The University of South Bohemia in České Budějovice
Faculty of Science

Master's Thesis

Uptake and metabolism of valsartan and candesartan in different plants

Bc. Laura Zellner, BSc

Thesis Supervisor:
Assoz.Univ.-Prof. DI Dr. Markus Himmelsbach
Institute for Analytical and General Chemistry
Johannes Kepler University Linz

Assistant Thesis Supervisor:
Dr. Franz Mlynek, MSc
Institute for Analytical and General Chemistry
Johannes Kepler University Linz

České Budějovice, 2022

Zellner, L., 2022: Uptake and metabolism of valsartan and candesartan in different plants. MSc. Thesis, in English. – 70 p., Faculty of Science, University of South Bohemia, České Budějovice, Czech Republic.

Annotation:

Due to the nowadays extensive pollution of the environment with pharmaceuticals and personal care products, plants are exposed to a significant concentration of xenobiotics. For this reason, a growing number of scientists is focussing on the interaction between these chemicals and plants. Likewise, the present work investigates the uptake and transformation of two blood pressure lowering drugs, namely candesartan and valsartan, in several plant species by high-performance liquid chromatography hyphenated with a drift-tube ion-mobility quadrupole time-of-flight mass spectrometer.

Statutory declaration

I declare that I am the author of this qualification thesis and that in writing it I have used the sources and literature displayed in the list of used sources only.

Reichenthal, 03.11.2022 _____

Place, date Signature

Acknowledgements

First and foremost, I would like to thank o.Univ.-Prof. DI Dr. Wolfgang Buchberger for the great chance to do my thesis at the Institute of Analytical Chemistry and to improve my skills in this, for me, particularly interesting field.

Next, I would like to express my gratitude to my supervisor, Assoc. Univ.-Prof DI Dr. Markus Himmelsbach for his support and expertise throughout my work. I appreciate that I was allowed to freely decide on the direction of my research.

Special thanks are also directed to Dr. Franz Mlynek without whom I would still be afraid of ruining the HPLC-DT-IM-QTOF. Thank you for your dedication and for the time you spent patiently explaining the instrumentation to me as well as for discussing my results. Not to forget, thanks for daily cheering me up with your hilarious insider jokes.

I also wish to extend my thanks to the whole team of the Institute, who very kindly welcomed and supported me. Special thanks to Thommy for the Python scripts, for your advice and for your help. Also, thanks to Alex, Thomas, and David – with all of you my time in the lab was truly amusing and I am glad that I got to know you.

Last but not least, I am grateful to my family and friends who supported me along the way and put up with my mood swings during stressful situations. Also, special thanks to those of you who contributed to this thesis by listening to me babbling about my daily progress in the lab, by giving your opinion on some formatting issues or by proofreading my writing.

Table of Contents

Abbreviations

ACE	angiotensin converting enzyme
ACEI	angiotensin-converting enzyme inhibitor
ACN	acetonitrile
AF	alternating frames
ARB	angiotensin receptor blocker
CAN	candesartan
CCS	collision cross section
CDC	candesartancilexetil
CE	collision energy
CID	collision induced dissociation
DT-IM	drift-tube ion-mobility
EU	European Union
FA	formic acid
FC	fold changes
GlcA	glucuronic acid
Glu	glucose
HCl	hydrochloric acid
HPLC	high performance liquid chromatography
IUPAC	international union of pure and applied chemistry
Mal	malonic acid
MeOH	methanol
MS	mass spectrometry
PPCPs	pharmaceuticals and personal care products
QTOF	quadrupole time of flight
RAAS	renin-angiotensin aldosterone system
RP	reversed-phase
RSD	relative standard deviation
RT	retention time
TWW	treated wastewater
VAL	valsartan
WWTPs	wastewater treatment plants

Abstract

As the climate changes and temperatures are constantly increasing, the reuse of treated wastewater, especially for irrigation of crops, is becoming essential to fight water scarcities in arid regions. However, employing reclaimed waters in agriculture raises another issue. More and more pharmaceuticals and personal care products (PPCPs) are released into the environment since wastewater treatment plants (WWTPs) are not able to remove all traces of these synthetic chemicals. Xenobiotics are then absorbed by plants, possibly metabolized, and might finally end up in the food chain.

The present work, therefore, engages with the uptake and transformation of two blood pressure lowering drugs, namely candesartan and valsartan, in several plant species. Cress, peas, maize, triticale, rye, barley, carrot, turnip greens and sorghum were grown hydroponically in water spiked with either of the pharmaceuticals. The resulting plant extracts were analyzed using high-performance liquid chromatography hyphenated with a drift-tube ion-mobility quadrupole time-of-flight mass spectrometer.

The acquired data were screened for common phase I and phase II metabolites using an in-house created theoretical database. Additionally, two new strategies for the identification of unknown transformation products were established. In the plantomics approach, the differences between drug-exposed and untreated plantlets were investigated. The alternating frames approach, in contrast, aimed to identify molecules containing the drug-backbone by searching for the characteristic fragmentation pattern of the xenobiotic based on matching drift times.

For both pharmaceuticals as well as for candesartancilexetil, the esterized prodrug of candesartan, a hydroxylated species was found. Also, extensive phase II metabolization was observed: species formed by conjugation with even multiple units of glucose, malonic acid and/or glucuronic acid could be detected. All compounds were tentatively identified based on their retention times, exact masses, fragmentation patterns and collision cross sections.

Finally, cress was cultivated in effluent samples of local WWTPs that contained candesartan and valsartan in the low µg L^{-1} range. In the extracts all parent drugs and glucosylated transformation products could be detected.

The newly developed strategies are promising, yet there is huge potential for optimization. Nevertheless, all herein presented approaches are applicable for screening plant tissue for any other pharmaceutical and its transformation products. Consequently, it should help to increase the understanding of the effects of PPCPs on the environment.

1. Introduction

Water is one of the most precious natural resources, which is reflected in the mission of transnational associations like the EU to protect its high quality and purity in the form of water policies [1]. Despite these efforts, water scarcity and droughts are becoming increasing threats which are even expected to worsen due to climate change [2]. For this reason, EU campaigns like “Water is too precious to waste” aim to draw humanity’s attention to these pressing challenges. Thereby special emphasis was set on the reuse of treated wastewater (TWW) for extending its lifecycle, thus saving water [3].

Amongst others, irrigation in agriculture is a promising area of application of TWW since it is the world’s largest water consumer, and water scarcities in agriculture threaten food security, especially in poor regions [4,5]. Though, such a policy comes along with another concern. TWW was proven to contain unwanted contaminants. For that reason, the European Commission proposed certain quality criteria that the reclaimed waters must meet to ensure high levels of environmental protection [3].

Nonetheless, these regulations do not address PPCPs yet, which are a part of the “emerging organic contaminants” in the environment [6]. Before blindly using TWW to fight water scarcities, the routes of pharmaceuticals into the environment and their influence on plants need to be understood.

1.1. Pharmaceutical pollution in the environment

PPCPs have been confirmed worldwide in drinking water, wastewater, groundwater, surface water, soils, and biota over the last years [7–9]. Their presence in the environment is particularly hazardous due to their strong biological activity, even at very low concentrations. As reported by several studies, some of these highly active compounds are already causing serious adverse effects on non-target organisms. An example of that would be the feminization of male fish by estrogenic drugs [9].

To understand the underlying cause of this ecotoxicological threat, the routes of PPCPs into the environment are discussed. The substances are released either from point or diffuse sources according to the classification of W.C. Li [10]. Point source pollution can be linked to a certain location, for example, the industrial effluent from pharmaceutical companies which contains drug-active substances. In contrast, diffuse pollution originates from a broad geographical

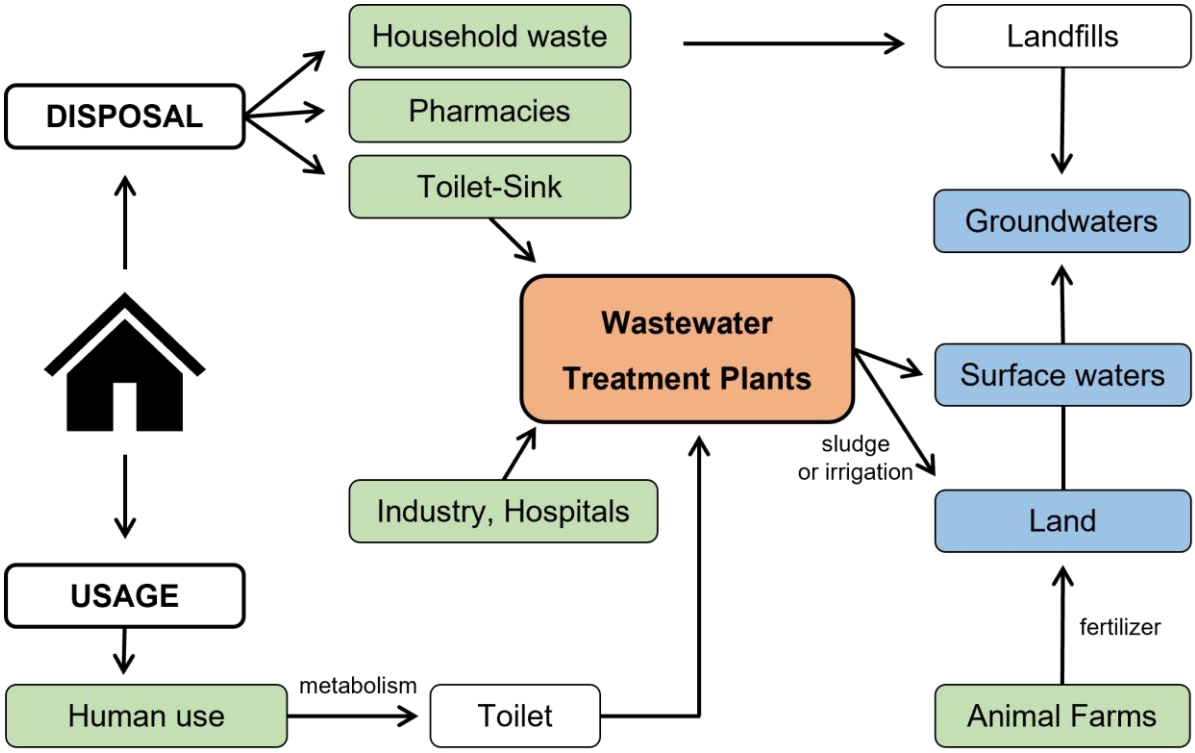

Figure 1: Possible pathways of pharmaceuticals into the environment, based on [11].

region and cannot be associated with one specific source. An example would be leakages of WWTPs. The various routes of pharmaceuticals from manufacture into the environment are visualized in Figure 1 [11].

First, organic contaminants of the environment can stem from improper water clearance in WWTPs [12]. High loads of drugs enter WWTPs either through direct disposal in toilets or as industrial/medical waste. Also, major amounts stem from human metabolism since part of the pharmaceutical is excreted unchanged via urine and feces.

Nowadays, sophisticated WWTPs that are equipped with an additional treatment step (e.g., ozonolysis, chlorination, absorption on charcoal) can greatly reduce the concentration of the high load of micropollutants in the water. However, wastewater is mostly still treated in conventional WWTPs. These cannot degrade the pharmaceuticals entirely, leading to contamination of sewage sludge and effluent with residues as well as metabolites of the substances [13].

For this reason, the utilization of sewage as organic fertilizer on farmland introduces these substances into the environment. In addition to that, the polluted TWW is directed to surface waters or used to irrigate crops to counteract water scarcities, as mentioned earlier, in arid or semi-arid regions like Israel or Spain [14].

Other sources of pollutants are soil fertilization with animal excreta or leakages from landfills caused by improper disposal of drugs in the household waste [11]. Via these routes, residues of human and veterinary medicines enter the environment and might end up in the groundwater.

The occurrence of xenobiotics in the environment has become a global issue due to the increasing availability and use of PPCPs [9]. Therefore, the attention of the scientific community for this topic was provoked worldwide. Advances in environmental analytical chemistry enabled to detect and quantify pharmaceuticals in a vast number of samples over the last thirty years in a concentration range of ng L^{-1} to µg L^{-1}. Nevertheless, impacts on human health, flora, fauna, etc., are yet poorly understood [15,16]. The next chapter engages in more detail with the influence of these drug remnants on plants, specifically how they are absorbed and metabolized.

1.2. Uptake and Metabolization of Xenobiotics in Plants

Due to the presence of PPCPs in soil and water, plants absorb the contaminants together with essential nutrients and trace elements. Most commonly, the compounds are taken up from the rhizosphere by passive diffusion into the roots. For visualization of the uptake process, which is described based on an article of Miller et al. [17], the typical root anatomy for a dicot vascular plant is shown in Figure 2.

The solutes must therefore pass the lipid bilayer (epidermis) on the outside of root tips and root hairs via one of three pathways [17]. These are (1) the transmembrane pathway (transport through cell walls and membranes), (2) the symplastic pathway (transport through the interconnecting plasmodesmata between cells) or the (3) apoplastic pathway (transport through the intercellular space). The preferred transport path is dictated by the physiochemical properties of the xenobiotic (e.g., charge, lipophilicity, polarity). While lipophilic compounds rapidly diffuse across the membrane and hence favour the symplastic pathway, ionized and highly polar substances are absorbed less frequently by plant roots. Nonetheless, such molecules are transported across the lipid bilayer actively with the help of transporter proteins.

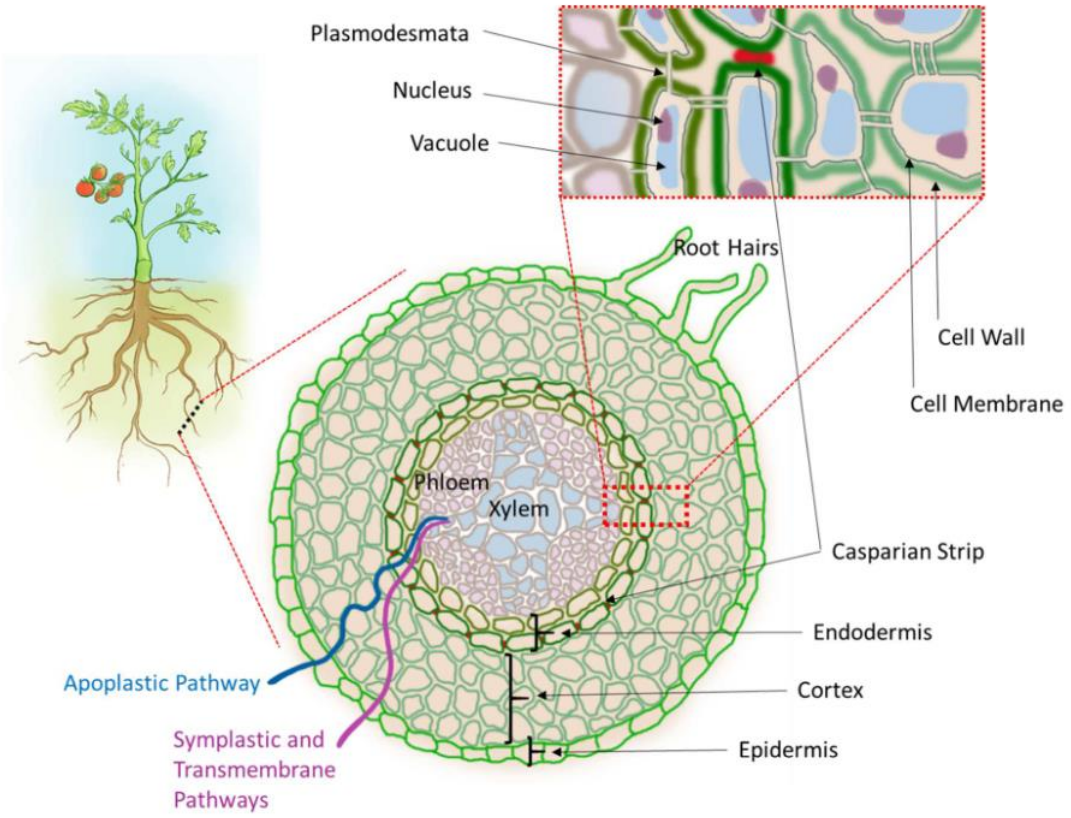

Figure 2: Cross-section of a dicot root. Apoplastic, symplastic and transmembrane pathways for solute uptake are indicated. The Casparian strips block apoplastic transport at the endodermis [17].

Once the epidermis is overcome, the compounds first diffuse through the cortex and finally cross the endodermis [17]. Since the Casparian strips in the endodermal cell walls block the apoplastic pathway, only symplastically transported xenobiotics can diffuse over this barrier and enter the vascular tissue. From there, the substances are transported upwards to the shoot, leaves, and fruits of the plant.

Transportation within the plant occurs via xylem or phloem [17]. In the xylem, xenobiotics are transported upwards together with water, inorganic nutrients, and other organic substances. This process is driven by hydrostatic pressure, which is created by transpiration in the upper regions (leaves) of the plant. Environmental conditions like temperature and humidity increase transpiration rates and consequently affect the accumulation of xenobiotics in plant leaves/fruits. The second long-distance transport pathway, namely via the phloem, is driven by osmotic pressure and carries substances from source areas to sink areas (e.g., carbohydrates from leaves to roots). Translocation of xenobiotics into fruits mainly occurs via this route.

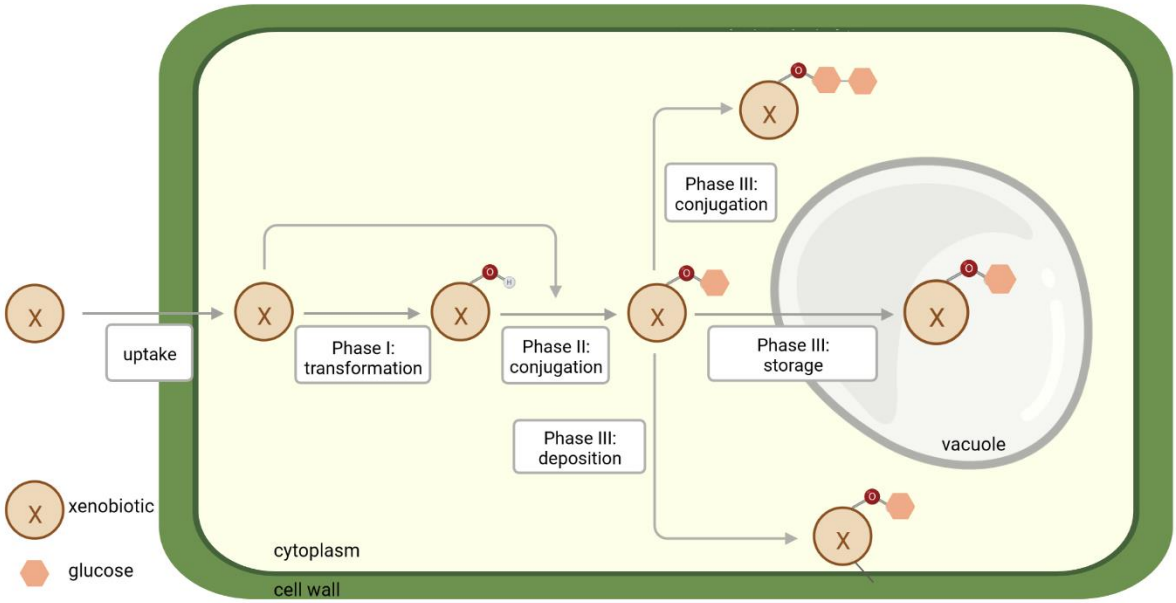

Figure 3: "Green liver concept" for detoxification of xenobiotics in plants, image created with Biorender.com based on [17].

So overall, whether xenobiotics remain in the roots, are transported to leaves in the xylem or end up in fruit due to phloem translocation depends on the compounds' ability to cross membranes.

Xenobiotics are a potential threat to plant metabolism. Thus, plants aim to protect themselves from these bioactive foreign compounds. Their protection mechanism is similar to the hepatic detoxification system in the human body and is therefore commonly called the "green liver concept" [18]. This metabolic pathway is frequently divided into three steps: (1) transformation and activation (phase I), (2) conjugation (phase II) and (3) compartmentation (phase III) (Figure 3).

During phase I, the reactivity and polarity of the xenobiotics are increased by hydrolysis, oxidation, or reduction reactions to make them suitable for further transformations. The reactive drug metabolites are then conjugated with polar molecules like sugars, malonic acid, amino acids, etc., in phase II. Already reactive parent compounds are directly conjugated without prior modifications. Phase II metabolites are overall more polar and less cytotoxic. Also, the conjugation unusually decreases the biological activity of the xenobiotic. These two metabolic processes take place in the cytosol of plant cells, and several enzymes like alcohol dehydrogenases and glycosyltransferases are involved. At this point in human metabolism, the metabolized compounds are secreted via urine or feces. Plants however, lack those excretory

pathways. For this reason, in phase III, the compounds are either stored in vacuoles, where they might be further transformed by peroxidases, or they are deposited onto insoluble compartments in the cells. Alternatively, often before compartmentation, the phase II metabolites are further conjugated [18,19].

Although this detoxification process minimizes the harmfulness of xenobiotics to plant metabolism, the toxicity of the transformation products is yet largely unknown. They might potentially pose a risk to humans or animals when accumulating in edible crops like maize. Also, the human/animal metabolism can convert unstable plant-derived xenobiotic conjugates back to the parent pharmaceutical active substance, which could lead to non-assessable drug exposure [20].

To gain information about such transformation products, already some effort was taken. Plant tissue was screened for metabolites of a group of drugs (amongst others, non-steroidal anti-inflammatory drugs and antibiotics), and the compounds were tentatively identified [21]. The present work continues this research by focussing on the metabolization of the drugs valsartan and candesartan in several different plant species. Of course, to increase the knowledge about the pharmaceuticals' behaviour in plants, first, their use, interactions, and mechanism of action in the human body need to be understood and are elucidated in the next chapter.

1.3. Candesartan and Valsartan

Candesartan and valsartan, besides azilsartan, irbesartan, losartan, olmesartan, and telmisartan, belong to the group of sartans which are used for the treatment of hypertension, congestive heart failure and albuminuria-related renal diseases [22]. By blocking the AT_1 angiotensin II receptor subtype, they suppress the hypertensive effects of the protein angiotensin II. Consequently, blood pressure and cardiac activity are reduced, aldosterone levels are lowered, and excretion of sodium is increased.

The peptide hormone angiotensin II acts within the renin-angiotensin-aldosterone system (RAAS), which is among other roles responsible for blood pressure regulation and renal function [23]. For understanding the mode of action of angiotensin receptor blockers (ARBs), first, the RAAS is discussed:

The RAAS (for visualization, see Figure 4) is a system that, in a prolonged manner, elevates blood volume and arterial resistance by increasing sodium and water reabsorption as well as vascular tone [24]. The process starts in the arterioles of the kidney, where prorenin is cleaved to renin due to activation of the juxtaglomerular cells. Activation of these cells is connected to low blood pressure or low sodium concentration in blood vessels. The enzyme renin is released into the blood and acts on angiotensinogen (produced in the liver) to cleave it into the inactive angiotensin I. By the action of the angiotensin-converting enzyme (ACE), which is mainly found in the lungs and kidney, angiotensin I is finally converted into the biologically active angiotensin II. The freshly created peptide hormone can subsequently interact with subtype AT_1 and AT_2 angiotensin II receptors in the kidney, adrenal cortex, arterioles, and brain, triggering several effects:

- Na-H exchange is stimulated by the peptide hormone in the kidney, which increases the sodium reabsorption from urine. The consequently higher osmolarity of the blood raises the water influx and, therefore, the arterial pressure.
- In the adrenal cortex, angiotensin II activates the synthesis of aldosterone from cholesterol which also causes sodium reabsorption while potassium is excreted. That leads to the same effects as mentioned previously, but aldosterone acts in a time-delayed fashion compared to angiotensin II.

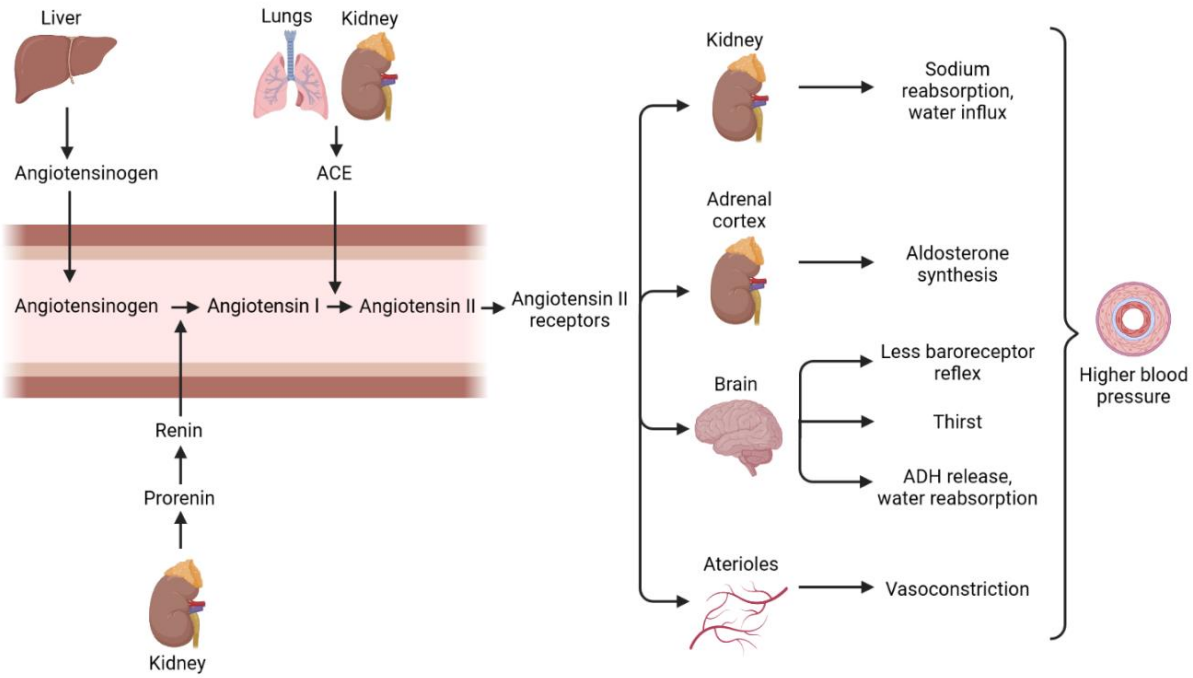

Figure 4: Renin-angiotensin-aldosterone system. Image created with biorender.com based on [24].

- Angiotensin II also has pressor effects. It leads to constriction of arterioles by triggering a secondary messenger cascade through binding to G protein-coupled receptors. Thereby total peripheral resistance in the arterioles is built up which causes higher blood pressure.
- In the brain, angiotensin II stimulates thirst by binding to the hypothalamus. Also, the release of antidiuretic hormone (ADH) by the posterior pituitary gland is provoked, which increases water reabsorption in the kidney. Furthermore, the baroreceptor reflex is desensitized, leading to less pronounced responses to the increased blood pressure.

Overall, these effects raise total water and sodium amounts in the body and, for that reason, lead to elevations of the blood pressure [24].

Inhibition of this cascade to treat hypertension is achieved by either using angiotensin-converting enzyme inhibitors (ACEIs) or ARBs. Since ACEIs, like ramipril or lisinopril, which block the conversion of angiotensin I by ACE enzyme inhibition, can have unwanted adverse effects, more selective ARBs were developed [23].

ARBs interfere with the RAAS by competitively and selectively blocking the AT_1 subtype of the angiotensin II receptor. They thus antagonize the formerly mentioned actions of angiotensin II and, consequently, the blood pressure decreases. Moreover, they lead to a dose-dependent increase in plasma renin activity as well as plasma concentration of angiotensin II. Also, the sartans can bind to the AT_2 subtype receptors but only to very small extents. Even at high concentrations, the drugs showed no affinity for any other receptors. One big advantage of ARBs is that they are well tolerated and show no specific, dose-dependent adverse effects [22,23].

1.3.1. Candesartan

Candesartan, which is sold amongst others under the name Atacand, is called 1-((2'-(1H-Tetrazole-5-yl)-[1,1'-biphenyl]-4-yl)methyl)-2-ethoxy-1H-benzo[d]imidazole-7-carboxylic acid according to IUPAC-nomenclature. The white crystalline powder is slightly soluble in water and physiological saline. The chemical and physical properties of the pharmaceutical are listed in Table 1, and its structure is depicted in Figure 5 [25,26].

Table 1: Chemical and physical properties of candesartan. [25,26]

Property	**Value**
Molecular formula	$C_{24}H_{20}N_6O_3$
Average molecular weight	440.4540
Monoisotopic molecular weight	440.1597
Melting Point	183 – 185 °C
logP	4.68
pK_a	3.44

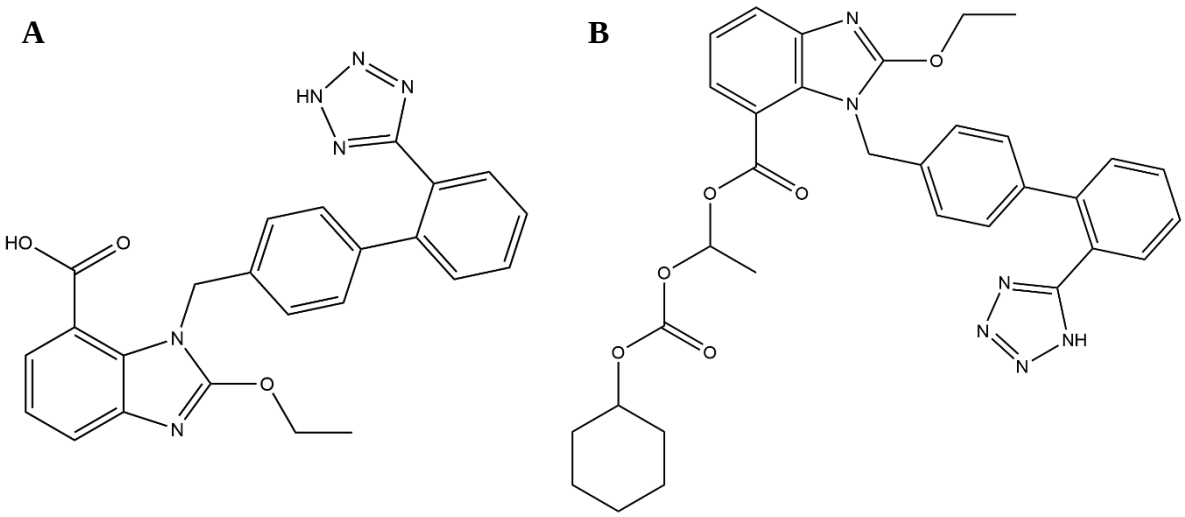

Figure 5: Structure of candesartan (A) and candesartancilexetil (B).

The molecule candesartan is only poorly absorbed by oral administration. For this reason, candesartancilexetil (Figure 5), an ester prodrug of candesartan, was synthesized. The prodrug is highly soluble in dimethyl sulfoxide, while it poorly dissolves in methanol, ethanol, or water. Candesartancilexetil shows no clinical efficiency before it is rapidly and completely hydrolyzed by a carboxylesterase in the intestinal wall to its active form candesartan. The prodrug is administered in doses from 4 to 32 mg per day, but due to incomplete absorption, candesartan shows an absolute oral bioavailability of only around 15 %. In humans, the drug shows plasma protein binding of over 99 %, a volume distribution of 0.13 L kg^{-1} after intravenous administration and a half-life of 3.5 to 11 hours. No relevant drug-food or food-food interactions of candesartan were yet reported [26,27].

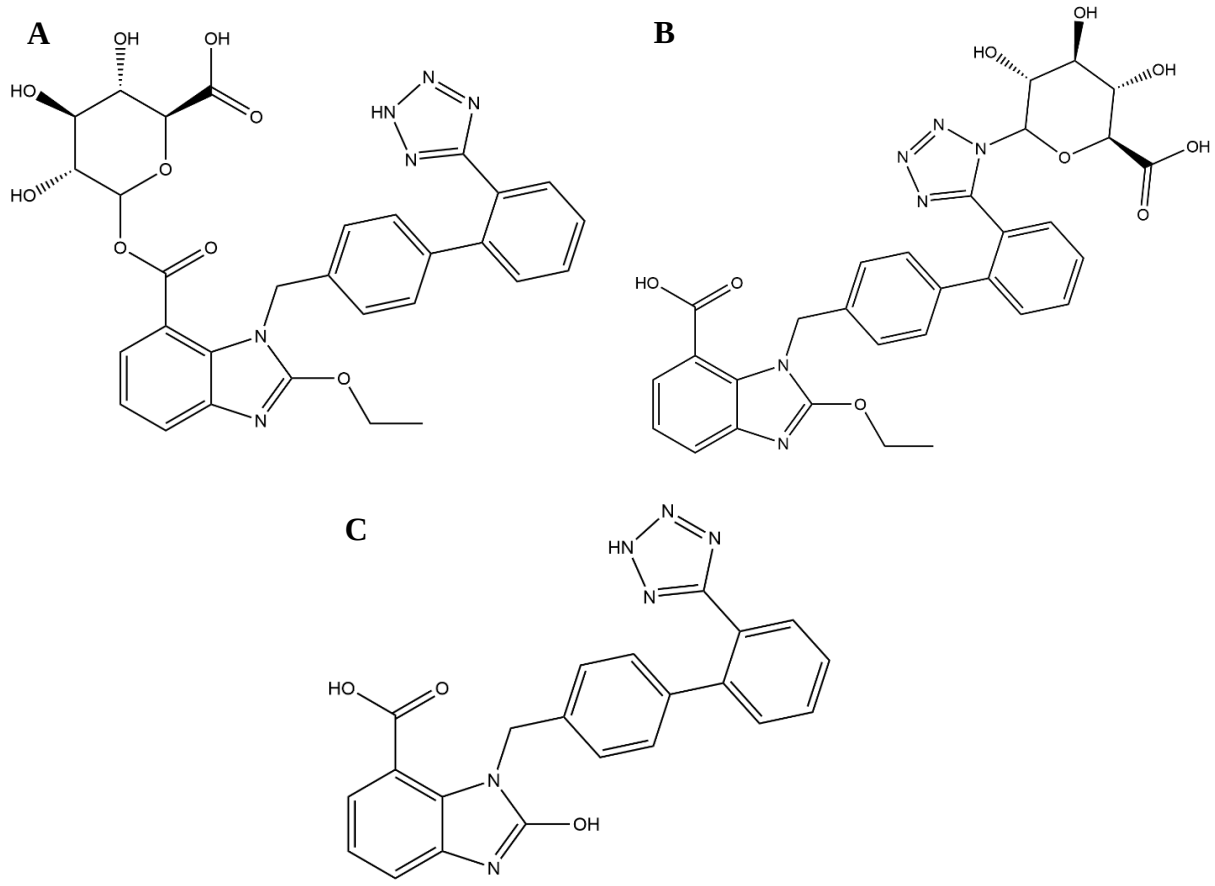

Figure 6: Structure of Candesartan O-glucuronide (A), Candesartan N-glucuronide (B) and O-Deethylated candesartan (C).

Candesartan clearance mainly takes place in the kidneys, but to a small extent, also the bile and the intestine are involved. It is eliminated mostly unchanged in urine and feces. So far, three clinically insignificant metabolites, namely candesartan O-glucuronide, candesartan N-glucuronide and O-Deethylated candesartan were identified (Figure 6) [26,27].

1.3.2. Valsartan

The IUPAC term for valsartan is N-(1-oxopentyl)-N-[[2'-(2H-tetrazole-5-yl)[1,1'-biphenyl]-4-yl]methyl]-L-valine and it is currently sold under the name Diovan. The drug is well soluble in ethanol, dimethyl sulfoxide and dimethylformamide, but it only poorly dissolves in aqueous media (water solubility 0.0234 mg mL $^{-1}$). In Figure 7 the molecular structure of Valsartan is depicted, and the most important chemical and physical properties of the compound are listed in Table 2 [25,28].

Table 2: Chemical and physical properties of valsartan. [25,28]

Property	**Value**
Molecular formula	$C_{24}H_{29}N_5O_3$
Average molecular weight	435.5188
Monoisotopic molecular weight	435.2270
Melting Point	116 – 117 °C
logP	1.499
pK_a	4.73

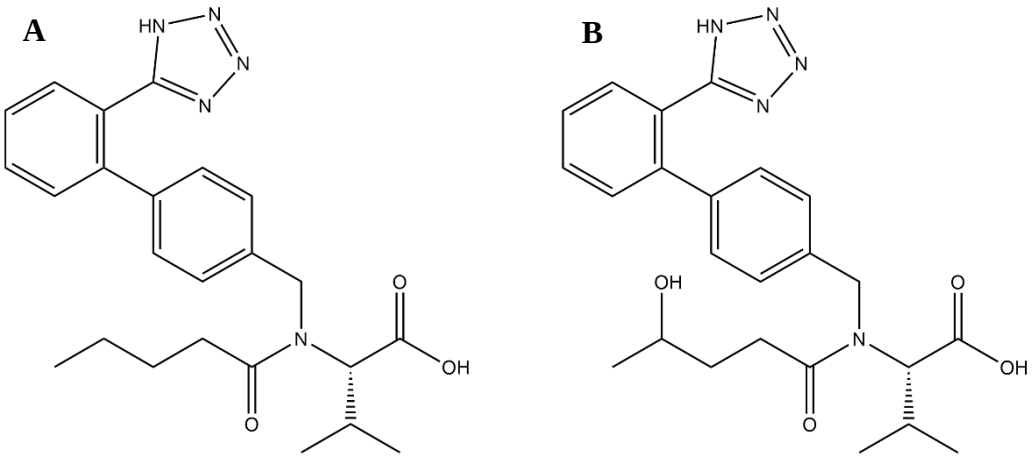

Figure 7: Structure of valsartan (A) and Valeryl-4-hydroxyvalsartan (B).

Two hours after oral administration of valsartan, the drug reaches its peak plasma concentration of 1.64 mg L^{-1}, which is, however, decreased by approximately 40 – 50 % by food intake. Valsartan is highly bound to serum proteins (85 – 99 %), shows a rather small volume of distribution of 17 L and is cleared from plasma at a rate of 2 L per hour. The absolute bioavailability of the drug is 23 %. It has a shorter half-life than other sartans. Nevertheless, a daily dose of 20 to 320 mg is sufficient to achieve the desired blood pressure lowering effects [23,28].

Valsartan is metabolized in the liver to minute extents. So far, only one primary metabolite, namely Valeryl-4-hydroxyvalsartan (Figure 7), is known. Nonetheless, the drug is secreted mostly unchanged in feces (83 % of the dose) and urine [23,28].

1.4. Analytical strategies

As already mentioned, several working groups have taken an effort to investigate the uptake and transformation of xenobiotics in plants. The workflow used for this purpose typically includes plant cultivation and treatment, preparation of plant extracts, instrumental analysis, and data processing. In the following, the strategies used in the scope of this work are elaborated (based on [21]).

For simplifying the experimental setup, plantlets are primarily grown hydroponically in drug-spiked water. Compared to soil cultivation, such a strategy shows a less complex matrix, and potential interferences of microorganisms are prevented. Usually, the cultivation medium contains a high concentration of the pharmaceutical to simplify the detection of formed metabolites. Moreover, it should not be forgotten that the used drug levels should not hamper the growth of the plant. Also, since transformation products might already form in the medium, it is necessary to analyse blank medium, which was kept under identical experimental conditions as the plantlets.

Plant extracts are, in most cases, simply prepared by extraction with appropriate solvents followed by homogenization. Frequently clean-up and preconcentration steps, like solid phase extraction, are included at this point. If plantlet sizes allow dividing the material into several distinct plant parts (roots, stem, leaves, etc.) during harvesting, separate extraction and analysis are recommended. Such a procedure namely provides additional information about the translocation of the parent drug and its metabolites within the plant.

Commonly, the main goal of the mentioned studies is to detect and identify new drug-related metabolites within the received plant extracts with the help of MS experiments. Depending on the analysis setup, the compounds can only be identified with a certain probability. For this reason, Schymanski et al. [29] defined a five-level identification confidence classification that ranges from confirmed to unknown structures (Figure 8). To reach high confidence, plant extracts are typically analysed with high-performance liquid chromatography (HPLC) hyphenated with quadrupole time-of-flight mass spectrometers (QTOF-MS) or Orbitrap-MS. MS^2 experiments are additionally performed to analyse the molecular fragmentation patterns. The thereby received data enable to propose tentative structures (level 3) since appropriate standards are frequently not commercially available and in-house synthesis is too laborious.

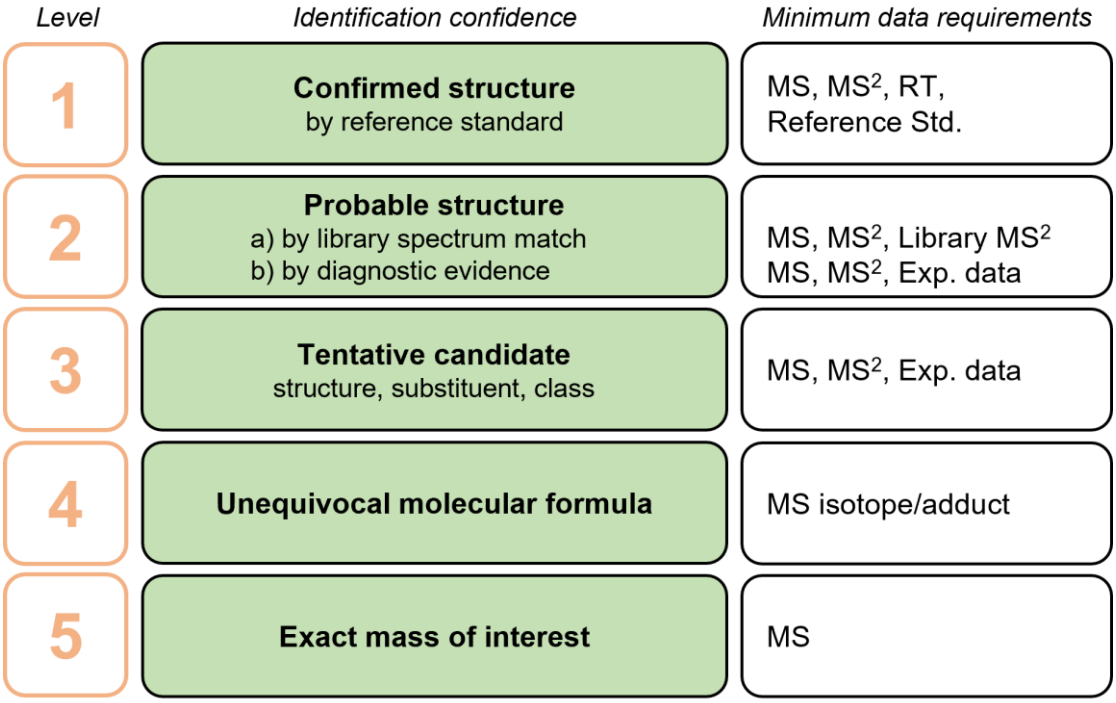

Figure 8: Identification confidence levels in mass spectrometric analysis, based on [29].

One of the latest accomplishments, also giving additional identification confidence, is using collision cross sections (CCS) as an additional characterizing parameter. The CCS values are received by equipping the MS device with a drift-tube ion-mobility (DTIM) device. It separates ions according to their mobility in an electric field in the presence of a buffer gas like nitrogen. With increasing size and shape of the analyte molecule, collisions with the neutral gas happen more frequently, leading to lower ion mobility and, hence, higher CCS values.

In general, there are two approaches for detecting plant-derived drug metabolites [21]. In untargeted analysis, extracts of treated and untreated plants are compared using suitable software. During a targeted approach, the extracts are screened for potential metabolites which were selected prior to analysis. A database containing these metabolites is usually created by checking literature data from similar plants, drawing analogies from human metabolism or using prediction tools.

During this work, in addition to the targeted approach, two strategies for untargeted metabolite identification were designed:

1.) Alternating frames (AF)-approach:

The first strategy aims to identify unknown transformation products within the plant extracts by screening MS data for the characteristic fragmentation pattern of the parent drugs. As mentioned in section 1.2. metabolites often result from simple conjugation with small biomolecules and should therefore show similar fragmentation as the pharmaceutical. For this approach, a complete fragmentation spectrum over the entire m/z range was acquired by applying an IM-MS all ions method. This technique is based on alternating collision energies (CE) and consequently records precursor molecules as well as their fragmentation pattern.

For this workflow IM measurements are critical. Since the ionized molecules pass the DT before being fragmented in the collision cell, parent as well as daughter ions show equal drift times and can therefore be related to each other.

2.) Plantomics-approach:

"Omics" in biology refers to the comprehensive analysis of large biological datasets which stem from a particular field of interest within an organism (metabolomics, proteomics, lipidomics, etc.). In plantomics usually all "-omics" fields are combined into a so-called multi-omic strategy that provides extensive insights into the complex plant systems [30]. The idea of plantomics was used in this work for comparisons between drug-exposed plantlets and ones grown in regular water. For this purpose, the multiomes of both groups were first analysed by HPLC-DT-IM-QTOF. Subsequently, the data were statistically evaluated to identify upregulated species in the treated samples, which could give a lead to drug metabolites.

2. Research objectives

As already mentioned, the present work aims to gather more information about the uptake and transformation of xenobiotics in plants by specifically looking at two blood pressure lowering drugs, namely valsartan and candesartan. The pharmaceuticals were chosen due to their regular and rather dominant appearance besides telmisartan in several TWW samples and water bodies (data collected at the Institute of Analytical Chemistry, JKU).

The primary goal was to tentatively identify metabolic transformation products of the pharmaceuticals in extracts of several model plants which were grown hydroponically under the influence of drug-spiked medium. For this purpose, the extracts were analysed with an HPLC-DT-IM-QTOF instrument, and the data were interpreted with the help of several bioinformatic tools.

Another objective was the quantification of candesartan and valsartan in effluent samples from WWTPs in the region (Hirschbach, Reichenthal). The water was then employed as cultivation medium for cress. Using the acquired analytical techniques, the thereby received plant extracts were screened for the formerly identified transformation products.

This thesis should increase the awareness of the influence of pharmaceuticals on the environment and therefore encourage further research in this area. Especially investigations concerning the toxicity and accumulation of the transformation products are crucial since upcoming water scarcities might intensify the need for reusing TWW for irrigation purposes in agriculture.

3. Materials and Methods

3.1. Chemicals, consumables, and plant seeds

Acetonitrile (ACN; ≥ 99.8 %) and methanol (MeOH; ≥ 99.8 %) were obtained from VWR (Vienna, Austria). Formic acid (FA; ≥ 99 %) and hydrochloric acid (HCl; ≥ 37 %) were acquired from Sigma Aldrich (Steinheim, Germany) and Merck (Darmstadt, Germany), respectively. All reagents were of HPLC grade.

Candesartancilexetil (CDC, 32 mg, 1A Pharma) and valsartan (VAL, 80 mg, Diovan) were purchased as pharmaceutical preparations in a local pharmacy.

Throughout the work, ultrapure water from a Milli-Q water purification system (Millipore, Bedford, Ma, USA) was used.

Garden cress (Cresto, *Lepidium sativum*), turnip greens (Namenia, *Brassica rapa* ssp. *silvestris*) and carrots (rote Riesen, *Daucus carots* ssp. *sativus*) were all purchased in a local garden shop (brand Kiepenkerl). Pea (Tiberius, *Pisum sativum*), maize (LG31272, *Zea mays*), sorghum (Armorik, *Sorghum bicolor L.*), triticale (Borowik, *Triticosecale neoblaringhemii*), rye (KWS Binntto, *Secale cereale*) and barley (Ernesta, *Hordeum vulgare*) were obtained from RWA (Korneuburg, Austria).

To remove insoluble parts prior to HPLC separation, the samples were filtered using 1 mL syringes (Omnifix-F, B. Braun Melsungen AG, Melsungen, Germany) equipped with nylon syringe filters (CHROMAFIL, pore size 0.45 µm, Ø 15 mm, Macherey-Nagel, Düren, Germany).

Further used consumables were conical centrifugation tubes from Greiner Bio-One (Kremsmünster, Austria), HPLC vials from Merck (Darmstadt, Germany) and INOX balls from Domel (Ø 5 mm, Železniki, Slovenia).

3.2. Preparation of reagents

Stock solutions of the pharmaceuticals were prepared by suspending one tablet, respectively, in 10 mL MeOH, followed by ultrasonication (Elmasonic s 60 H, Elma, Singen, Germany) for 20 min. Thereby solutions of 3 200 mg L^{-1} CDC and 8 000 mg L^{-1} VAL were obtained. Insoluble parts were removed using nylon syringe filters.

Further solutions of 1000 mg L^{-1}, 100 mg L^{-1} and 10 mg L^{-1} for both drugs were prepared in Milli-Q water. For external calibration, these solutions were additionally diluted to 2.5, 5, 7.5, 10 and 25 µg L^{-1} of CDC and VAL, respectively. To achieve full hydrolysis of CDC to candesartan (CAN), the dilution was done in 1 M NaOH. The base was prepared by dissolving NaOH beads in Milli-Q water followed by ultrasonication for 20 min.

As medium for plant cultivation, a 10 mg L^{-1} solution for each pharmaceutical was prepared in tap water. All solutions were stored at 4 °C

3.3. Laboratory cultivation of plants

For the study, garden cress, peas, maize, triticale, rye, barley, carrot, turnip greens and sorghum were selected as model plants. They were cultivated under hydroponic conditions without supplying nutrients. Besides the plantlets which were exposed to cultivation medium, always negative controls were grown in tap water.

Cress seeds (5 g) were soaked for 1 – 2 h in tap water before they were distributed on the grid of a cultivation set (local garden shop). They were allowed to germinate for two days (watering once a day with a spray bottle), and then the cultivation set was filled with approximately 300 mL of the respective solution (regular water or cultivation medium). The cress was grown on a laboratory bench with direct sunlight for 7 days. The medium was refilled to assure constant supply. Figure 9 exemplary shows a batch of cress right before harvesting.

Figure 9: Hydroponic cultivation of cress in a cultivation set.

Figure 10: Cultivation of peas and maize. (A) Germinated peas after two days of growth in darkness. (B) Peas (left) and maize (right) planted into iron-on beads.
(C) Maize plantlets in Erlenmeyer flasks in exposure to the cultivation medium.

Pea and maize seeds were soaked overnight in tap water. Then the seeds were spread on wet paper towels and left in darkness to germinate for two days. After that, the sprouts were planted into beds of wetted iron-on beads and grown for a few days. Once they reached a certain height, the plantlets were transferred into small Erlenmeyer flasks filled with 50 mL tap water or cultivation medium. The whole process of cultivation can be seen in Figure 10.

Triticale, rye, and barley sprouts were grown likewise as pea and maize. They were, though, not transferred onto iron-on beads but further cultivated on petri dishes with a paper towel soaked in water/cultivation medium (Figure 11).

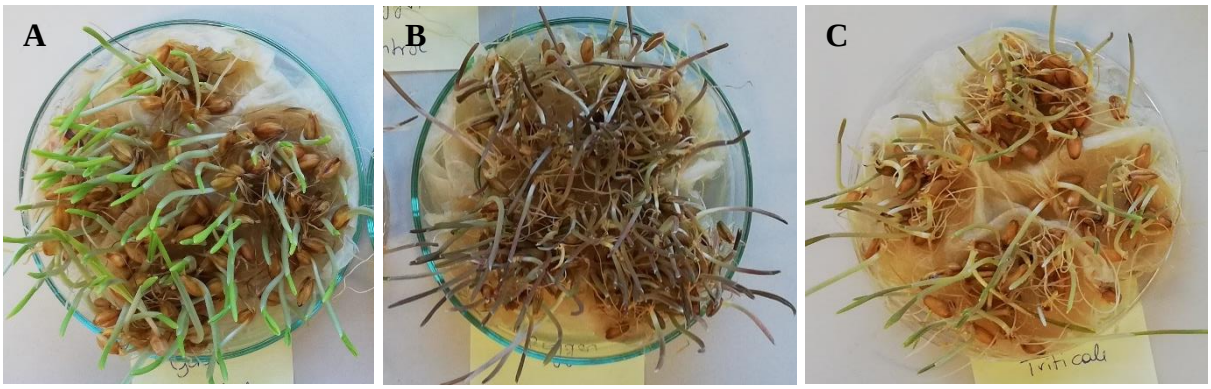

Figure 11: (A) Barley, (B) rye, and (C) triticale growing in petri dishes on paper towels soaked in cultivation medium.

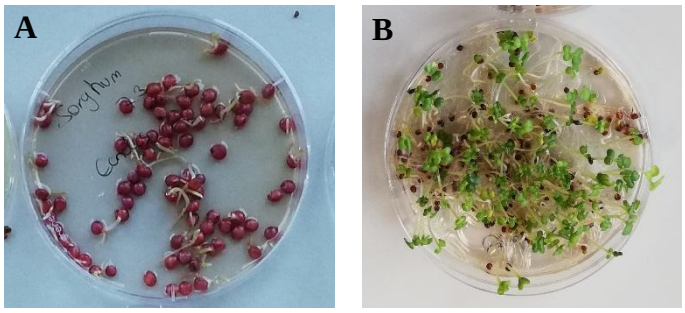

Figure 12: (A) Sorghum and (B) turnip green germs growing on petri dishes.

Carrot, turnip greens and sorghum seeds were germinated with small amounts of water under light exclusion on petri dishes. After two days, the buds were exposed to light and further grown for 5 days (Figure 12). Cultivation medium was supplied to the plantlets on daily basis.

3.4. Preparation of plant extracts

The plantlets were removed from their cultivation set-ups and divided into up to three parts (roots, stem, and leaves), depending on plantlet size (Figure 13). The material was then extensively rinsed with tap water and dried with a paper towel. Next, about 1.5 g (0.5 g for cress) of the material were weighted into 15 mL centrifugation tubes, and 3 mL of extraction solvent as well as four beads were added. If the sample weight deviated, the volume of the solvent was adjusted.

The samples were extracted for 15 min at 20 Hz using a ball mill (‘Star Beater’, VWR, Vienna, Austria) followed by centrifugation (‘MegaStar’ 1.6 R, VWR, Vienna) at 4 700 rpm for 8 min to pellet the insoluble plant material (Figure 13). The liquid supernatant was taken up with a syringe and filtered into 1.5 mL HPLC glass vials. The samples were stored at -80 °C prior to analysis.

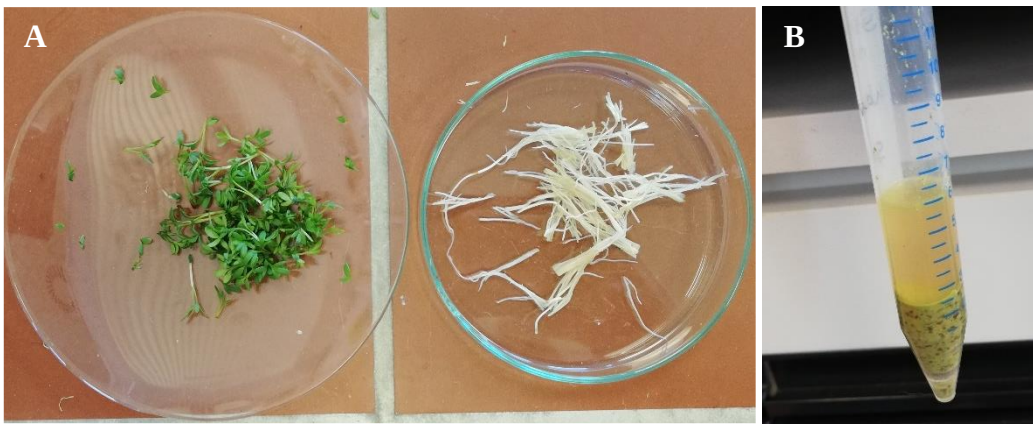

Figure 13: (A) Cress separated in leaves (left) and roots (right).
(B) Turnip greens sample after extraction and subsequent centrifugation.

For optimizing the extraction, following solvents were screened: MeOH, 0.1 M HCl / ACN 2:1, 0.1M HCl / MeOH 1:1, 0.1 M HCl / MeOH 4:1, ACN and H_2O / MeOH 1:1 (v/v).

3.5. HPLC-DT-IM-QTOF instrumentation and settings

The plant extracts were analyzed using reversed-phase (RP) HPLC hyphenated with a high-resolution DT-IM-QTOF. The 1260 Infinity II HPLC system comprised a 1260 Flexible Pump, Autosampler and Multicolumn Thermostat (Agilent Technologies, Waldbronn, Germany). For separation, it was equipped with an Agilent InfinityLab Poroshell 120 EC-C18 column (3.0 x 75 mm, 2.7 µm), which was protected by a C18 guard column (4 x 3 mm, Phenomenex, Aschaffenburg, Germany).

The mobile phase consisted of (A) water with 0.1 % FA and (B) ACN with 0.1 % FA. The applied gradient can be seen in Table 3. The flow rate of the mobile phase was set to 0.5 mL min^{-1}, the column was held at a temperature of 30 °C, and 20 µl of the samples were injected.

As detector, an Agilent Technologies 6560 DT-IM-QTOF mass spectrometer equipped with a Dual Jet Stream Electrospray Ionization source was operated in positive ion mode. As sheath and drying gas, N_2 was used. All other MS parameters are listed in Table 4.

Table 3: Mobile phase gradient for HPLC separation.
(Solvent A: H_2O with 0.1 % FA; Solvent B: ACN with 0.1 % FA)

Time / min	Solvent A / %	Solvent B / %
0	90	10
0.5	90	10
4.5	65	35
9.0	5	95
12.0	5	95
12.1	90	10
18.0	90	10

Table 4: MS parameters.

Parameter	**Value**
Drying/sheath gas temperature / °C	275
Drying/sheath gas flow / L min^{-1}	11
Nebulizer / psi	40
Capillary voltage / V	4 000
Nozzle voltage / V	1 000
Fragmentor voltage / V	400
Acquisition rate / spectra s^{-1}	1
m/z range	100 – 1 700

Table 5: IM-QTOF MS parameters.

Parameter	**Value**
Trap fill time / µs	1 800
Trap release time / µs	250
Frame rate / frames sec^{-1}	0.9
Transient rate / transients $frame^{-1}$	17
Maximum DT / ms	60

When operating in the DT-IM mode, the instrument was auto-tuned in the 2-GHz extended dynamic range setting in the 1700 m/z fragile ion mode. High purity nitrogen was used as drift gas, and 5-bit multiplexing was applied. Further IM settings are stated in Table 5.

The AF setting (DT-IM mode) was used to collect complete fragmentation spectra over the whole m/z range. CEs were therefore set to alternate between 0 V and 5 V over the individual frames.

The collected DT were converted to $^{DT}CCS_{N2}$ values using single field calibration with the Agilent Tune Mix, which was measured before the plant samples. Electric field parameters for DT measurements were set to 1567 V, 217 V, 210.5 V and 38 V at the drift tube entrance, the drift tube exit, the rear funnel entrance, and the rear funnel exit, respectively [31].

3.6. Analysis of standards and window solutions

To obtain CDC, CAN and VAL retention times (RT), 1 mg L^{-1} standards of the respective drug were analyzed by HPLC-MS. Fragmentation patterns were gained by recording MS^2 spectra with 3 (only for VAL), 5, 10, 15, 20 and 25 V CE.

Light-dependent degradation or hydrolysis of the pharmaceutical compounds was investigated by analyzing so-called "window solutions". These were standard solutions which were diluted to 10 mg L^{-1} with tap water and stored at the window in the same conditions as the plants. Samples of the window solution were analyzed likewise the plant extracts by HPLC-MS^2 and screened for the parent drugs as well as the detected metabolites.

3.7. Metabolite screening in hydroponically grown plants

As a first approach to identify drug metabolites, the plant material and negative control samples, which were obtained according to section 3.4., were analyzed with an HPLC-DT-IM-QTOF instrument in QTOF-only mode. Data were processed with MassHunter Qualitative B.07.00 software (Agilent).

Metabolites were identified using a targeted approach with the help of an in-house prepared theoretical database library (PCDL). Therefore, phase I metabolites, formed by human metabolism [26,28], were conjugated in several possible variations with frequently found groups like glucose, malonic acid, or glucuronic acid [32] (see Table 14 – Table 16 in the Appendix). The resulting database was compared to the MS data and matches with a tolerance of ± 5 ppm were searched (option "Find compounds by formula" of the MassHunter Qualitative software). Promising signals were further investigated by targeted MS^2.

The negative control samples were searched for the identified metabolites to assure that the compounds were formed as a consequence of the exposure to pharmaceuticals.

In a second approach, the spectra received by the AF mode of the instrument were searched for the characteristic fragments of the parent drugs. For this purpose, the raw data were demultiplexed using the PNNL Reprocessor 4.0 (Pacific Northwest National Laboratory, Richland, WA, USA) and features were extracted with the help of the Mass Profiler (Version 10.0, Agilent Technologies, Waldbronn, Germany). Settings for the Mass Profiler are summarized in Table 6.

Features that showed the drug-specific fragmentation pattern were identified using a Python script provided by a colleague. The script took a list of target fragments and screened the features for them based on matching drift times. Subsequently, the features were ranked according to the number of found fragments in an output file. In the next step, the drift spectra of the features showing the highest number of hits were manually reviewed in the IM-MS Browser 10.0 (Agilent Technologies, Waldbronn, Germany), and promising signals were subjected to targeted MS^2.

3.1. Plantomics – statistical analysis

For the statistical comparison of plants grown with and without drug influence, garden cress was planted and grown (section 3.3.). Five random samples of roots and leaves were harvested according to section 3.4. for cress in tap water, in CDC solution and VAL solution, each. Additional five samples of tap water and extraction solvent were included to detect signals not stemming from the plant material (background correction).

Table 6: Mass Profiler settings.

Parameter	Setting
Ion intensity / counts	>= 2 500.0
RT tolerance / %	0.2
DT tolerance / %	1.5
Mass tolerance / ppm	5.0
Q-Score	>= 60.0

The samples were analysed randomly to eliminate any biases with an HPLC-DT-IM-QTOF instrument in IM-QTOF mode. The random worklist was created using a random number generator in Microsoft Excel.

IM raw data was again demultiplexed using the PNNL Reprocessor. $^{DT}CCS_{N2}$ values were determined, and a mass correction was applied with the help of the IM Reprocessor (Version 10.00, Agilent Technologies, Waldbronn, Germany) and IM-MS Browser. For feature extraction, the Mass Profiler was used (for the settings, see Table 6).

For pre-processing of the received features, a script was created in PyCharm 2021.2.2 (Python 3.9) with pandas 1.3.4 and numpy 1.21.4. The script performs the following tasks (see Appendix Source code 1 for the complete code):

- Creation of a unique identifier for each feature
- Excluding features showing equal intensity over all samples (background signals stemming from the solvent, the tap water, etc.)
- Excluding features stemming from tap water or extraction solvent
- Replacing missing signals by text (NaN)
- Remodeling the file format for further analysis

In addition to that, all features outside an RT window of 3 to 14 min were deleted.

The pre-processed data was subsequently statistically analysed with the web-based platform MetaboAnalyst [33]. The drug-treated plant samples were compared to the untreated ones by a one-factor analysis. The files were uploaded to the online platform, and missing value estimation was employed. Also, the data were normalized by the median, log-transformed, and Pareto scaled. For visualization of the results, Python was utilized (matplotlib 3.5.2, seaborn 0.11.2 and bioinfokit 2.0.8). Fold changes (FC, threshold 2.0) and *p*-values (threshold 0.05) were illustrated in volcano plots to see significantly up- or downregulated signals. Additionally, hierarchical clustering heatmaps were compiled.

The most promising upregulated features of the drug-treated groups were further analyzed by targeted MS^2.

3.2. Analysis of wastewater samples

To demonstrate the presence of xenobiotics in the environment, samples from two WWTPs in upper Austria (Hirschbach and Reichenthal) were collected. The water samples were analyzed with HPLC-MS and CDC, CAN and VAL amounts were quantified using external calibration with standards in the range of 2.5 – 25 µg L^{-1} of the respective drug.

As a next step, garden cress was grown as described in section 3.3 using the wastewater. Again HPLC-MS spectra of the extracted plant material were recorded, and the received data were screened for the parent drugs and metabolites. Detected compounds were subjected to targeted MS^2, and their presence was additionally checked within the drift spectra of the samples.

4. Results and Discussion

4.1. Optimization of extraction solvent

The extraction procedure was optimized by screening of six different solvents. Of the tested media, MeOH yielded the highest signals for CAN (Figure 14). However, to facilitate extraction of the typically more polar metabolites (compared to the parent drugs), 0.1 M HCl / ACN 2:1 was chosen. Another reason for the solvent choice was its good performance during previous work of our group.

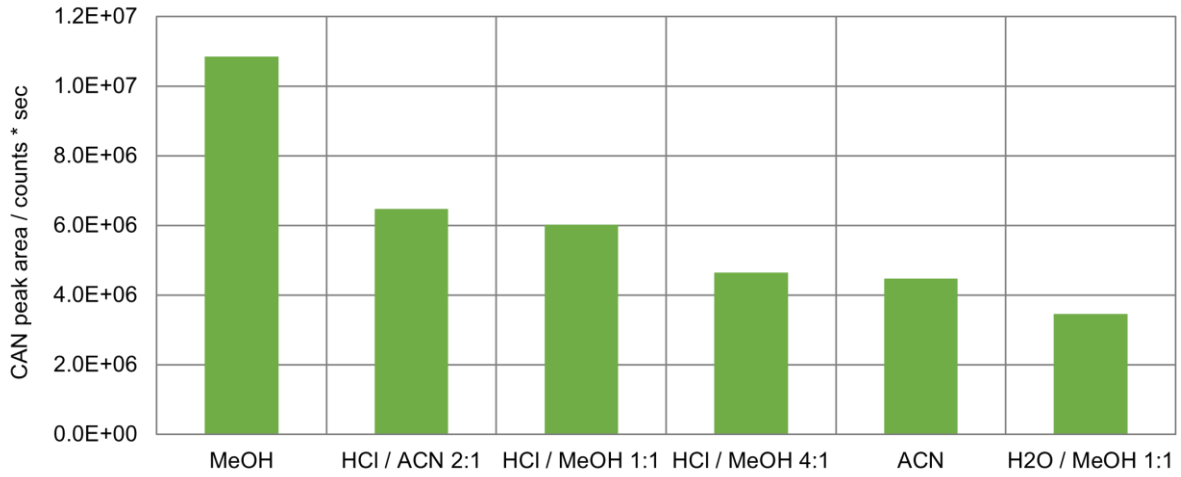

Figure 14: Comparison of extraction solvents.
CAN signals for cress roots after HPLC-MS depending on the medium used for extraction.

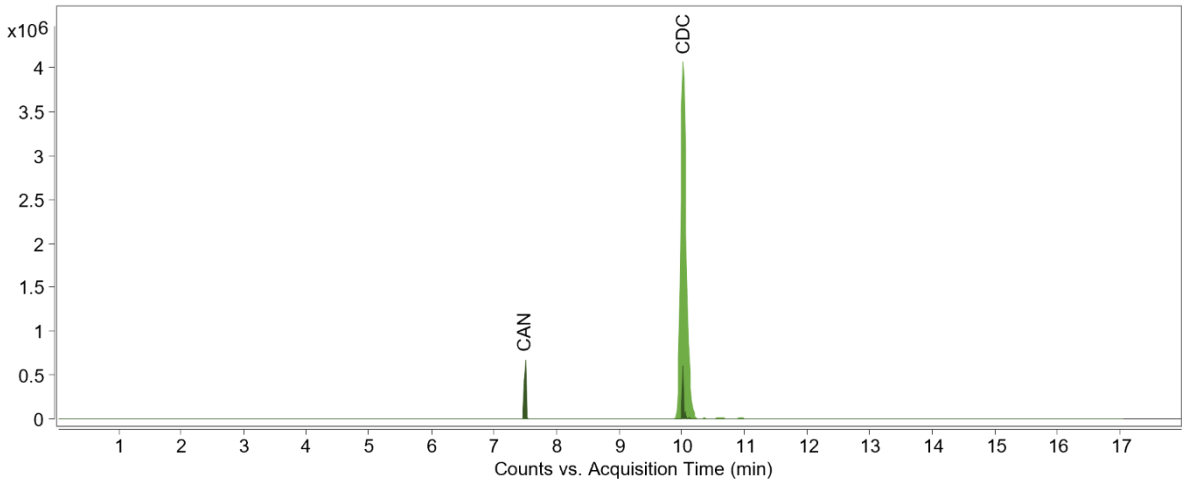

Figure 15: Extracted ion chromatogram of m/z 441.165 and m/z 611.262 of a 1 mg L^{-1} CDC standard.

4.2. Analysis of standards and window solutions

The chromatographic aim was to define a method suitable for CAN as well as VAL. Finally, applying the method stated in section 3.5., CAN and CDC eluted approximately at 7.5 min and 9.9 min (ΔRT = 0.1 min, Figure 15), respectively, while VAL showed an RT of 8.3 min (ΔRT = 0.1 min, Figure 16). Additionally, the method allows to properly separate the more polar metabolites, which elute earlier from the column.

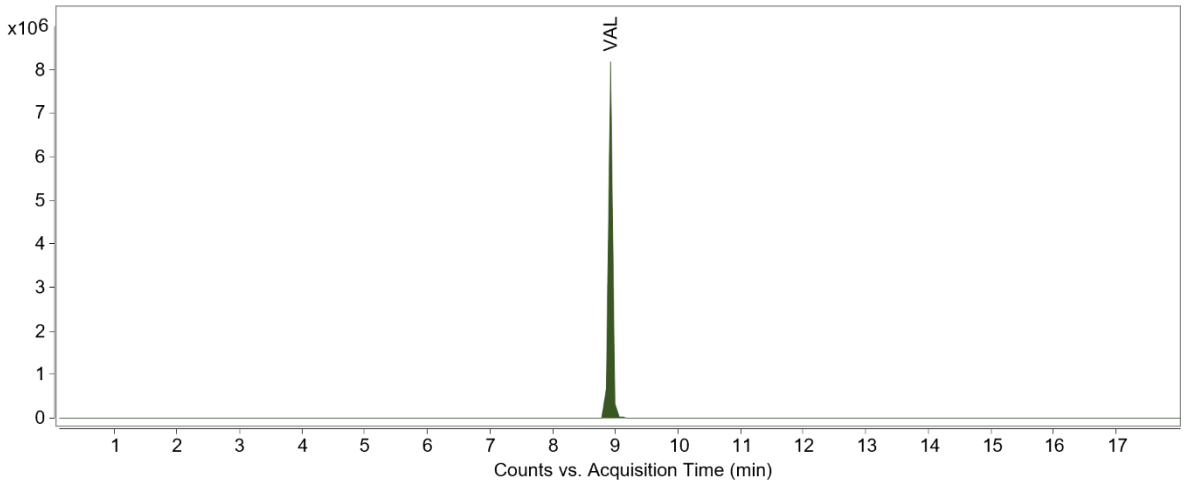

Figure 16: Extracted ion chromatogram of m/z 436.233 of a 1 mg L^{-1} VAL standard.

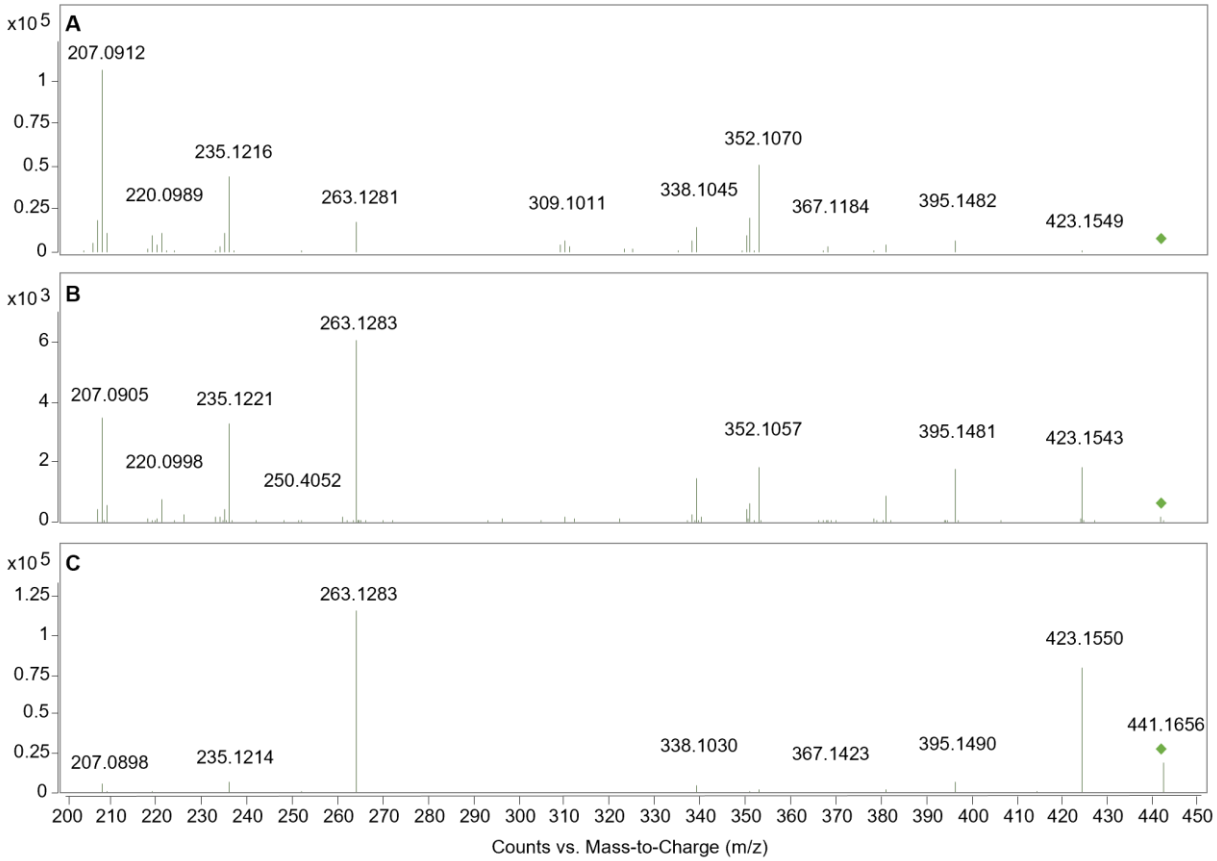

Figure 17: MS^2 spectrum of CAN at a CE of (A) 25 V, (B) 15 V and (C) 5 V.

Upon conducting MS^2 experiments with different CE, the specific fragmentation patterns of the parent drugs were received. For CAN, the protonated molecular ion peak was observed at m/z 441.165, and major fragments were found at m/z 423.155, 263.128, 235.121 and 207.091 (Figure 17). The characteristic fragments were chosen according to (1) their intensity and (2) their variation with changing CEs since upon applying higher CE, the bigger fragments should get less pronounced.

The fragmentation spectra of CDC are depicted in Figure 19. At m/z 611.262 its protonated molecular ion peak could be seen. As expected, the fragmentation pattern of the prodrug equaled the one of CAN.

VAL showed its protonated molecular ion peak at m/z 436.233, and the most dominant fragments were detected at m/z 418.223, 291.149, 235.098 and 207.091 (Figure 19). For all three parent drugs, the fragmentation patterns were in line with predicted spectra and literature findings [28].

In the window solutions, no transformation products could be detected, and the signals of the pharmaceuticals remained merely constant, indicating high resistance against photo- and hydrolysis. This fact is especially interesting for CDC. As it can be seen in Figure 15 when measuring a CDC standard solution directly after preparation roughly 5 % of the prodrug

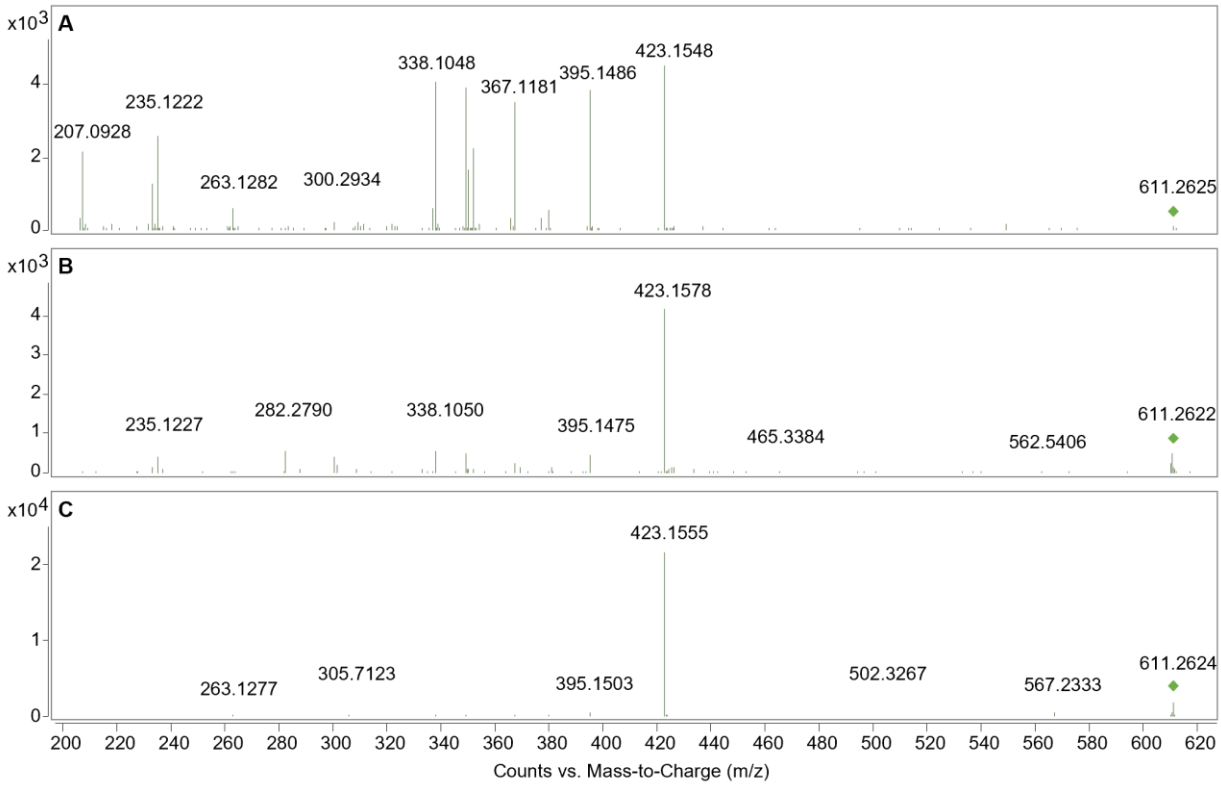

Figure 18: MS^2 spectrum of CDC at a CE of (A) 25 V, (B) 15 V and (C) 5 V.

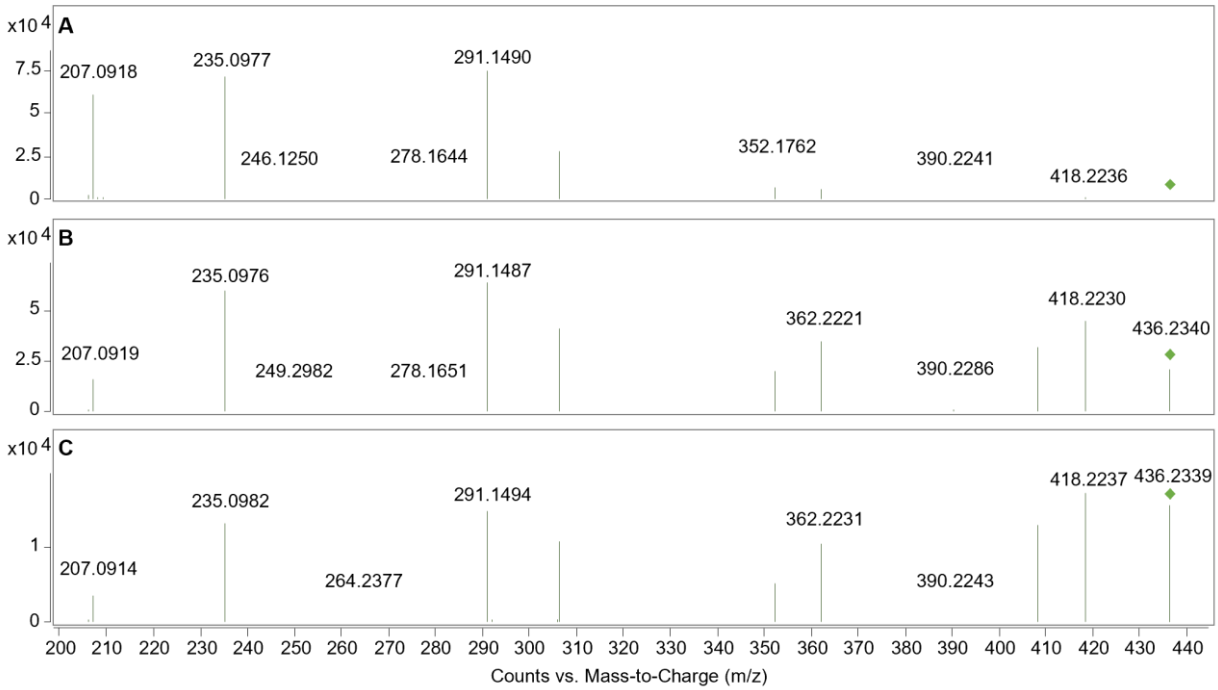

Figure 19: MS^2 spectrum of VAL at a CE of (A) 15 V, (B) 5 V and (C) 3 V.

(calculated based on peak areas) were already converted to CAN. Even after 15 and 30 days, the proportion of the active drug did not change, suggesting that the hydrolysis reaction of the prodrug to the active form is rather slow under aqueous conditions.

In addition to that, the chromatogram including CAN and CDC (Figure 15) shows a tiny peak for m/z 441.165 at the RT of the prodrug. That signal most probably stems from in-source fragmentation of CDC and was observed in all experiments.

4.3. Tentative identification of Valsartan and Candesartan metabolites formed in plants

The plant extract samples were analysed by HPLC-DT-IM-QTOF, and the received data were screened for the parent drugs as well as transformation products using suitable software. CAN, CDC, and VAL were confirmed in the samples by comparing RTs and fragmentation patterns to the information obtained from standard measurements (see section 4.2.). All detected metabolites could only be identified tentatively based on their m/z values, MS^2 data and CCS values since higher identification confidence cannot be reached without appropriate reference standards. In Table 7, a summary of all found compounds in the different plants can be seen.

The table neatly implies that the metabolic pathways vary between plant species by demonstrating differences in the formation and translocation of drug metabolites, which are discussed in the following. CAN and VAL were detected in all screened plants and distributed over the whole tissue. CDC, however, could not be found in sorghum, suggesting high hydrolysis rates in that plant species.

Overall, the pharmaceuticals and metabolites were more frequently and in higher abundance found in plant roots compared to stem and leaves, which indicates that the sartan-drugs migrated at low rates through the plant tissue. Moreover, cress translocated the formed metabolites to a higher extent than peas and maize, which might be a consequence of the complexity of the plantlets. While cress was already fully grown after 10 days, peas and maize were harvested in the seedling or vegetative stage. Also, the data demonstrated that in general, the bigger the metabolite was, the less it was formed within the plants. Interestingly, turnip greens and carrot showed, besides cress, the highest amount of transformation products while triticale, rye, and barley hardly conjugated the xenobiotic.

Nonetheless, the absence of metabolite species in several plants does not necessarily signify that the compounds were not formed. The signals could have also been below the methods limit of detection, or, for very fibrous plant material, the extraction might have been insufficient to recover all transformation products. Furthermore, in plant species with low xenobiotic uptake rates, the time of exposure may have been too low to form adducts.

Table 7: Overview of tentative formulas for CAN, CDC, and VAL phase I and phase II metabolites found in various plant extracts

Compound	Sum formula	theoretic m/z $[M+H]^+$	RT / min	$^{DT}CCS_{N2}$ / Å²	RSD CCS / %	Cress		Peas			Maize			Carrot	Turnip greens	Sorghum	Triticale	Rye	Barley
						Roots	Leaves	Roots	Stem	Leaves	Roots	Stem	Leaves						
CAN	**$C_{24}H_{20}N_6O_3$**	**441.1675**	**7.5**	**197.1**	**0.43%**	**yes**	**yes**	**yes**	**yes**	**yes**	**yes**	**yes**	**yes**	**yes**	**yes**	**yes**	**yes**	**yes**	**yes**
OH-CAN	$C_{24}H_{20}N_6O_4$	457.1624	5.3	205.8	2.99%	yes	–	yes	–	–	yes	yes	yes	yes	yes	–	–	–	yes
CAN-Glc	$C_{30}H_{30}N_6O_8$	603.2203	6.9	221.7	5.28%	yes	yes	yes	–	–	yes	–	yes	yes	yes	yes	yes	yes	yes
CAN-Glc-Glc	$C_{36}H_{40}N_6O_{13}$	765.2731	6.4	269.9	1.61%	yes	–	yes	–	–	yes	–	–	–	yes	yes	–	yes	yes
CAN-Glc-Mal	$C_{33}H_{32}N_6O_{11}$	689.2207	7.1	250.0	0.06%	yes	yes	yes	–	–	yes	–	–	yes	yes	–	–	yes	–
CAN-Glc-Glc-Mal	$C_{39}H_{42}N_6O_{16}$	851.2735	6.5	278.0	0.23%	yes	–	yes	–	–	yes	–	–	–	yes	–	–	–	–
CAN-Glc-Glc-Mal-Mal	$C_{42}H_{44}N_6O_{19}$	937.2739	6.7	284.8	-	–	–	–	–	–	–	–	–	–	yes	–	–	–	–
CDC	**$C_{33}H_{34}N_6O_6$**	**611.2618**	**10.0**	**242.1**	**0.23%**	**yes**	**yes**	**yes**	**yes**	**yes**	**yes**	**yes**	**yes**	**yes**	**yes**	**–**	**yes**	**yes**	**yes**
OH-CDC	$C_{33}H_{34}N_6O_7$	627.2567	8.6	234.7	0.30%	yes	–	yes	–	–	–	yes	–	–	yes	–	–	–	–
OH-CDC	$C_{33}H_{34}N_6O_7$	627.2567	9.6	243.7	0.25%	yes	–	yes	–	–	yes	yes	–	–	–	–	–	–	–
OH-CDC-Glc-Glc-GlcA	$C_{51}H_{62}N_6O_{23}$	1127.3944	7.0	313.9	-	–	–	–	–	–	yes	–	–	–	–	–	–	–	–
CDC-Glc	$C_{39}H_{44}N_6O_{11}$	773.3146	9.3	272.7	-	–	–	–	–	–	yes	–	–	–	–	–	–	–	–
VAL	**$C_{24}H_{29}N_5O_3$**	**436.2348**	**8.3**	**204.8**	**0.42%**	**yes**	**yes**	**yes**	**yes**	**yes**	**yes**	**yes**	**yes**	**yes**	**yes**	**yes**	**yes**	**yes**	**yes**
OH-VAL	$C_{24}H_{29}N_5O_4$	452.2298	7.1	206.9	1.38%	yes	yes	yes	–	–	yes	–	–	–	–	–	–	–	–
OH-VAL-Glc	$C_{30}H_{39}N_5O_9$	614.2748	6.7	235.0	-	yes	–	–	–	–	–	–	–	–	–	–	–	–	–
VAL-Glc	$C_{30}H_{39}N_5O_8$	598.2877	7.8	242.0	0.14%	yes	yes	yes	–	–	yes	yes	–	yes	yes	yes	yes	yes	yes
VAL-Glc-Glc	$C_{36}H_{49}N_5O_{13}$	760.3405	7.2	267.1	0.02%	yes	–	yes	–	–	yes	–	–	yes	yes	yes	–	–	–
VAL-Glc-Glc-Glc	$C_{42}H_{59}N_5O_{18}$	922.3933	7.0	292.2	0.03%	yes	–	yes	–	–	–	–	–	–	yes	–	–	–	–
VAL-Glc-Mal	$C_{33}H_{41}N_5O_{11}$	684.2880	7.9	250.9	0.32%	yes	yes	yes	yes	yes	–	–	–	yes	yes	–	–	–	–
VAL-Glc-Glc-Mal	$C_{39}H_{51}N_5O_{16}$	846.3409	7.3	280.0	0.75%	yes	–	–	–	–	–	–	–	yes	yes	–	–	–	–
VAL-Glc-Glc-Mal-Mal	$C_{42}H_{53}N_5O_{19}$	932.3413	7.4	284.8	0.25%	yes	–	–	–	–	–	–	–	yes	yes	–	–	–	–
VAL-UM	-	551.2958*	8.3	226.9	0.33%	–	–	yes	–	–	yes	yes	–	yes	–	–	yes	yes	yes

* measured m/z

4.3.1. Candesartan

CDC seemed to be highly resistant to hydrolysis, as already stated in the previous section. For this reason, the proportion of CAN compared to the prodrug was examined in several plant extracts (Figure 20). Particularly in cress, the percentage exceeded the 5 %, which were observed in standards as well as window solutions. These findings imply that the plant likely expresses enzymes that can hydrolyze CDC to its active form. However, the main part of the pharmaceutical was still present in its ester form, which was rather surprising since carboxylesterases were reported to be highly active during a plant's detoxification process [34].

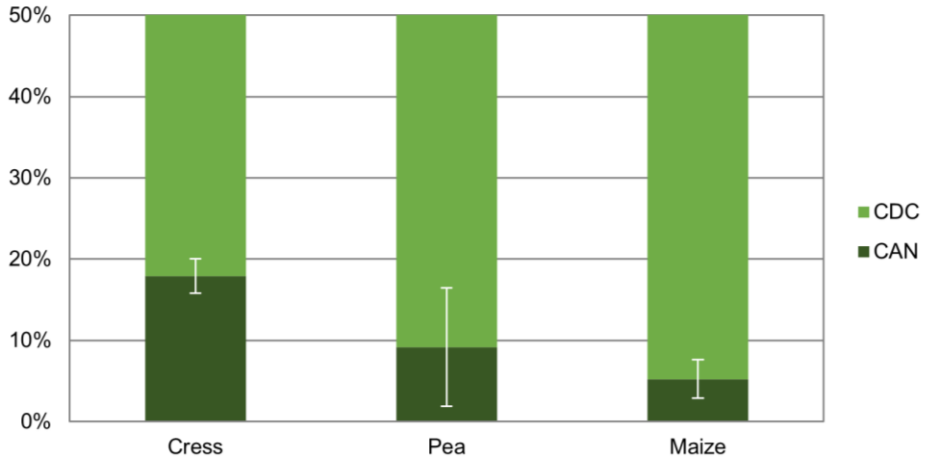

Figure 20: Percentual proportion of CAN (dark green) compared to CDC (light green) in cress, pea, and maize. Error bars represent standard deviations.

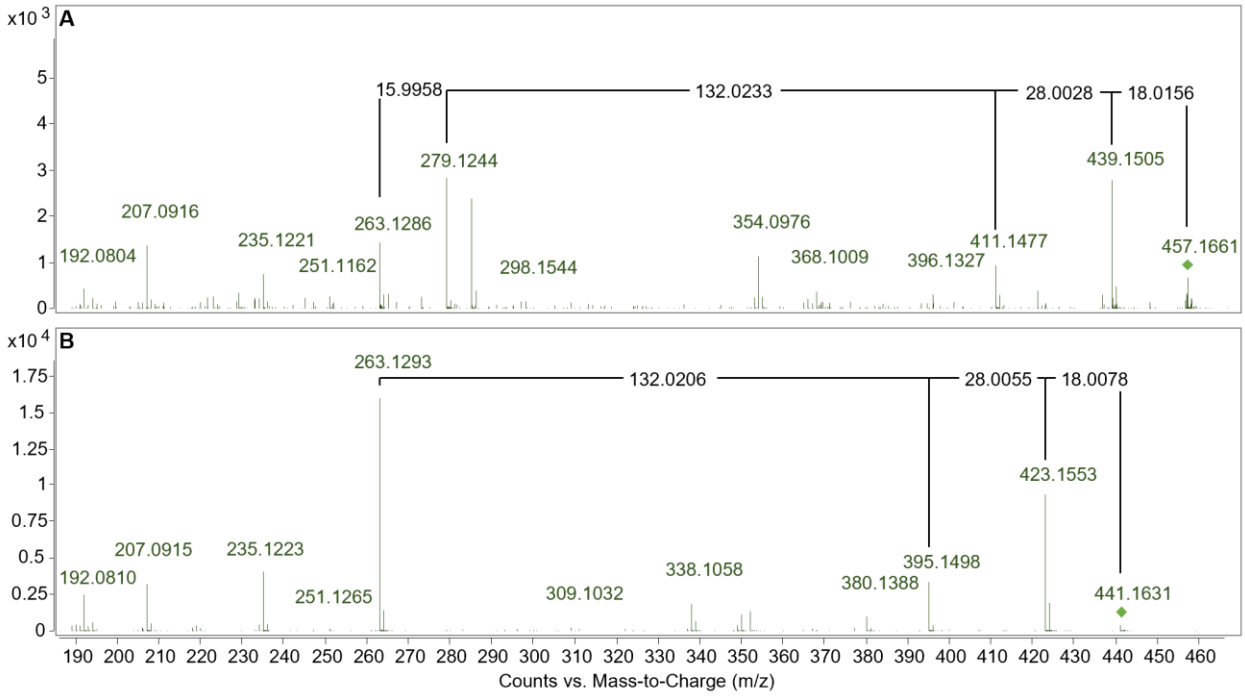

Figure 21: MS^2 spectrum of OH-CAN (m/z 457.17; A) in a cress root sample fragmented with a CE of 10 V in comparison to an MS^2 spectrum of CAN (441.16; B)

Overall, in addition to CAN and CDC, nine metabolites were found in the plant samples. Six thereof were related to the active form of the drug, and the other three were based on CDC. Although lower amounts of CAN were taken up by the plants, the active drug was metabolized to greater extents than CDC. In reference to the "green liver system" of plant metabolism, this might signify that the prodrug was too inert for phase II metabolization while CAN could be conjugated readily.

All detected metabolites showed, as expected, higher polarity than the parent compounds and eluted earlier from the column (for RTs, see Table 7).

Concerning the phase I metabolites, none of the more reactive species, which are known from human metabolism [26], were detected. This fact might suggest that plant metabolism requires lower reactivity for conjugation steps. Nonetheless, for both CAN and CDC, hydroxylated species were found. They showed the same characteristic fragmentation pattern as their parent compounds, but the m/z values were shifted by 18.01, which corresponds to the loss of a water molecule (Figure 21 and Figure 22, respectively).

Interestingly, OH-CDC frequently was found twice with varying RT and CCS value. A possible explanation for that might be different sites of hydroxylation that influence the overall polarity and arrangement of the metabolite. Also, the signal could stem from an unknown secondary metabolite that was already fragmented in-source.

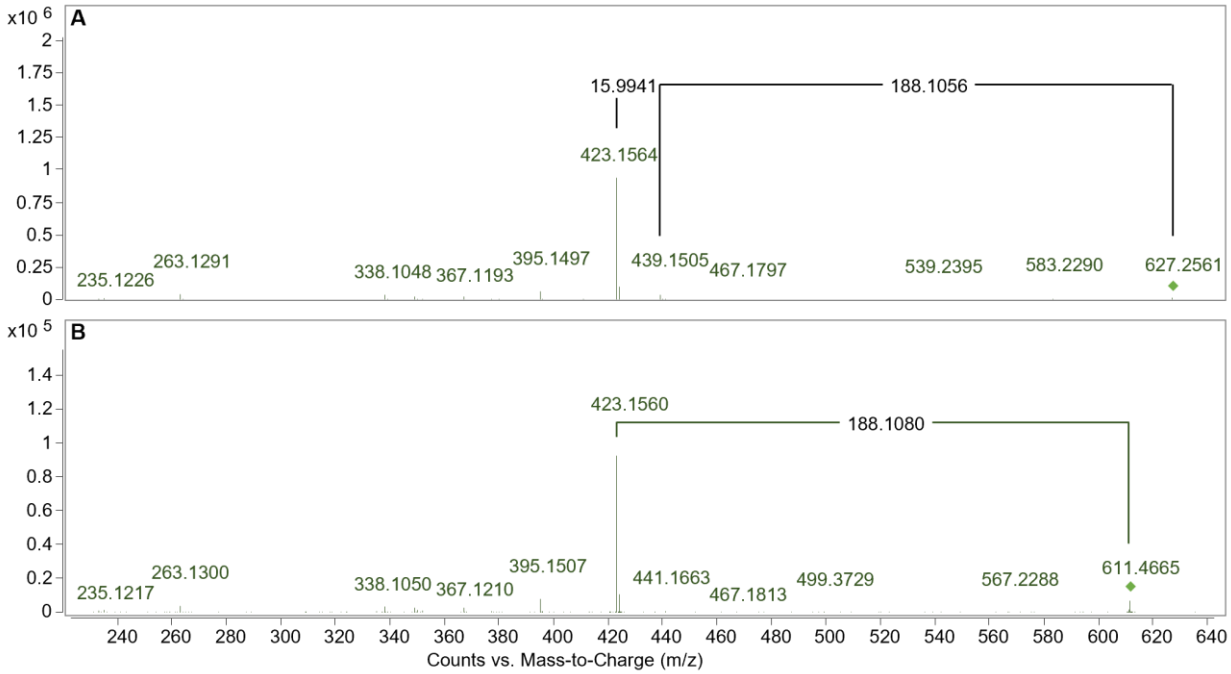

Figure 22: MS^2 spectrum of OH-CDC (m/z 627.26; A) in a triticale root sample fragmented with a CE of 5 V in comparison to an MS^2 spectrum of CDC (611.26; B)

Phase II metabolites were formed by conjugation with glucose, malonic- or glucuronic acid (Table 7). Even multiple units of sugars were frequently attached to CAN. Upon collision-induced dissociation (CID), all transformation products showed the specific fragmentation pattern of either CAN, CDC, or OH-CDC. The adducts were identified by looking at the difference in m/z between the metabolite's and the drug's $[M+H]^+$ signals. A Δ m/z of 162.0528 corresponds to a glucose unit while 176.0321 points towards glucuronic- and 86.0004 towards malonic acid (one molecule of water is split off during conjugation).

In the following, the MS^2 spectra of CAN-Glu and CAN-Glu-Mal are exemplarily discussed. All further spectra can be found in the Appendix. Figure 23 shows the fragmentation of CAN-Glu. The characteristic fragments were present in high abundance, and a Δ m/z of 162.0535 hinted towards conjugation of CAN with a glucose unit. For CAN-Glu-Mal (Figure 24), the Δ m/z of 248.0526 suggested the presence of a glucose and a malonic acid moiety (162.0528 + 86.0004 = 248.0532) that were lost simultaneously, indicating that they were with high probability conjugated to each other.

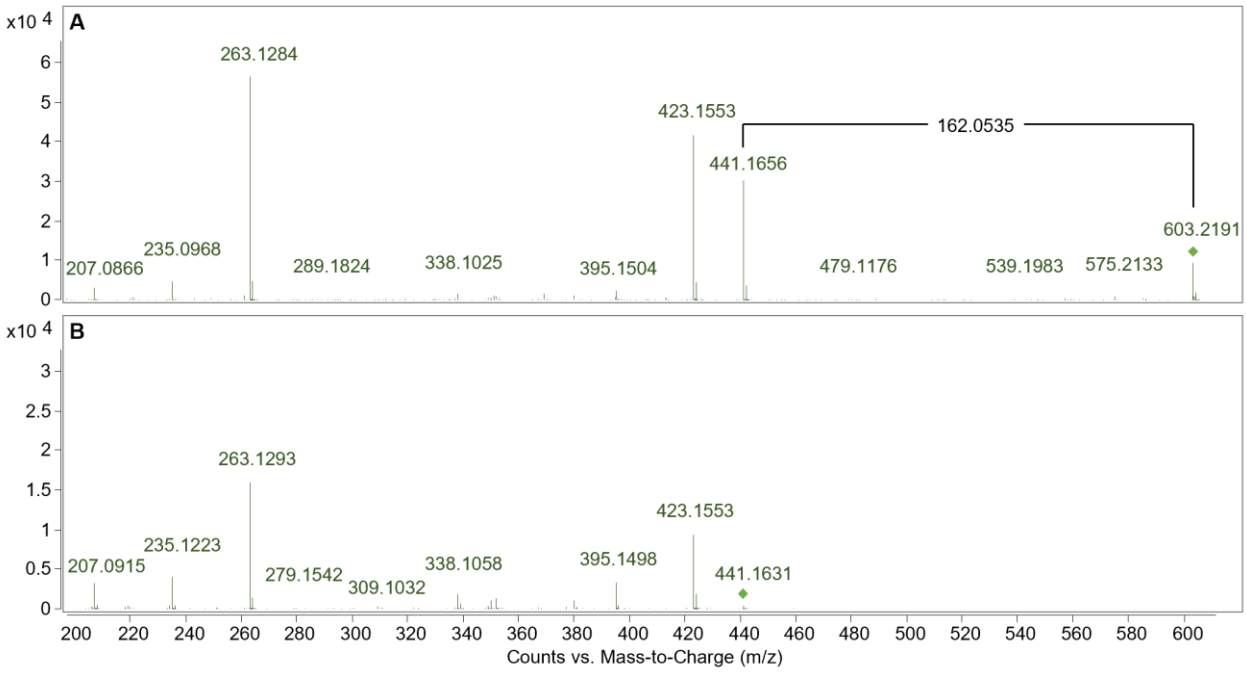

Figure 23: MS^2 spectrum of CAN-Glc (m/z 603.22; A) in a pea root sample fragmented with a CE of 10 V in comparison to an MS^2 spectrum of CAN (441.16; B)

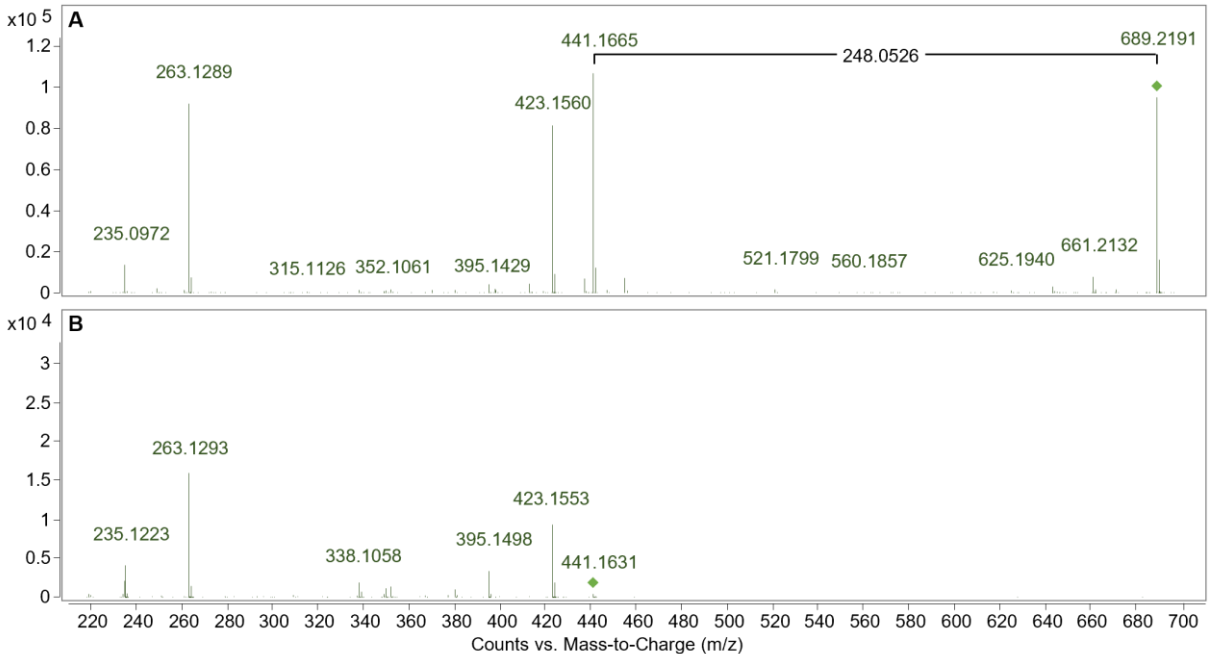

Figure 24: MS^2 spectrum of CAN-Glc-Mal (m/z 689.22; A) in a cress leaves sample fragmented with a CE of 10 V in comparison to an MS^2 spectrum of CAN (441.16; B)

One very special metabolite, namely OH-CDC-Glc-Glc-GlcA, was found exclusively in maize roots (Figure 25). Checking the characteristic fragments as well as the Δ m/z values of the adducts, the data strongly suggested that OH-CDC was connected to two sugar moieties and glucuronic acid. So far, only a few papers reported transformation products in plants that contained GlcA adducts, though, recently diclofenac was found to form two such metabolites also in maize [35].

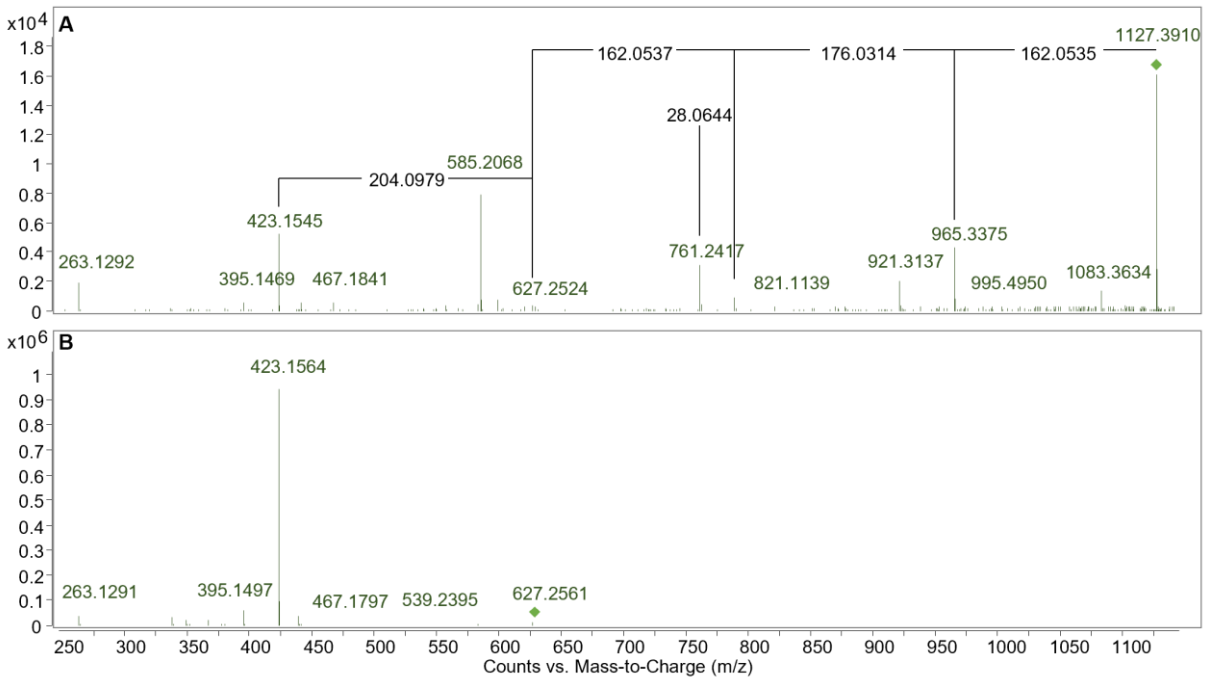

Figure 25: MS^2 spectrum of OH-CDC-Glc-Glc-GlcA (m/z 1127.39; A) in a maize root sample fragmented with a CE of 10 V in comparison to an MS^2 spectrum of OH-CDC (627.26; B)

4.3.2. Valsartan

In plants treated with VAL-spiked medium, one phase I metabolite and seven phase II metabolites were suggested. In addition to that, an unknown transformation product which contained the VAL structure as a backbone was found (see section 4.3.4.). Likewise, CAN and CDC conjugates, the metabolites showed shorter retention during chromatography (Table 7).

The detected OH-VAL (Figure 26) would match the m/z ratio of Valeryl-4-hydroxyvalsartan, which is the only phase I metabolite that is formed in humans [28]. As for the hydroxylated form of CAN and CDC, OH-VAL showed the characteristic fragmentation pattern of valsartan with a Δ m/z shift of 15.99. However, just by interpreting the MS^2 data, it was not possible to locate the site of hydroxylation in the molecule hence the identity of the transformation product could not be confirmed. Also, the CCS value was of no use since Valeryl-4-hydroxyvalsartan is not included in any database yet.

Using the same identification workflow as explained in section 4.3.1., various combinations of VAL with glucose and malonic acid moieties were detected. The MS^2 spectra for these compounds can again be found in the Appendix, except for some extraordinary examples, which are studied in the following.

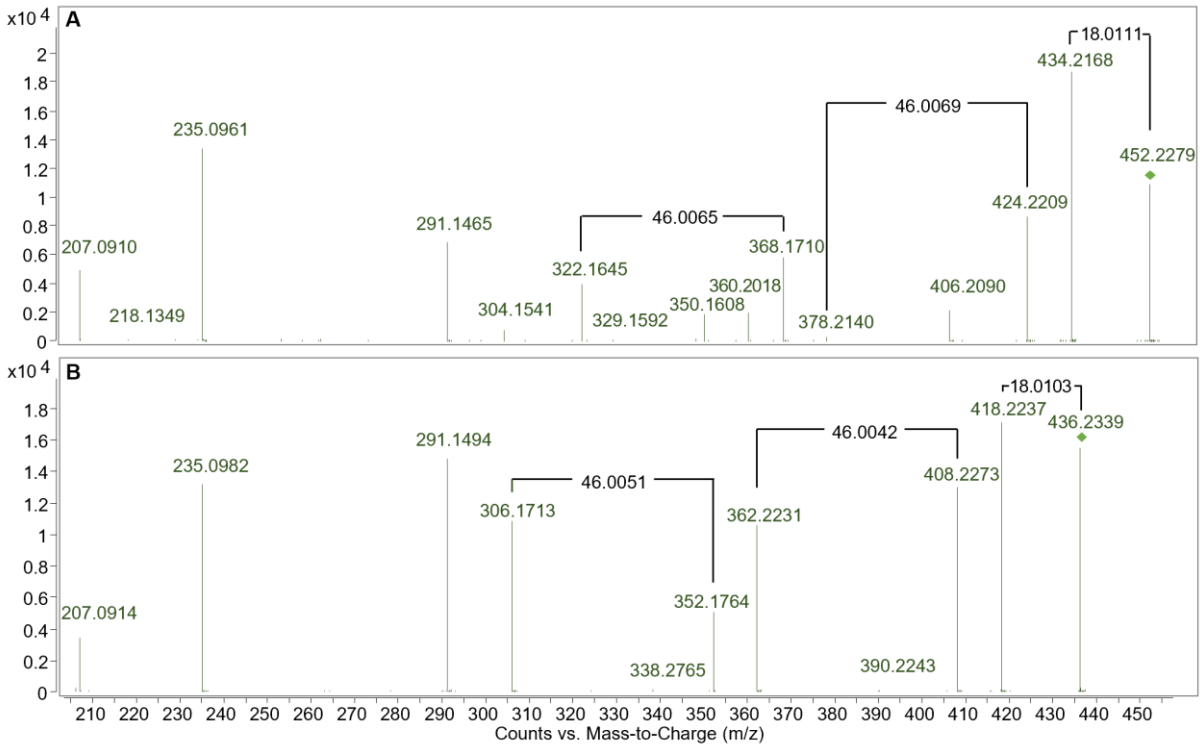

Figure 26: MS^2 spectrum of OH-VAL (m/z 452.23; A) in a pea root sample fragmented with a CE of 3 V in comparison to an MS^2 spectrum of VAL (436.23; B)

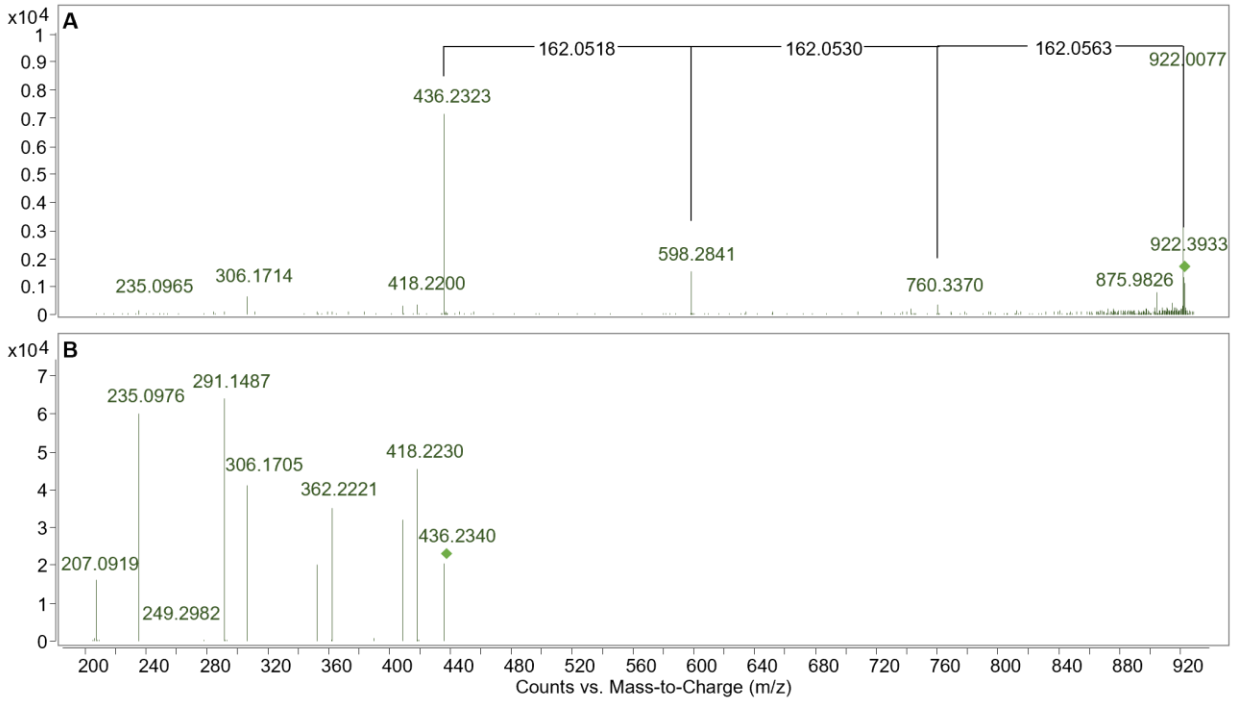

Figure 27: MS^2 spectrum of VAL-Glc-Glc-Glc (m/z 922.39; A) in a pea root sample fragmented with a CE of 5 V in comparison to an MS^2 spectrum of VAL (436.23; B)

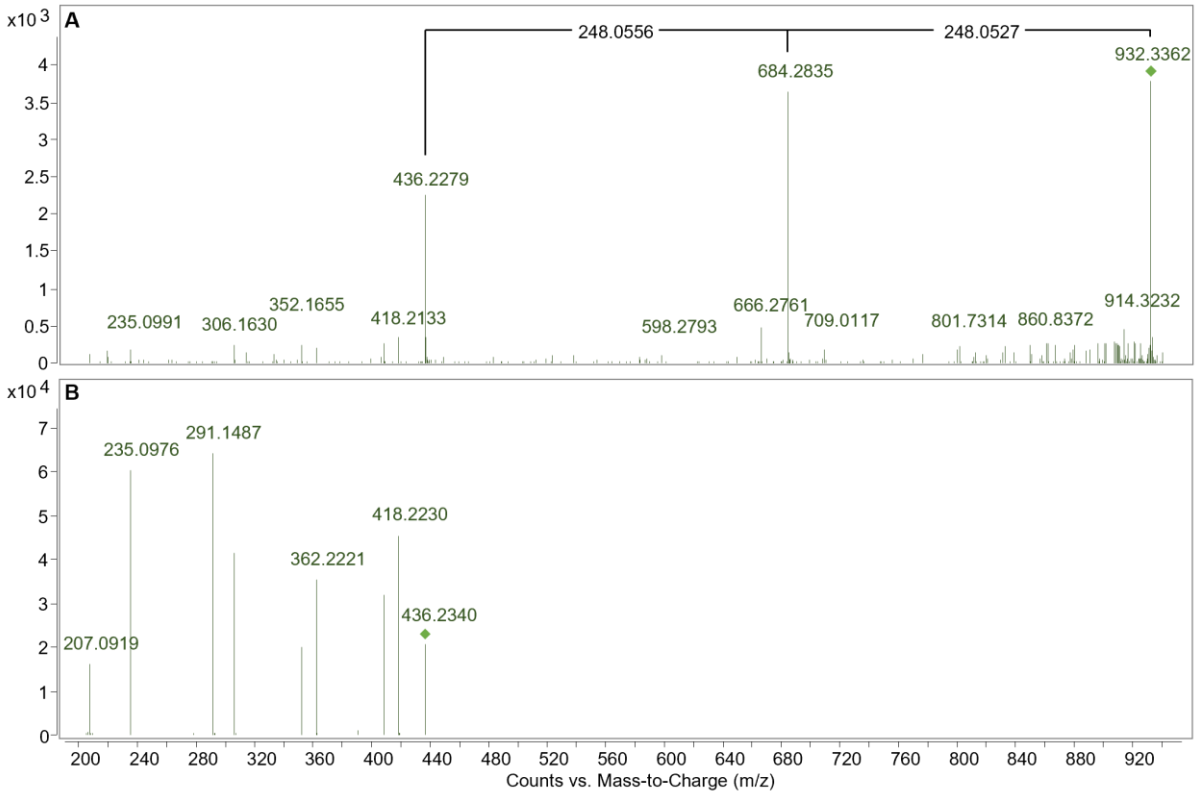

Figure 28: MS^2 spectrum of VAL-Glc-Glc-Mal-Mal (m/z 932.34; A) in a carrot sample fragmented with a CE of 5 V in comparison to an MS^2 spectrum of VAL (436.23; B)

In Figure 27, the spectrum for VAL-Glc-Glc-Glc can be observed. Apart from the backbone fragments at m/z 235.1, 418.22 and 436.23, signals hinting toward the loss of three sugar units were seen (Δ m/z = 162.05). In the case of VAL-Glc-Glc-Mal-Mal (Figure 28), glucose and malonic acid were lost again together. Surprisingly, also a signal at m/z 598.26, corresponding to VAL-Glc, was noticed. It proposes that the drug either first lost Glc-Mal-Mal followed by the second glucose molecule or that one malonic acid split off on its own (however, such behavior was yet never reported in literature).

4.3.3. $^{DT}CCS_{N2}$ values

Apart from identifying drug-related metabolites, a goal of this work was to find out their CCS values, which were used as a further dimension of resolution. Also, the values can contribute to building extensive CCS databases that will help to identify ions in future measurements.

CCS values have so far only been reported or predicted (in the case of CAN) for the parent drugs [36,37]. The measured values of 197.1 $Å^2$, 242.1 $Å^2$, and 204.8 $Å^2$ for CAN, CDC, and VAL, respectively, only marginally deviated from literature findings (CAN 197.21 $Å^2$; CDC 241.5 $Å^2$, 0.09 RSD; VAL 202.0 $Å^2$, 0.05 RSD) speaking for the robustness of the parameter.

The measured CCS values showed good reproducibility with relatively low relative standard deviations (RSD) (Table 7). For OH-CAN, CAN-Glc, CAN-Glc-Glc and OH-VAL, in contrast, comparably higher RSDs were observed. On the condition that the overall polarity of the metabolites was not altered (meaning stable RT times), these observations may be explained by either varying hydroxylation/glucosylation sites or different conformations of the molecule.

4.3.4. AF approach

All-ion fragmentation spectra over the entire m/z range of the plant extract samples were acquired using an HPLC-DT-IM-QTOF instrument in the AF mode. From these spectra, features were extracted and subsequently, a Python script was used to filter the features for the drug-specific fragments based on matching drift times of parent and daughter ions. The drift spectra of the most promising hits (more than one of the characteristic fragments for either CAN, CDC, or VAL) were checked, and a targeted MS^2 was set up for the respective parent ions.

In the inspected sample stemming from cress roots exposed to CAN medium, 47 promising hits were found. Nevertheless, the characteristic drug fragments were only present in the drift spectra of 26 features in question. Upon looking at the masses of these features, twelve of them corresponded to signals of either the parent drug or already known metabolites (CAN, CDC, CAN-Glc, CAN-Glc-Mal). The remaining 14 hits were subjected to targeted MS^2. None of the received spectra, though, showed the CAN characteristic fragmentation pattern.

For VAL, 114 features with more than one characteristic fragment were found. 59 thereof were proven by looking at the drift spectra, and 37 parent ions were fragmented by targeted MS^2. As a result, two compounds with the correct fragmentation pattern could be detected. A phase II metabolite for OH-VAL, namely a glucose adduct (Figure 29) and the already formerly mentioned unidentified metabolite.

The unidentified metabolite (Figure 30) showed its molecular ion peak at 551.296 and was found in several plants (peas, maize, carrot, triticale, rye, and barley). The fragmentation pattern of the compound strongly suggested a VAL backbone, but the Δ115.064 could not be assigned to any known small biomolecule. In an attempt to identify the adduct, the METLIN Neutral Loss Database (http://metlin.scripps.edu [38]) was searched. Thereby the only reasonable hit was aspartic acid ($C_4H_7NO_4$, 133.037 g mol^{-1}) which shows a rather high mass error (62 ppm) which is not expected in high-resolution MS.

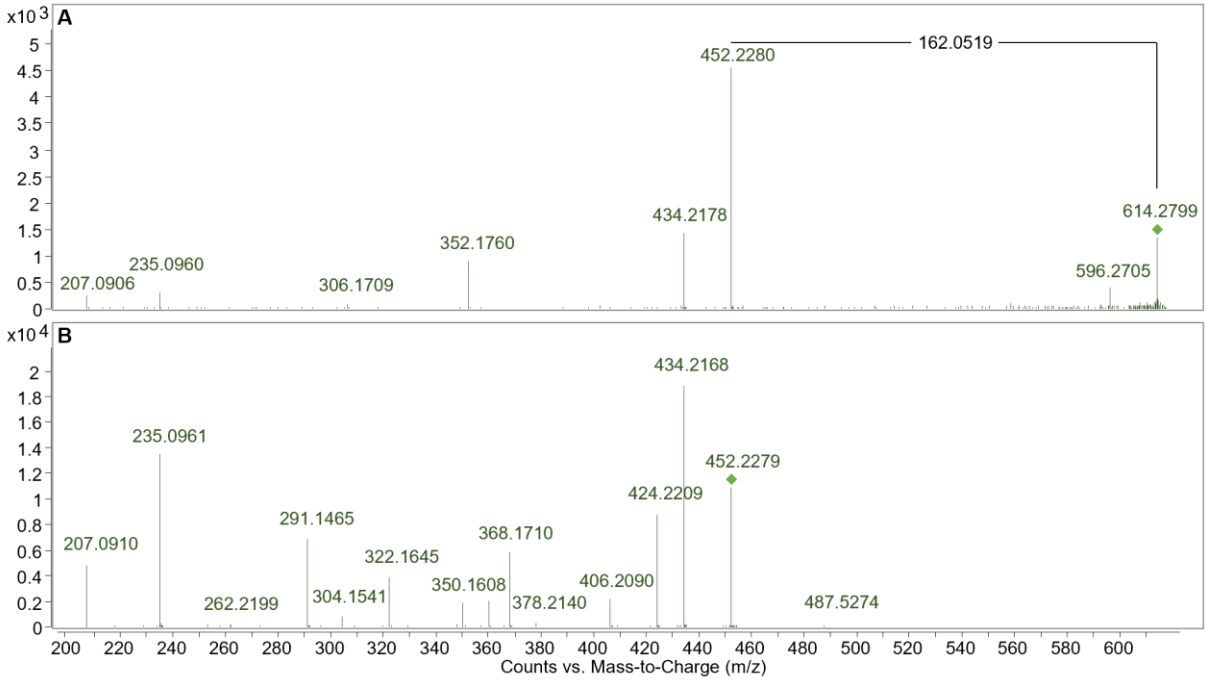

Figure 29: MS^2 spectrum of OH-VAL-Glc (m/z 614.28; A) in a cress root sample fragmented with a CE of 3 V in comparison to an MS^2 spectrum of OH-VAL (452.23; B)

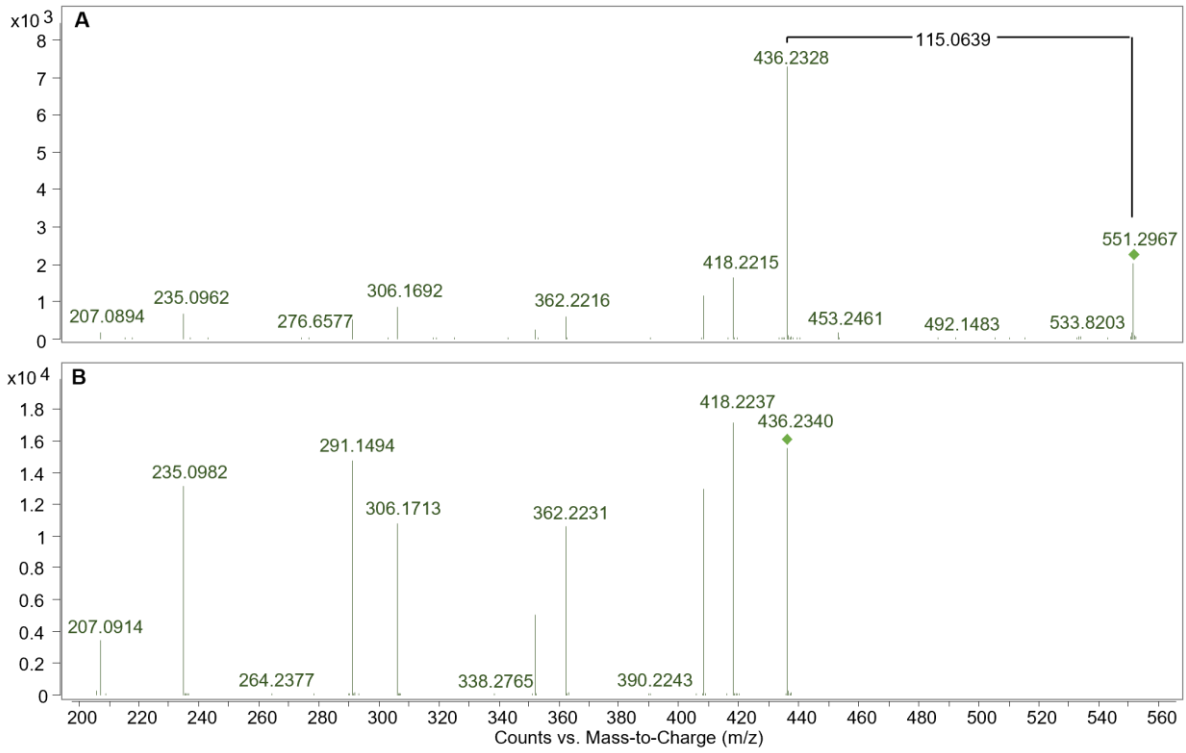

Figure 30: MS^2 spectrum of VAL-UM (m/z 551.30; A) in a pea root sample fragmented with a CE of 3 V in comparison to an MS^2 spectrum of VAL (436.23; B)

Overall, the AF approach did not provide many new insights. The fact that almost no unknown metabolites were found might simply indicate that all drug transformation products were already identified. Also, it is conceivable that phase I metabolites, which were possibly formed within the plant, produce different fragments than the parent drug and consequently cannot be detected with this approach. Anyway, the strategy still needs to be optimized since a high number of hits were wrong positives. Often the MassHunter software linked signals that showed considerably deviating drift times and hence yielded incorrect features. One attempt to solve or minimize this problem would be to test different settings for the feature extraction.

4.4. Plantomics – investigation of pharmaceutical-related changes in plants

In the plantomics approach, the measurement data from pharmaceutical-treated and untreated plantlets were combined to obtain an insight into the changes that were induced by the pharmaceutical. For a first overview, hierarchical cluster heatmaps displaying the 30 most significant differences between the two sample sets were generated based on *t*-tests. Subsequently, two-dimensional volcano plots were created from *p*-values and FCs to visualize which features were mainly responsible for the mentioned differences. Within the volcano plots, significantly up-regulated features are depicted on the top-right side (dark green), while downregulated signals appear top-left (light green). For detecting unknown metabolites, all significantly up-regulated features were subjected to targeted MS^2.

In the following, the maps and plots for CAN and VAL, cress roots and leaves, respectively, are discussed.

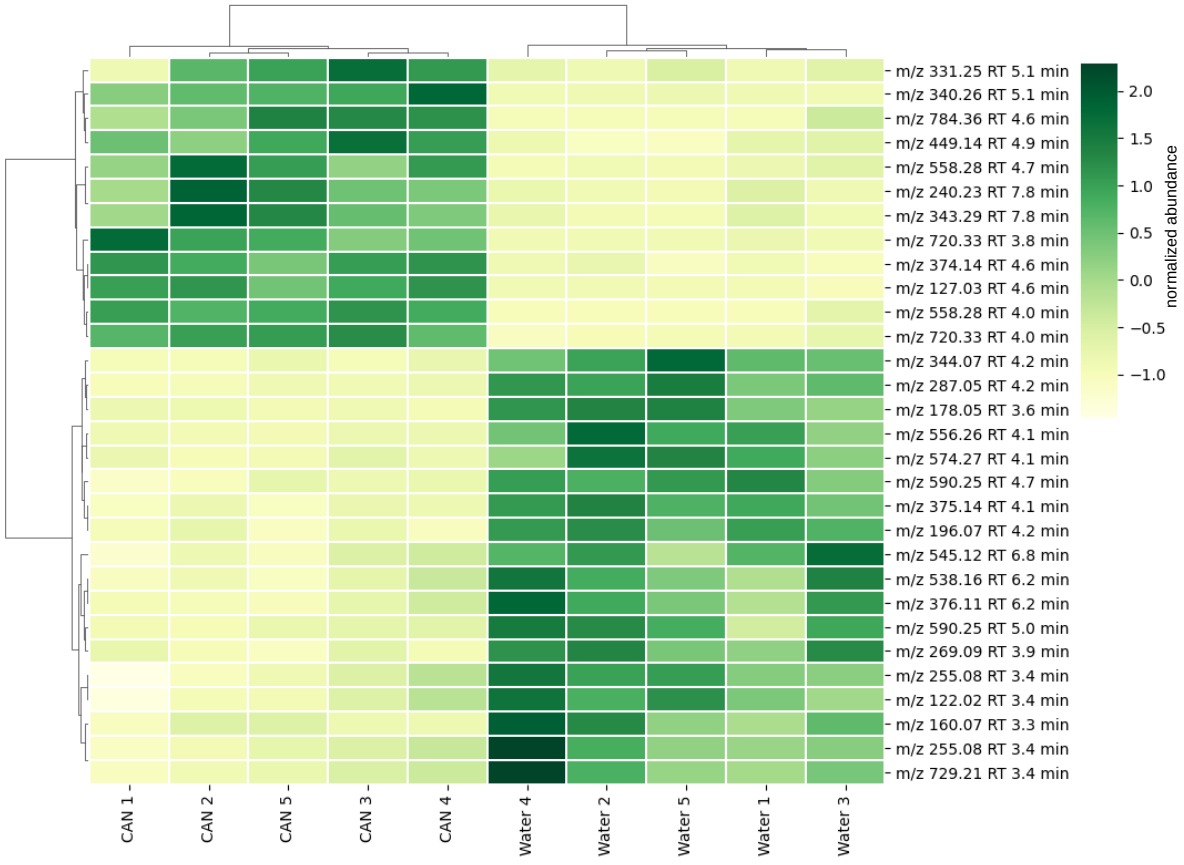

Figure 31: Heatmap of the features detected in cress roots treated with CAN-medium (n = 5) and tap water (n = 5). The 30 most significant features were clustered (Euclidean distance, ward algorithm) based on *t*-tests.

4.4.1. Candesartan – cress roots

The clustering in the created heatmap (Figure 31) clearly enables to distinguish between treated and untreated samples, which confirms that CAN induced pronounced change within the root tissue of cress.

In the volcano plot (Figure 32), the 15 most upregulated features are depicted. Further details to them can be found in Table 8. None of the already known CAN or CDC-related compounds was included in the significantly upregulated species, as revealed by the measured m/z values. Also, no further metabolites could be identified by targeted MS^2 because the fragmentation patterns of the upregulated features were not indicative of the CAN backbone.

Table 8: 15 top upregulated features in cress roots grown in CAN-medium.

ID	RT / min	$[M+H]^+$	$^{DT}CCS_{N2}$ / Å^2	FC	*p*-value
1	3.8	720.33	253.3	36.85	1.8E-05
2	4.0	558.28	230.5	13.29	3.3E-05
3	7.8	343.29	196.6	5.61	9.8E-05
4	7.8	240.23	172.8	5.26	9.4E-05
5	4.6	784.36	270.3	6.36	2.1E-05
6	4.0	768.30	259.4	7.94	6.0E-04
7	7.6	472.36	220.0	9.74	8.5E-04
8	7.8	176.07	135.0	11.34	1.5E-03
9	9.1	1039.67	331.1	20.88	3.6E-03
10	3.6	770.31	257.8	5.82	6.5E-04
11	7.8	240.23	198.6	7.20	1.1E-03
12	7.5	212.05	144.8	9.98	8.0E-03
13	9.1	997.62	320.7	12.45	1.6E-02
14	9.0	494.32	225.3	8.61	8.9E-03
15	11.0	882.61	361.6	4.48	8.1E-04

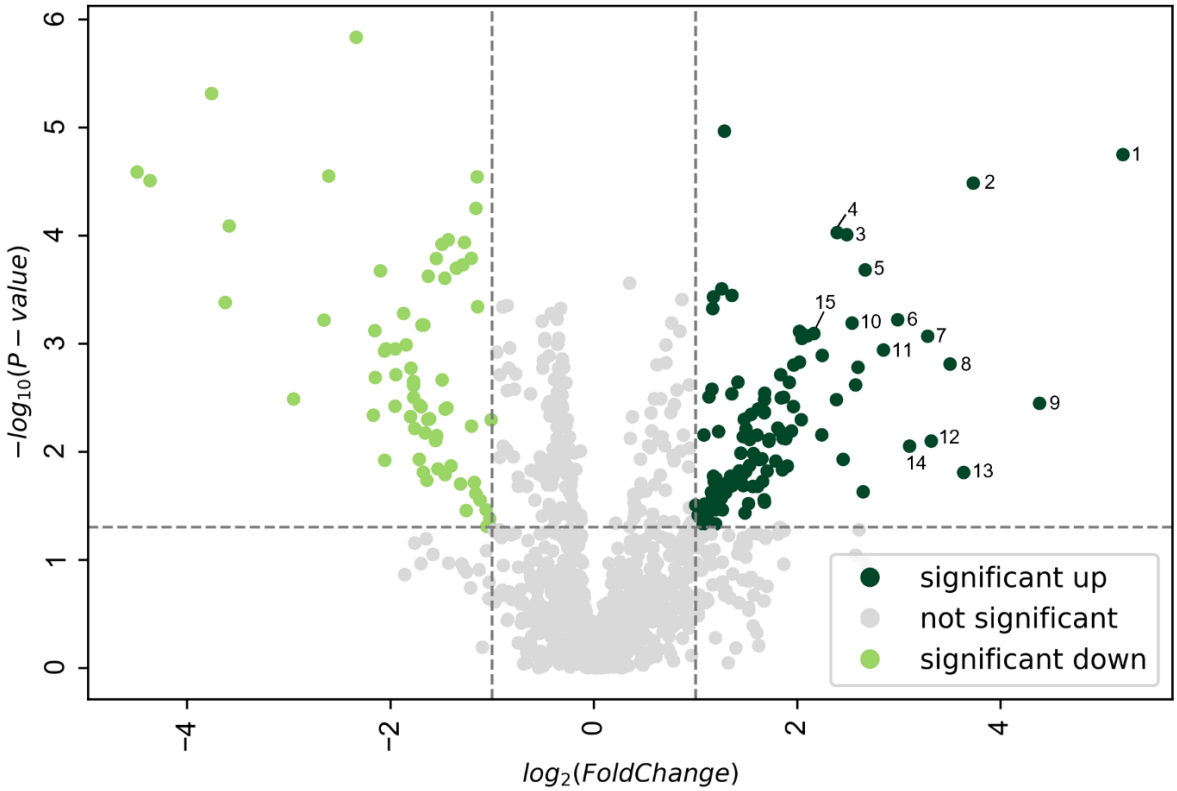

Figure 32: Up- and dysregulated features in cress roots grown in CAN-medium visualized in a volcano plot based on *p*-values and FCs (labelled features are listed in Table 8).

4.4.2. Candesartan – cress leaves

For the leave tissue, no clear difference between the control and drug-exposed samples was seen (Figure 33). The fluctuations in signal abundance were most likely affiliated with the amount of plant material that was used for extraction. When comparing the volcano plot of roots and leaves, the features showed overall lower FCs in the latter (Figure 32 and Figure 34). These observations are in line with the smaller signals of the parent drugs as well as of the metabolites in the upper parts of the plants, as mentioned in section 4.3.

Exactly like in the roots, the significantly upregulated features showed no relation to CAN or CDC (Table 9) and no familiar fragmentation patterns were observed upon subjecting them to CID. Interestingly, the FCs of features 1 – 3 were particularly high, although overall little change was induced by the pharmaceutical in the leave tissue. A possible explanation might be that the signals stem from molecules, like stress messengers, that under normal conditions are not or only in very low concentrations present in the plant.

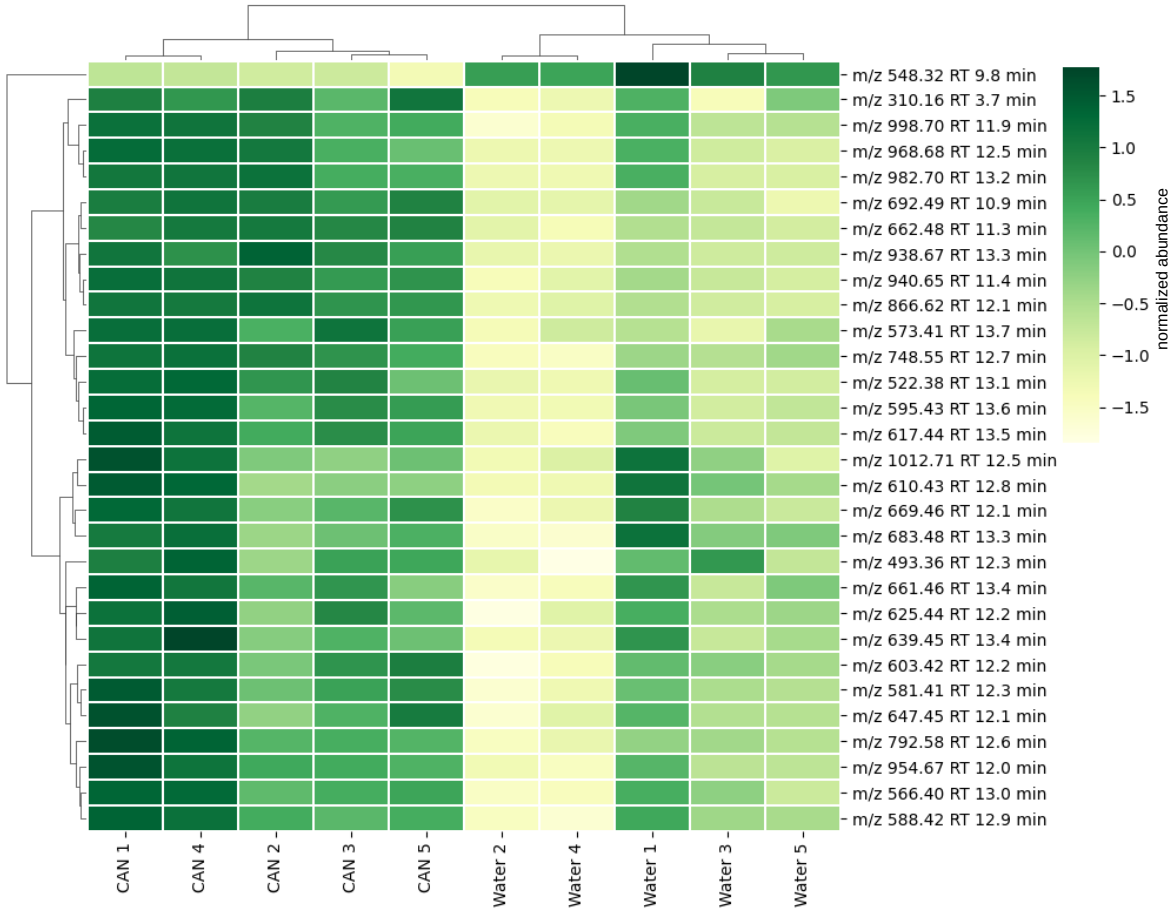

Figure 33: Heatmap of the features detected in cress leaves treated with CAN-medium (n = 5) and tap water (n = 5). The 30 most significant features were clustered (Euclidean distance, ward algorithm) based on t-tests.

Table 9: 12 top upregulated features in cress leaves grown in CAN-medium.

ID	RT / min	$[M+H]^+$	$^{DT}CCS_{N2}$ / Å^2	FC	p-value
1	7.3	726.42	255.7	19.90	7.5E-06
2	7.4	814.48	273.5	13.47	2.0E-05
3	7.4	460.28	363.2	12.87	2.2E-05
4	7.5	858.50	282.1	8.73	7.5E-05
5	5.7	369.12	235.8	5.20	1.3E-03
6	3.9	287.05	210.1	4.14	9.9E-04
7	4.8	576.24	238.2	4.04	1.1E-03
8	11.7	808.58	65.1	3.97	8.9E-04
9	7.5	482.30	373.7	4.71	1.8E-03
10	11.4	662.48	34.1	4.71	3.3E-03
11	10.7	824.57	65.9	4.34	3.2E-03
12	4.4	326.15	289.2	4.21	3.8E-03
13	3.9	694.27	261.3	4.04	3.5E-03
14	4.1	620.27	242.7	3.67	1.1E-03
15	5.2	679.51	40.9	3.64	1.5E-03

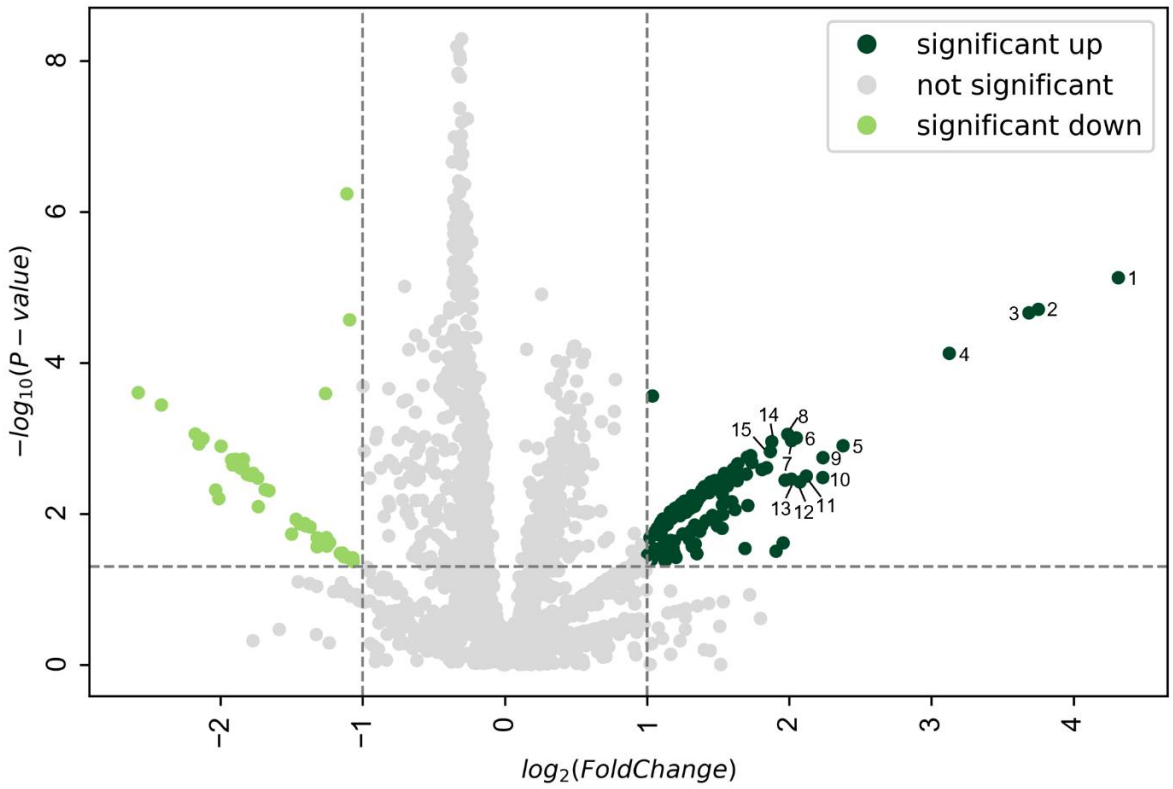

Figure 34: Up- and dysregulated features in cress leaves grown in CAN-medium visualized in a volcano plot based on *p*-values and FCs (labelled features are listed in Table 9).

4.4.3. Valsartan – cress roots

In cress roots treated with VAL medium, similar clustering as for CAN was seen (Figure 35). It was possible to distinguish between the sample groups based on the drug-induced changes.

The volcano plot (Figure 36) shows numerous significantly upregulated features whereby one indeed corresponded to VAL. Nonetheless, no further drug-related species were found within the hits. Several of the upregulated features seen in the VAL-exposed extracts were also found in those of CAN (m/z 720.33 RT 3.8 min, m/z 343.29 RT 7.8 min, m/z 240.23 RT 7.8 min, m/z 212.05 RT 7.5 min, m/z 558.28 RT 4.0 min and 770.31 RT 3.6 min, Table 10), which suggests that these molecules might be involved in metabolic pathways connected to xenobiotic detoxification. Identification of these molecules would be very interesting from the omics science point of view. For this reason, the METLIN database (http://metlin.scripps.edu [38]) was searched for the corresponding m/z values, but no satisfactory hits were found for any of them.

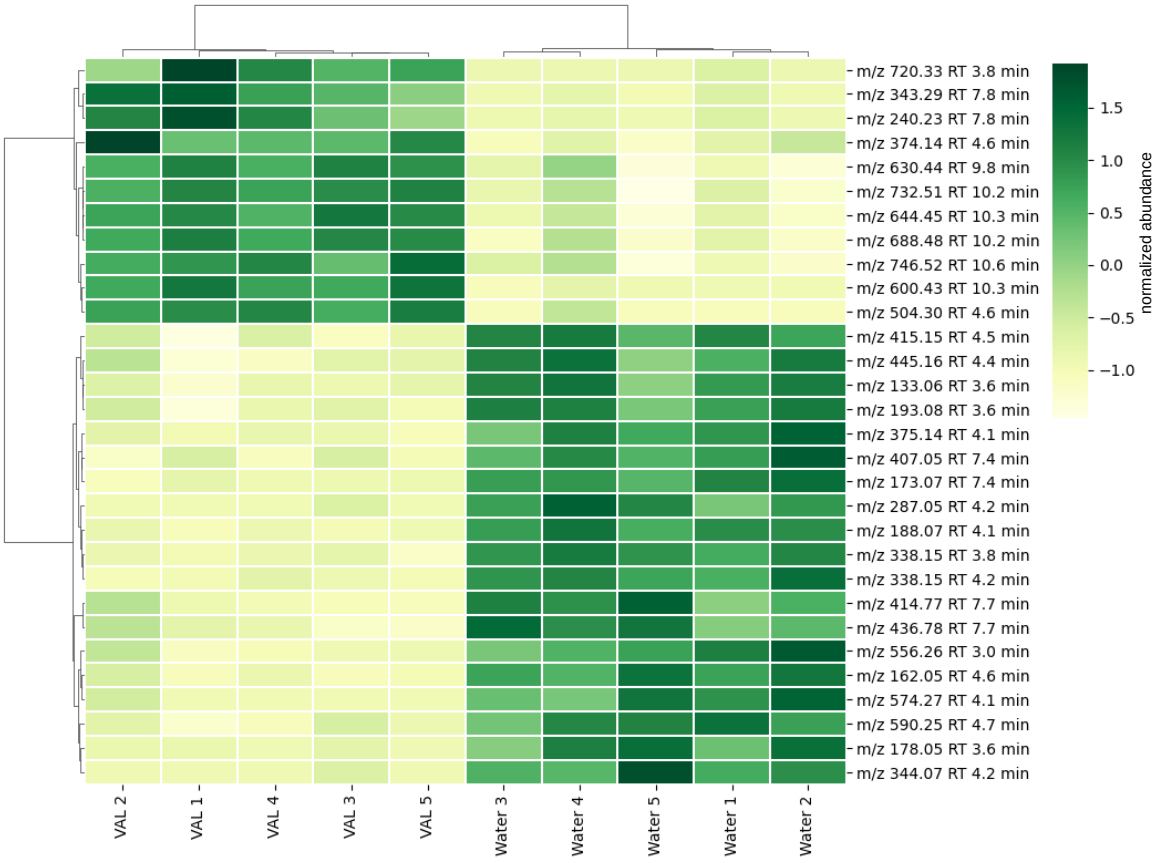

Figure 35: Heatmap of the features detected in cress roots treated with VAL-medium (n = 5) and tap water (n = 5). The 30 most significant features were clustered (Euclidean distance, ward algorithm) based on t-tests.

Table 10: 15 top upregulated features in cress roots grown in VAL-medium.

ID	RT / min	$[M+H]^+$	$^{DT}CCS_{N2}$ / Å^2	FC	p-value
VAL	8.3	436.24	203.7	3.96	3.9E-03
1	3.8	720.33	253.3	16.53	7.6E-05
2	7.8	343.29	196.6	7.43	3.5E-05
3	7.8	240.23	172.8	7.56	5.4E-05
4	4.6	504.30	204.7	7.49	9.5E-05
5	5.4	362.25	186.3	9.82	4.0E-04
6	7.8	240.23	198.6	9.74	5.6E-04
7	7.5	212.05	144.8	9.57	6.0E-04
8	5.4	326.23	186.9	9.18	1.7E-03
9	9.6	332.33	201.8	13.47	4.6E-02
10	4.7	558.28	231.3	6.94	6.9E-04
11	4.0	558.28	230.5	5.52	5.1E-04
12	3.6	770.31	257.8	6.32	1.3E-03
13	4.3	574.27	228.5	7.56	3.2E-03
14	11.0	804.56	283.9	4.87	4.3E-04
15	10.6	424.32	206.3	4.86	6.2E-04

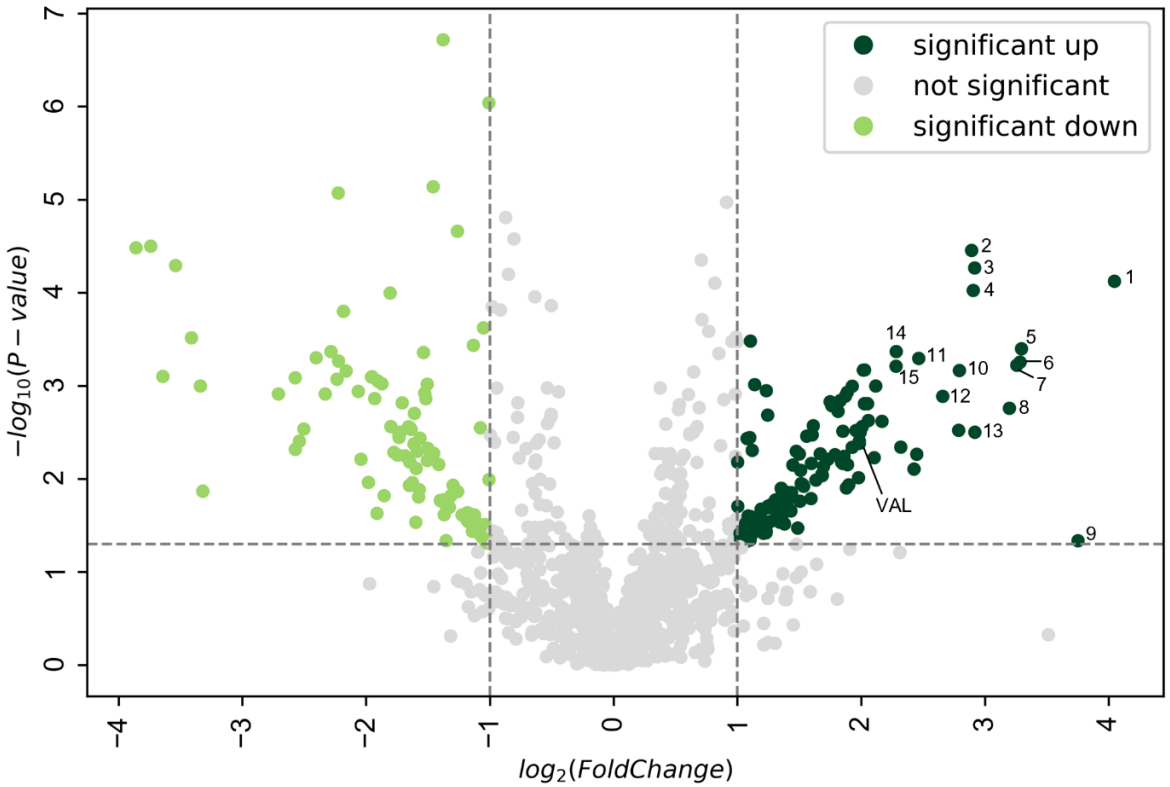

Figure 36: Up- and dysregulated features in cress roots grown in VAL-medium visualized in a volcano plot based on *p*-values and FCs (labelled features are listed in Table 10).

4.4.4. Valsartan – cress leaves

In contrast to CAN, the VAL-treated cress leaves could be distinguished from the control group, as seen in the heatmap (Figure 37). Nevertheless, the changes were not as pronounced as for the root tissue.

As it can be seen in the volcano plot (Figure 38), VAL was no longer included in the most upregulated species, meaning that the drug itself was no longer mainly responsible for the changes induced in the plantlet's upper parts. In comparison to the plot seen for CAN-treated leaf material (Figure 34), more significant differences could be observed.

As previously, no further drug-related species were found in these samples upon targeted MS^2. The only common feature with CAN leaves samples was m/z 694.27 RT 3.8 min (Table 11).

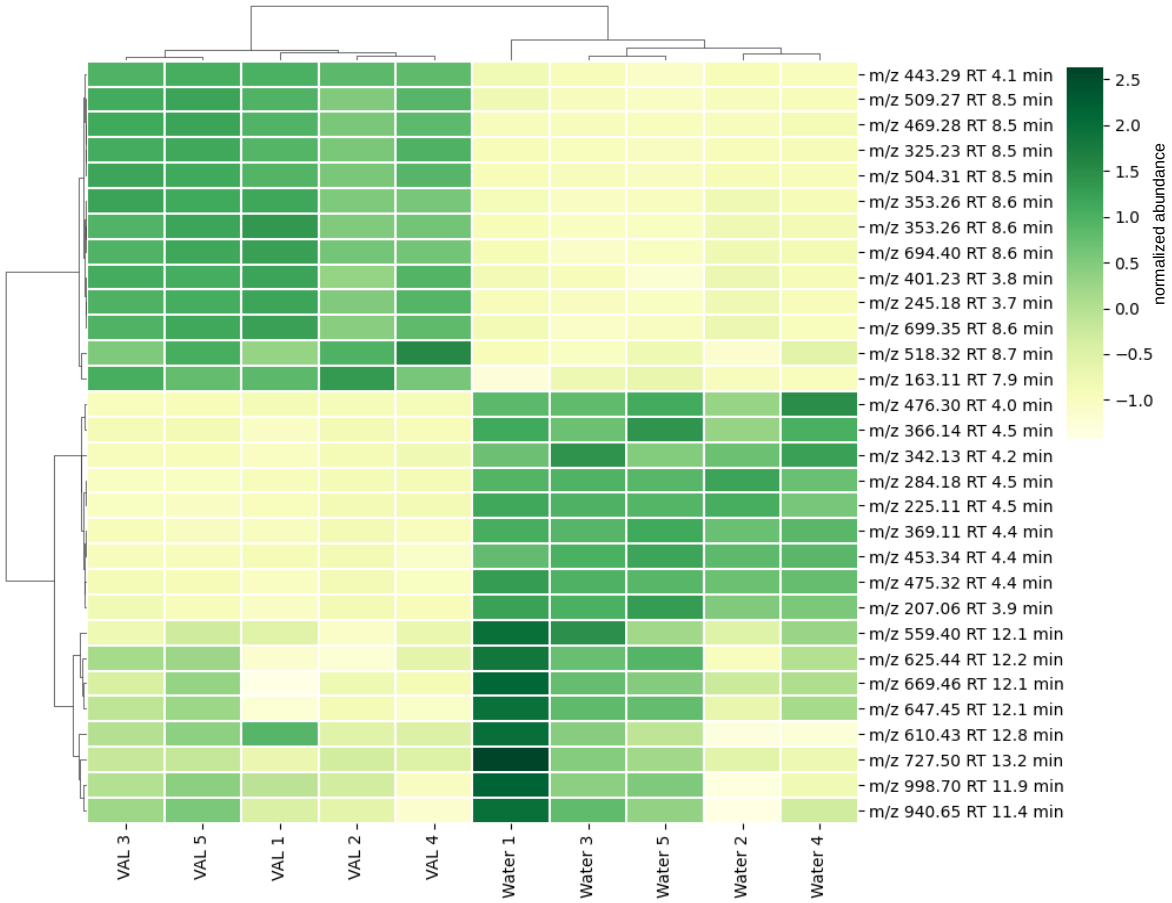

Figure 37: Heatmap of the features detected in cress leaves treated with VAL-medium (n = 5) and tap water (n = 5). The 30 most significant features were clustered (Euclidean distance, ward algorithm) based on t-tests.

Table 11: 15 top upregulated features in cress leaves grown in VAL-medium.

ID	RT / min	$[M+H]^+$	$^{DT}CCS_{N2}$ / Å²	FC	p-value
1	9.3	532.34	227.7	17.56	2.3E-05
2	9.3	353.26	188.5	17.15	2.3E-05
3	8.5	325.23	223.3	7.83	2.0E-09
4	8.5	469.28	221.2	7.40	3.1E-09
5	8.5	504.31	221.0	7.33	3.5E-09
6	8.5	509.27	215.0	6.67	5.0E-08
7	3.7	245.18	167.6	6.96	2.1E-07
8	5.0	358.27	191.4	14.18	7.2E-05
9	9.3	537.30	221.8	13.94	1.4E-04
10	9.3	353.26	229.4	14.75	3.5E-04
11	8.6	659.36	250.5	11.93	4.6E-05
12	4.0	663.39	392.6	12.29	6.4E-05
13	3.8	694.27	261.2	13.49	2.6E-04
14	5.9	489.30	216.5	12.41	3.4E-04
15	8.5	325.23	177.1	10.93	1.3E-04

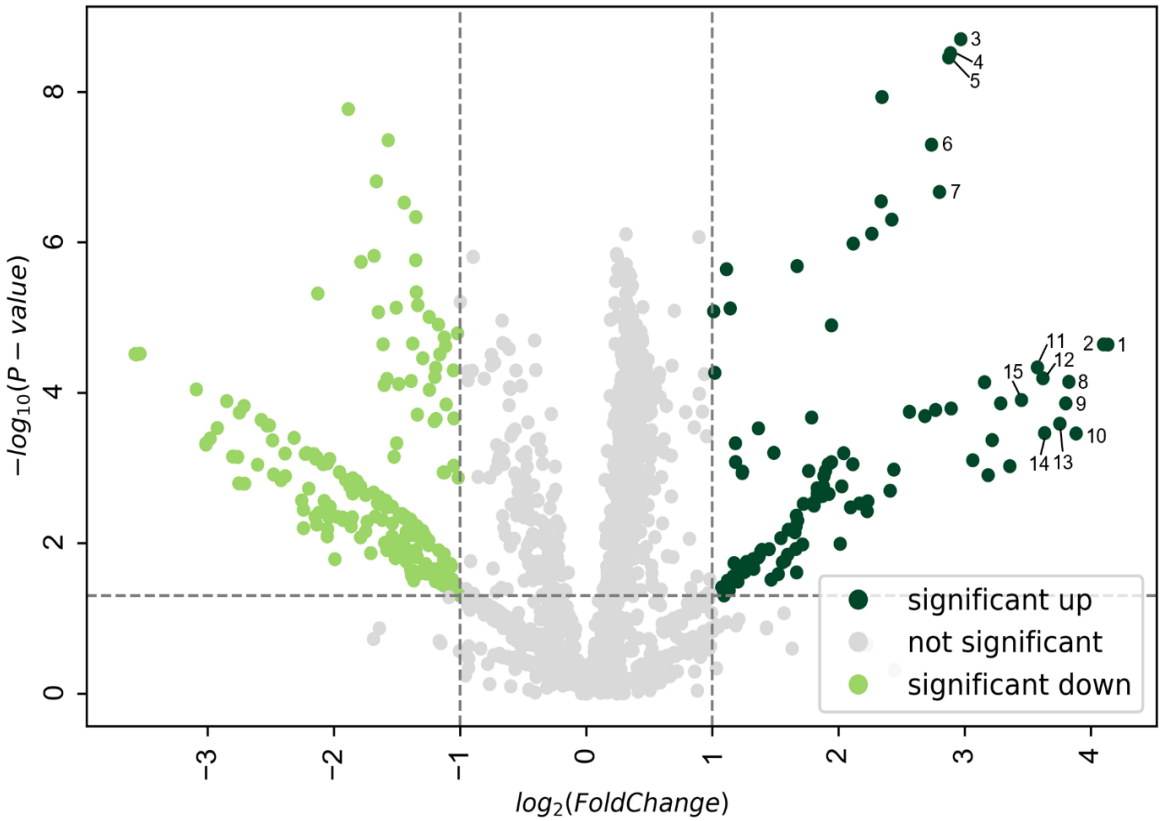

Figure 38: Up- and dysregulated features in cress leaves grown in VAL-medium visualized in a volcano plot based on *p*-values and FCs (labelled features are listed in Table 11).

Overall, the plantomics approach did not help to identify any new metabolites. Nevertheless, it showed that great changes within the plants were induced by the pharmaceuticals and therefore emphasizes the importance of further research in that area.

The findings of this approach are in line with the ones from section 4.3. The higher drug abundance in the root tissue induces more pronounced changes while leaves are only marginally influenced. As already mentioned, this might indicate that the pharmaceuticals diffuse slowly within the plant, or the time of exposure was too short.

None of the inspected features corresponded to any formerly detected drug-related substances (expect of VAL) which shows that the reaction of the plant metabolism to the foreign chemical substances is much more pronounced than the concentration of xenobiotic itself. It is likely that the significantly upregulated features correspond to stress molecules, that are expressed as response to the CAN/VAL contamination. On the contrary, the down-regulated features might stem from molecules involved with non-essential processes within the plant that are shut down to sustain viability. Though, to confirm any of these assumptions, further targeted and untargeted '-omics' approaches, which aim to identify these compounds, are required.

4.5. Valsartan and Candesartan in local wastewater

The final aim of this thesis was to investigate whether the identified metabolites are formed when plants are exposed to CAN and VAL concentrations that are frequently found in the environment. For this purpose, water samples from the effluents of local WWTPs (Hirschbach, Reichenthal) were collected and CDC, CAN, and VAL were quantified using the HPLC-QTOF instrumentation. Subsequently, the water was employed as cultivation medium for cress, and the resulting plant extracts were screened for the parent drugs and transformation products using the already described approaches (section 4.3.).

4.5.1. Candesartan

External calibration was done using standard solutions in the range of 2.5 – 25 µg L^{-1}. For CAN, a linear function with high regression coefficient (R^2) could be achieved (Figure 39). It was, however, not possible to quantify CDC because a portion of the prodrug readily hydrolyzed to its active form, yielding non-reproducible results. Nonetheless, CDC showed a similar abundance as CAN in the WWTP samples, which again emphasizes its high stability.

For CAN, concentrations of 5.8 µg L^{-1} and 4.1 µg L^{-1} were measured in the samples from Hirschbach and Reichenthal, respectively (Table 12).

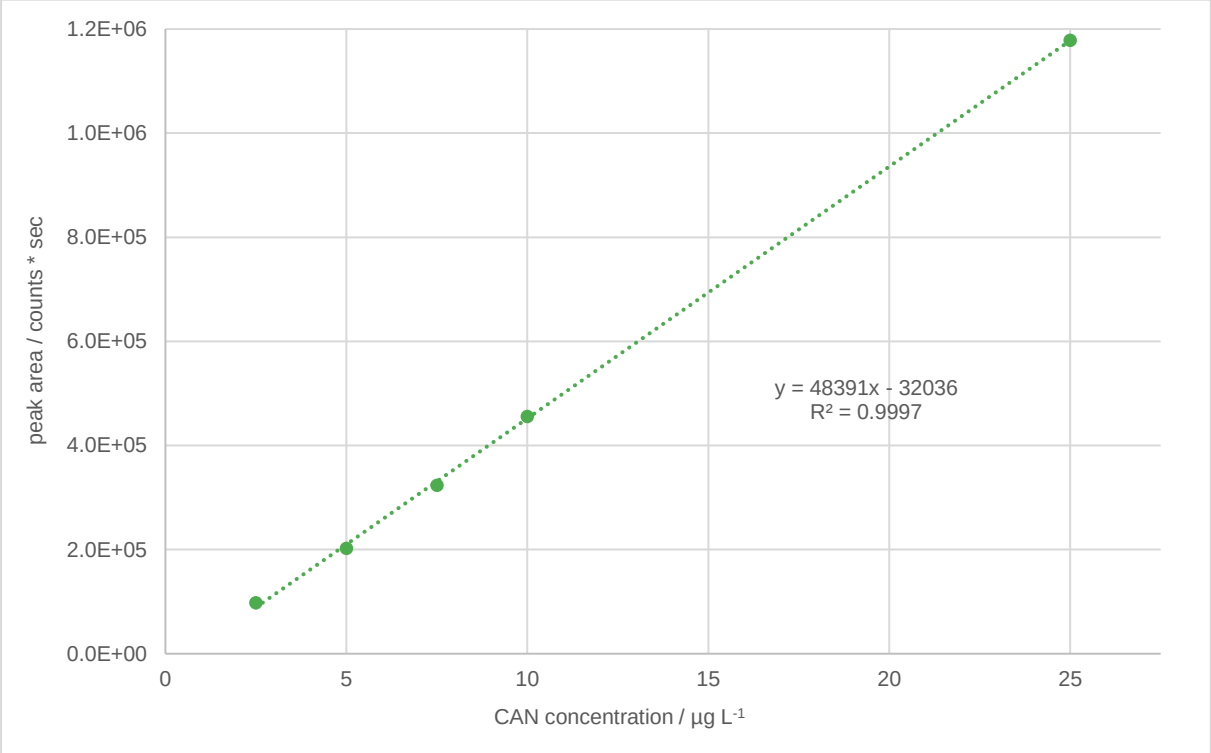

Figure 39: External calibration curve for CAN based on linear regression of CAN signals of five standard solutions in the range of 2.5 – 25 µg L^{-1}.

Table 12: Concentration of CAN in the WWTP samples.

Wastewater	RT / min	peak intensity / counts * s	concentration / µg L^{-1}
Hirschbach	7.5	248 202	5.8
Reichenthal	7.5	166 745	4.1

In cress grown in water from Hirschbach, signals corresponding to CAN, CDC and CAN-Glc were detected in root as well as leaf tissue. For Reichenthal, CAN-Glc was not found in the leaves. The presence of the compounds was confirmed by targeted MS^2 and drift time measurements. Concentrations could not be determined since all signals were below the limit of quantification.

4.5.2. Valsartan

External calibration (Figure 40) enabled the detection of a concentration of 23.0 µg L^{-1} in the water sample from Hirschbach (Table 13). For Reichenthal, the signal of VAL was below the limit of quantification, but a small peak with corresponding m/z was detected at 7.5 min.

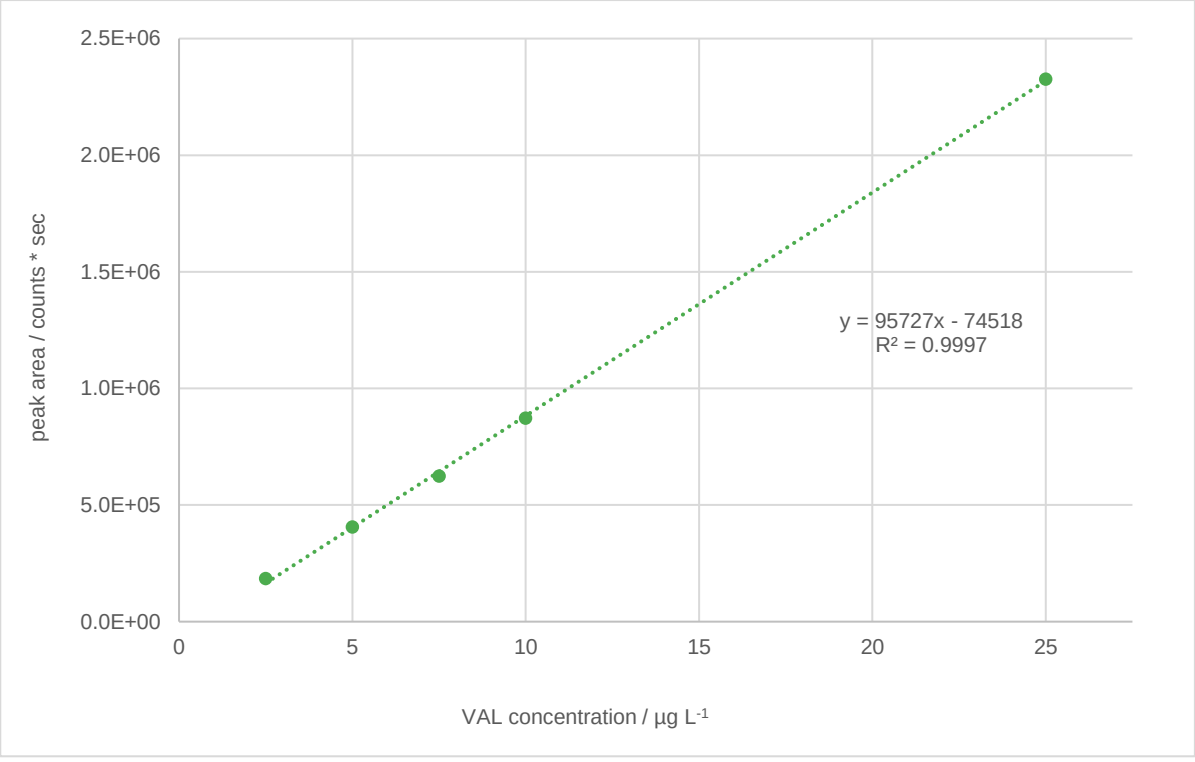

Figure 40: External calibration curve for VAL based on linear regression of VAL signals of five standard solutions in the range of 2.5 – 25 µg L^{-1}.

Table 13: Concentration of VAL in the WWTP samples.

Wastewater	**RT / min**	**peak area / counts * s**	**concentration / µg L^{-1}**
Hirschbach	8.3	2 126 044	23.0
Reichenthal	8.3	23 539	-

As for CAN, VAL and a glucosylated transformation product were identified in the cress extracts. Cress exposed to the water from Hirschbach showed the compounds again in both roots and leaves, while the very low drug concentration in the sample from Reichenthal made it impossible to detect VAL-Glc in the upper parts of cress. Again, VAL and its metabolite were present only in traces but were confirmed using MS^2 experiments. All observed metabolites for CAN and VAL were formed within cress since they could not be detected in the WWTP samples.

The measured concentrations of CAN and VAL in the WWTP samples lie within the range that is frequently observed for xenobiotics in the environment [21] and correspond to data collected previously at the Institute of Analytical Chemistry (JKU). The outcomings emphasize that the low drug concentrations in wastewater are sufficient to lead to accumulation of the parent drug as well as of transformation products within the plant.

5. Conclusion

The nowadays extensive use of PPCPs in daily life poses an imminent threat to the environment. For this reason, the present thesis contributed to increasing the understanding of the uptake and transformation of xenobiotics in plants.

Several model plants were exposed to either CAN or VAL, which both lower blood pressure. Parent drugs, as well as formed transformation products were tentatively identified in the plant extracts using RP-HPLC coupled to a DT-IM-QTOF. Thereby, in total, nine and seven metabolites were found for CAN and VAL, respectively. Besides hydroxylated phase I transformation products, various conjugates of the pharmaceuticals with glucose, malonic acid and/or glucuronic acid were observed. For more confident identification of the herein detected metabolites, nuclear magnetic resonance (NMR) spectroscopy would be the method of choice.

The newly designed AF approach enabled the identification of two additional transformation products for VAL. It might facilitate "fast-screening" of plant extracts for metabolites, provided that the characteristic fragmentation pattern of the parent drug is known. For that purpose, however, considerable optimizations concerning feature extraction would be required.

Using the plantomics-related method, no further drug-related metabolites were found, but it demonstrated that the pharmaceuticals induced pronounced changes in the plant tissue. This strategy shows high potential for further investigations of the uptake and metabolization of xenobiotics in plants and should be refined to achieve more valuable results. Including more plant species might highlight features that are exclusively related to the pharmaceuticals and using more replicates per group will enhance the reliability of the findings.

The environmental relevance of the acquired knowledge was finally demonstrated by exposing cress to water samples from effluents of WWTPs that contained VAL and CAN in much lower concentrations. In the corresponding extracts, the parent drugs and glucosylated transformation products could be identified.

Concluding, little is yet known about the uptake and biotransformation of xenobiotics in plants. Therefore, further work needs to be directed especially towards the toxicological significance of the accumulated pharmaceutical preparations and metabolites for the environment as well as for human health. In addition, special risks posed by the synergistic effects of the plethora of PPCPs in waterbodies need to be considered.

References

[1] EUR-Lex - 32000L0060 - EN - EUR-Lex. https://eur-lex.europa.eu/legal-content/EN/TXT /?uri=CELEX%3A32000L0060&qid=1658221430673 (accessed July 19, 2022).

[2] A.Y. Hoekstra, Water scarcity challenges to business, Nat Clim Chang. 4 (2014) 318–320. https://doi.org/10.1038/nclimate2214.

[3] Water Reuse - Environment - European Commission. https://ec.europa.eu/environment/water/reuse.htm (accessed July 19, 2022).

[4] F.A. Ward, M. Pulido-Velazquez, Water conservation in irrigation can increase water use, Proc Natl Acad Sci U S A. 105 (2008) 18215–18220. https://doi.org/10.1073/pnas.0805554105.

[5] Y. Yin, Q. Tang, X. Liu, X. Zhang, Water scarcity under various socio-economic pathways and its potential effects on food production in the Yellow River basin, Hydrol Earth Syst Sci. 21 (2017) 791–804. https://doi.org/10.5194/hess-21-791-2017.

[6] X. Wu, L.K. Dodgen, J.L. Conkle, J. Gan, Plant uptake of pharmaceutical and personal care products from recycled water and biosolids: A review, Science of the Total Environment. 536 (2015) 655–666. https://doi.org/10.1016/j.scitotenv.2015.07.129.

[7] P. Łukaszewicz, A. Białk-Bielińska, J. Dołżonek, J. Kumirska, M. Caban, P. Stepnowski, A new approach for the extraction of tetracyclines from soil matrices: application of the microwave-extraction technique, Anal Bioanal Chem. 410 (2018) 1697–1707. https://doi.org/10.1007/s00216-017-0815-7.

[8] M. Patel, R. Kumar, K. Kishor, T. Mlsna, C.U. Pittman, D. Mohan, Pharmaceuticals of emerging concern in aquatic systems: Chemistry, occurrence, effects, and removal methods, Chem Rev. 119 (2019) 3510–3673. https://doi.org/10.1021/acs.chemrev.8b00299.

[9] T. aus der Beek, F.A. Weber, A. Bergmann, S. Hickmann, I. Ebert, A. Hein, A. Küster, Pharmaceuticals in the environment-Global occurrences and perspectives, Environ Toxicol Chem. 35 (2016) 823–835. https://doi.org/10.1002/etc.3339.

[10] W.C. Li, Occurrence, sources, and fate of pharmaceuticals in aquatic environment and soil, Environmental Pollution. 187 (2014) 193–201. https://doi.org/10.1016/j.envpol.2014.01.015.

[11] M. Kostopoulou, A. Nikolaou, Analytical problems and the need for sample preparation in the determination of pharmaceuticals and their metabolites in aqueous environmental matrices, TrAC - Trends in Analytical Chemistry. 27 (2008) 1023–1035. https://doi.org/10.1016/j.trac.2008.09.011.

[12] J.B. Ellis, Pharmaceutical and personal care products (PPCPs) in urban receiving waters, Environmental Pollution. 144 (2006) 184–189. https://doi.org/10.1016/j.envpol.2005.12.018.

[13] X. Wu, L.K. Dodgen, J.L. Conkle, J. Gan, Plant uptake of pharmaceutical and personal care products from recycled water and biosolids: A review, Science of the Total Environment. 536 (2015) 655–666. https://doi.org/10.1016/j.scitotenv.2015.07.129.

[14] T. Sato, M. Qadir, S. Yamamoto, T. Endo, A. Zahoor, Global, regional, and country level need for data on wastewater generation, treatment, and use, Agric Water Manag. 130 (2013) 1–13. https://doi.org/10.1016/j.agwat.2013.08.007.

[15] W.W. Buchberger, Current approaches to trace analysis of pharmaceuticals and personal care products in the environment, J Chromatogr A. 1218 (2011) 603–618. https://doi.org/10.1016/j.chroma.2010.10.040.

[16] K. Kümmerer, Pharmaceuticals in the environment, Annu Rev Environ Resour. 35 (2010) 57–75. https://doi.org/10.1146/annurev-environ-052809-161223.

[17] E.L. Miller, S.L. Nason, K.G. Karthikeyan, J.A. Pedersen, Root Uptake of Pharmaceuticals and Personal Care Product Ingredients, Environ Sci Technol. 50 (2016) 525–541. https://doi.org/10.1021/acs.est.5b01546.

[18] H. Sandermann, Plant metabolism of xenobiotics, Trends Biochem Sci. 17 (1992) 82–84. https://doi.org/10.1016/0968-0004(92)90507-6.

[19] H. Bártíková, L. Skálová, L. StuchÍková, I. Vokřál, T. Vaněk, R. Podlipná, Xenobiotic-metabolizing enzymes in plants and their role in uptake and biotransformation of veterinary drugs in the environment, Drug Metab Rev. 47 (2015) 374–387. https://doi.org/10.3109/03602532.2015.1076437.

[20] Q. Fu, T. Malchi, L.J. Carter, H. Li, J. Gan, B. Chefetz, Pharmaceutical and Personal Care Products: From Wastewater Treatment into Agro-Foo Systems, Environ Sci Technol. 53 (2019) 14083–14090. https://doi.org/10.1021/acs.est.9b06206.

[21] F. Mlynek, M. Himmelsbach, W. Buchberger, C.W. Klampfl, Analytical approaches for the determination and identification of drug metabolites in plants after uptake, in: Handbook of Environmental Chemistry, Springer Science and Business Media Deutschland GmbH, 2021: pp. 493–523. https://doi.org/10.1007/698_2020_629.

[22] A. Barreras, C. Gurk-Turner, Angiotensin II Receptor Blockers, Baylor University Medical Center Proceedings. 16 (2003) 123–126. https://doi.org/10.1080/08998280.2003.11927893.

[23] A. Markham, K.L. Goa, Valsartan. A review of its pharmacology and therapeutic use in essential hypertension, Drugs. 54 (1997) 299–311. https://doi.org/10.2165/00003495-199754020-00009.

[24] Physiology, Renin Angiotensin System - StatPearls - NCBI Bookshelf. https://www.ncbi.nlm.nih.gov/books/NBK470410/ (accessed July 21, 2022).

[25] CAS Common Chemistry. https://commonchemistry.cas.org/detail?cas_rn=137862-53-4 (accessed July 21, 2022).

[26] Candesartan cilexetil: Uses, Interactions, Mechanism of Action | DrugBank Online. https://go.drugbank.com/drugs/DB00796 (accessed July 26, 2022).

[27] C.H. Gleiter, C. Jägle, U. Gresser, K. Mörike, Candesartan, Cardiovasc Drug Rev. 22 (2006) 263–284. https://doi.org/10.1111/j.1527-3466.2004.tb00146.x.

[28] Valsartan: Uses, Interactions, Mechanism of Action | DrugBank Online. https://go.drugbank.com/drugs/DB00177 (accessed July 21, 2022).

[29] E.L. Schymanski, J. Jeon, R. Gulde, K. Fenner, M. Ruff, H.P. Singer, J. Hollender, Identifying small molecules via high resolution mass spectrometry: Communicating confidence, Environ Sci Technol. 48 (2014) 2097–2098. https://doi.org/10.1021/es5002105.

[30] E. Gemperline, C. Keller, L. Li, Mass Spectrometry in Plant-omics, Anal Chem. 88 (2016) 3422–3434. https://doi.org/10.1021/acs.analchem.5b02938.

[31] S.M. Stow, T.J. Causon, X. Zheng, R.T. Kurulugama, T. Mairinger, J.C. May, E.E. Rennie, E.S. Baker, R.D. Smith, J.A. McLean, S. Hann, J.C. Fjeldsted, An Interlaboratory Evaluation of Drift Tube Ion Mobility-Mass Spectrometry Collision Cross Section Measurements, Anal Chem. 89 (2017) 9048–9055. https://doi.org/10.1021/acs.analchem.7b01729.

[32] C.W. Klampfl, Metabolization of pharmaceuticals by plants after uptake from water and soil: A review, TrAC - Trends in Analytical Chemistry. 111 (2019) 13–26. https://doi.org/10.1016/j.trac.2018.11.042.

[33] Z. Pang, G. Zhou, J. Ewald, L. Chang, O. Hacariz, N. Basu, J. Xia, Using MetaboAnalyst 5.0 for LC–HRMS spectra processing, multi-omics integration and covariate adjustment of global metabolomics data, Nat Protoc. (2022). https://doi.org/10.1038/s41596-022-00710-w.

[34] M.C. Gershater, R. Edwards, Regulating biological activity in plants with carboxylesterases, Plant Science. 173 (2007) 579–588. https://doi.org/10.1016/j.plantsci.2007.08.008.

[35] F. Mlynek, M. Himmelsbach, W. Buchberger, C.W. Klampfl, A new analytical workflow using HPLC with drift-tube ion-mobility quadrupole time-of-flight/mass spectrometry for the detection of drug-related metabolites in plants, Anal Bioanal Chem. 412 (2020) 1817–1824. https://doi.org/10.1007/s00216-020-02429-7.

[36] K.M. Hines, D.H. Ross, K.L. Davidson, M.F. Bush, L. Xu, Large-Scale Structural Characterization of Drug and Drug-Like Compounds by High-Throughput Ion Mobility-Mass Spectrometry, Anal Chem. 89 (2017) 9023–9030. https://doi.org/10.1021/acs.analchem.7b01709.

[37] P.L. Plante, É. Francovic-Fontaine, J.C. May, J.A. McLean, E.S. Baker, F. Laviolette, M. Marchand, J. Corbeil, Predicting Ion Mobility Collision Cross-Sections Using a Deep Neural Network: DeepCCS, Anal Chem. 91 (2019) 5191–5199. https://doi.org/10.1021/acs.analchem.8b05821.

[38] C.A. Smith, G. O'Maille, E.J. Want, C. Qin, S.A. Trauger, T.R. Brandon, D.E. Custodio, R. Abagyan, G. Siuzdak, METLIN: A metabolite mass spectral database, in: Ther Drug Monit, Ther Drug Monit, 2005: pp. 747–751. https://doi.org/10.1097/01.ftd.0000179845.53213.39.

Appendix

Table 14: List of human phase I metabolites of candesartancilexetil [26].

Analyte	Abbreviation	Sum formula	Exact mass [M]	$[M+H]^+$
Candesartancilexetil	CDC	$C_{33}H_{34}N_6O_6$	610.2540	611.2618
Hydroxylated candesartancilexetil	OH-CDC	$C_{33}H_{34}N_6O_7$	626.2489	627.2567
Candesartan	CAN	$C_{24}H_{20}N_6O_3$	440.1597	441.1675
Candesartan O/N-glucuronide	O/NG-CAN	$C_{30}H_{28}N_6O_9$	616.1918	617.1996
O-deethylated candesartan	ODE-CAN	$C_{22}H_{16}N_6O_3$	412.1284	413.1362
Hydroxylated candesartan	OH-CAN	$C_{24}H_{20}N_6O_4$	456.1546	457.1624

Table 15: List of human phase I metabolites of valsartan [28].

Analyte	Abbreviation	Sum formula	Exact mass [M]	[M+H]+
Valsartan	VAL	$C_{24}H_{29}N_5O_3$	435.5188	436.2349
Hydroxyvalsartan	OH-VAL	$C_{24}H_{29}N_5O_4$	451.2220	452.2298
Valsartan acid	VA	$C_{14}H_{10}N_4O_2$	266.0804	267.0882

Table 16: Conjugates for phase II metabolites of xenobiotics (X) that are commonly observed in plants.

Abbreviation	Conjugate sum formula	Conjugate exact mass
X-Glc	$C_6H_{10}O_5$	162.0528
X-Glc-Glc	$C_{12}H_{20}O_{10}$	324.1056
X-Glc-Glc-Glc	$C_{18}H_{30}O_{15}$	486.1585
X-Glc-Glc-Glc-Glc	$C_{24}H_{40}O_{20}$	648.2113
X-Glc-Mal	$C_9H_{12}O_8$	248.0532
X-Glc-Glc-Mal	$C_{15}H_{22}O_{13}$	410.1060
X-Glc-Glc-Glc-Mal	$C_{21}H_{32}O_{18}$	572.1589
X-Glc-Glc-Glc-Glc-Mal	$C_{27}H_{42}O_{23}$	734.2117
X-Glc-Mal Methylester	$C_{10}H_{14}O_8$	262.0689

Abbreviation	Conjugate sum formula	Conjugate exact mass
X-Glc-Glc-Mal Methylester	$C_{16}H_{24}O_{13}$	424.1217
X-Glc-Glc-Glc-Mal Methylester	$C_{22}H_{34}O_{18}$	586.1745
X-Glc-Glc-Glc-Glc-Mal Methylester	$C_{28}H_{44}O_{23}$	748.2273
X-Mal	$C_3H_2O_3$	86.0004
X-Mal-Mal	$C_6H_4O_6$	172.0008
X-Mal-Mal-Mal	$C_9H_6O_9$	258.0012
X-Mal Methylester	$C_4H_4O_3$	100.0160
X-Mal-Mal Methylester	$C_7H_6O_6$	186.0164
X-Mal-Mal-Mal Methylester	$C_{10}H_8O_9$	272.0168
X-Glc-Mal-Mal	$C_{12}H_{14}O_{11}$	334.0536
X-Glc-Glc-Mal-Mal	$C_{18}H_{24}O_{16}$	496.1064
X-Glc-Glc-Glc-Mal-Mal	$C_{24}H_{34}O_{21}$	658.1593
X-Glc-Glc-Glc-Glc-Mal-Mal	$C_{30}H_{44}O_{26}$	820.2121
X-Glc-Mal-Mal-Mal	$C_{15}H_{16}O_{14}$	420.0540
X-Glc-Glc-Mal-Mal-Mal	$C_{21}H_{26}O_{19}$	582.1068
X-Glc-Glc-Glc-Mal-Mal-Mal	$C_{27}H_{36}O_{24}$	744.1597
X-Glc-Glc-Glc-Glc-Mal-Mal-Mal	$C_{33}H_{46}O_{29}$	906.2125
X-GlcA	$C_6H_8O_6$	176.0321
X-GlcA-GlcA	$C_{12}H_{16}O_{12}$	352.0642
X-GlcA-GlcA-GlcA	$C_{18}H_{24}O_{18}$	528.0963
X-GlcA-GlcA-GlcA-GlcA	$C_{24}H_{32}O_{24}$	704.1284
X-GlcA-Mal	$C_9H_{10}O_9$	262.0325
X-GlcA-GlcA-Mal	$C_{15}H_{18}O_{15}$	438.0646
X-GlcA-GlcA-GlcA-Mal	$C_{21}H_{26}O_{21}$	614.0967
X-GlcA-GlcA-GlcA-GlcA-Mal	$C_{27}H_{34}O_{27}$	790.1287
X-Glc-GlcA	$C_{12}H_{18}O_{11}$	338.0849
X-Glc-GlcA-GlcA	$C_{18}H_{26}O_{17}$	514.1170
X-Glc-GlcA-GlcA-GlcA	$C_{24}H_{34}O_{23}$	690.1491
X-Glc-GlcA-GlcA-GlcA-GlcA	$C_{30}H_{42}O_{29}$	866.1812
X-Glc-Glc-GlcA	$C_{18}H_{28}O_{16}$	500.1377
X-Glc-Glc-GlcA-GlcA	$C_{24}H_{36}O_{22}$	676.1698
X-Glc-Glc-GlcA-GlcA-GlcA	$C_{30}H_{44}O_{28}$	852.2019
X-Glc-Glc-GlcA-GlcA-GlcA-GlcA	$C_{36}H_{52}O_{34}$	1028.2340
X-Glc-GlcA-Mal	$C_{15}H_{20}O_{14}$	424.0853

Abbreviation	Conjugate sum formula	Conjugate exact mass
X-Glc-GlcA-GlcA-Mal	$C_{21}H_{28}O_{20}$	600.1174
X-Glc-GlcA-GlcA-GlcA-Mal	$C_{27}H_{36}O_{26}$	776.1495
X-Glc-GlcA-GlcA-GlcA-GlcA-Mal	$C_{33}H_{44}O_{32}$	952.1816
X-Glc-GlcA-Mal-Mal	$C_{18}H_{22}O_{17}$	510.0857
X-Glc-GlcA-GlcA-Mal-Mal	$C_{24}H_{30}O_{23}$	686.1178
X-Glc-GlcA-GlcA-GlcA-Mal-Mal	$C_{30}H_{38}O_{29}$	862.1499
X-Glc-GlcA-GlcA-GlcA-GlcA-Mal-Mal	$C_{36}H_{46}O_{35}$	1038.1820
X-Glc-Glc-GlcA-Mal	$C_{21}H_{30}O_{19}$	586.1381
X-Glc-Glc-GlcA-GlcA-Mal	$C_{27}H_{38}O_{25}$	762.1702
X-Glc-Glc-GlcA-GlcA-GlcA-Mal	$C_{33}H_{46}O_{31}$	938.2023
X-Glc-Glc-GlcA-GlcA-GlcA-GlcA-Mal	$C_{39}H_{54}O_{37}$	1114.2344
X-Glc-Glc-GlcA-Mal-Mal	$C_{24}H_{32}O_{22}$	672.1385
X-Glc-Glc-GlcA-GlcA-Mal-Mal	$C_{30}H_{40}O_{28}$	848.1706
X-Glc-Glc-GlcA-GlcA-GlcA-Mal-Mal	$C_{36}H_{48}O_{34}$	1024.2027
X-Glc-Glc-GlcA-GlcA-GlcA-GlcA-Mal-Mal	$C_{42}H_{56}O_{40}$	1200.2348
X-GSH	$C_{10}H_{15}N_3O_6S$	305.0682
X-GSH+OH	$C_{10}H_{16}N_3O_7S$	322.0709
X-taurine	$C_2H_5NO_2S$	107.0041
X-sulfate	SO_3	79.9568
X-ethanolamine	C_2H_5N	43.0422
X-glycerol	$C_3H_6O_2$	74.0368

Source code 1: pre-processing.py

```
import pandas as pd
import numpy as np
import os
import re

################################################################################
# the following variables need to be defined individually:

# filename without path
# in case the file might be a corrupted .xls file, save the file in a correct
  manner before running the script
file = r'mydocument.xlsx'

# common prefix that was added to the sample names - will be deleted
prefix = ' 220322 g5 AF10CE '

# list of names of all background correction groups
correction_groups = ['W ', 'S ']
################################################################################


def boundary_checker(*args) -> bool:
    """checks if several measurements yielded equal signal

    This function checks if all passed arguments are within a certain boundary
    based on the first argument.

    Returns
    -------
    int
        Returns True or False
    """
    for n, arg in enumerate(args):
        first_argument = 0
        if n == 0:
            first_argument = int(arg)
        ############################################################################
        # define criteria for considering signal differences as random
          fluctuations
        if first_argument * 0.9 < int(arg) < first_argument * 1.1:
            continue
        else:
            return False
        ############################################################################
    return True


# reading data from the input file
data = pd.read_excel((os.path.join(os.path.dirname(file), file)), header=4, engine='openpyxl')

# deletion of the prefixes
data = data.rename(columns=lambda col_name: col_name.replace(prefix, ''))
```

```
# insertion of Identifier column and deletion of not required data
data.insert(loc=0, column='Identifier', value='')
data["Identifier"] = data["RT"].astype(str) + '_' + data["m/z"].astype(str) + '_' + data["CCS"].astype(str)
data = data.drop(['ID', 'RT', 'm/z', 'SD', 'SD.1', 'SD.2', 'SD.3', 'CCS', 'DT', 'Abundance', 'RSD','Ions', 'Z',
'Freq.', 'Q Score', 'Sat.', 'Mark'], axis=1)
data = data.replace('NaN', 0.001)

measurement_data = data.copy()

# extraction of the background correction groups, checking which features
  yielded comparable intense signals
row_index_dict = {}
for group in correction_groups:
    correction_group_list = data.filter(regex=f'^{group}', axis=1).head()
    correction_data = data[correction_group_list.columns].values.tolist()
    measurement_data = data.drop(correction_group_list, axis=1)
    measurement_data = measurement_data.drop('Identifier', axis=1)
    index = 0
    for row in correction_data:
        if boundary_checker(*row):
            row_index_dict[index] = np.mean(row)
        index += 1

# searching and deleting of features that show similar intensities as
  correction groups
for key in row_index_dict:
    target_row = measurement_data.iloc[int(key)]
    target_row_values = target_row.values.tolist()
    if boundary_checker(row_index_dict[key], *target_row_values):
        data = data.drop(int(key))

# creation of a row comprising the sample group names
pattern = r'(\D*)'
sample_groups = data.columns.tolist()
for i in range(len(sample_groups)):
    sample_groups[i] = re.match(pattern, sample_groups[i]).group(0)
data.loc[-1] = sample_groups
data.index = data.index + 1
data = data.sort_index()

# replacing missing signals by text
data = data.replace(0.001, 'NaN')

# saving new file
filename = file.split('.')[0] + '_cleaned.csv'
data.to_csv((os.path.join(os.path.dirname(file), filename)), index=False)
```

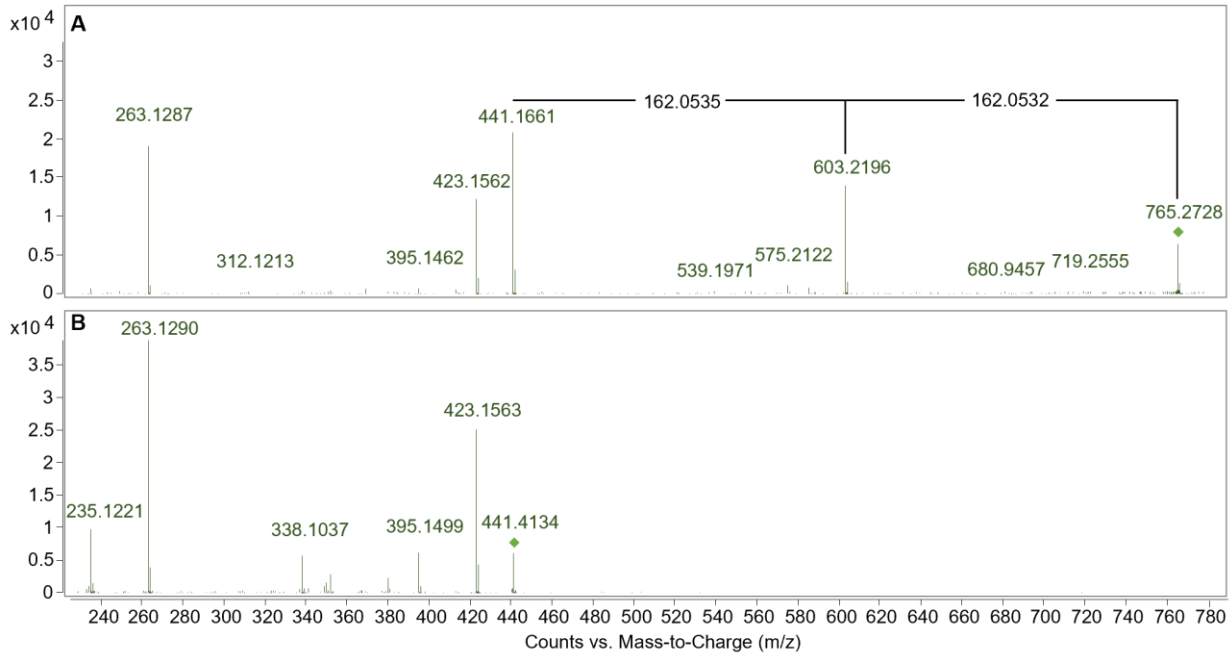

Figure 41: MS^2 spectrum of CAN-Glc-Glc (m/z 765.27; A) in a cress root sample fragmented with a CE of 10 V in comparison to an MS^2 spectrum of CAN (441.16; B)

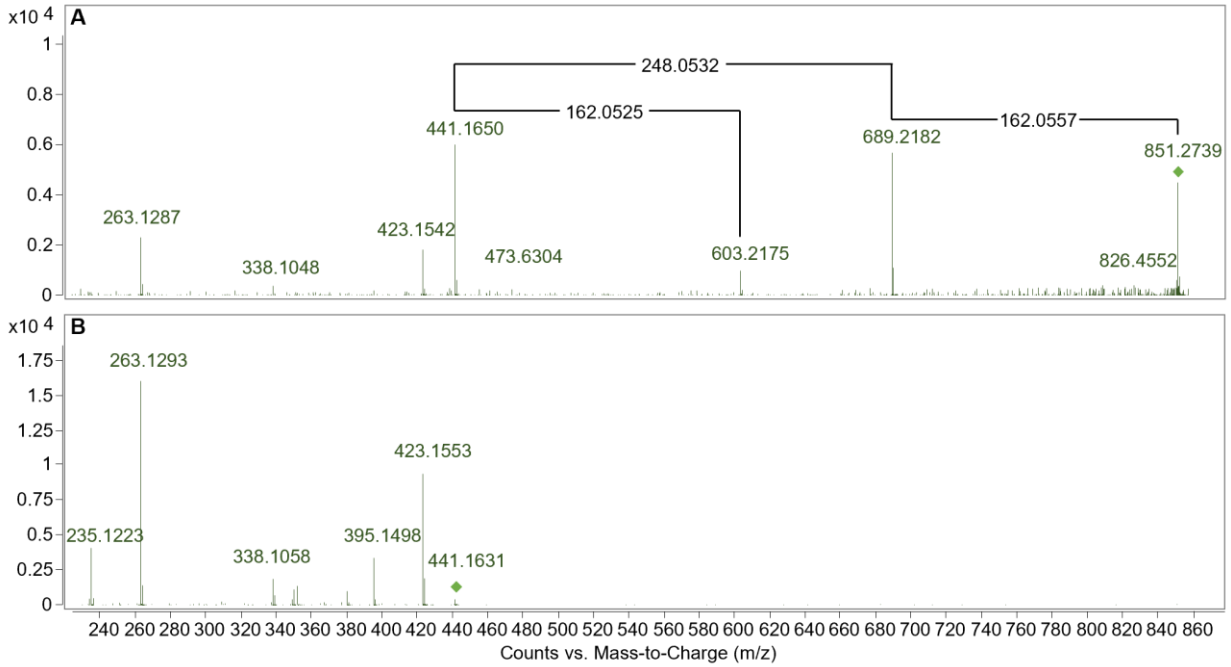

Figure 42: MS^2 spectrum of CAN-Glc-Glc-Mal (m/z 851.27; A) in a pea root sample fragmented with a CE of 10 V in comparison to an MS^2 spectrum of CAN (441.16; B)

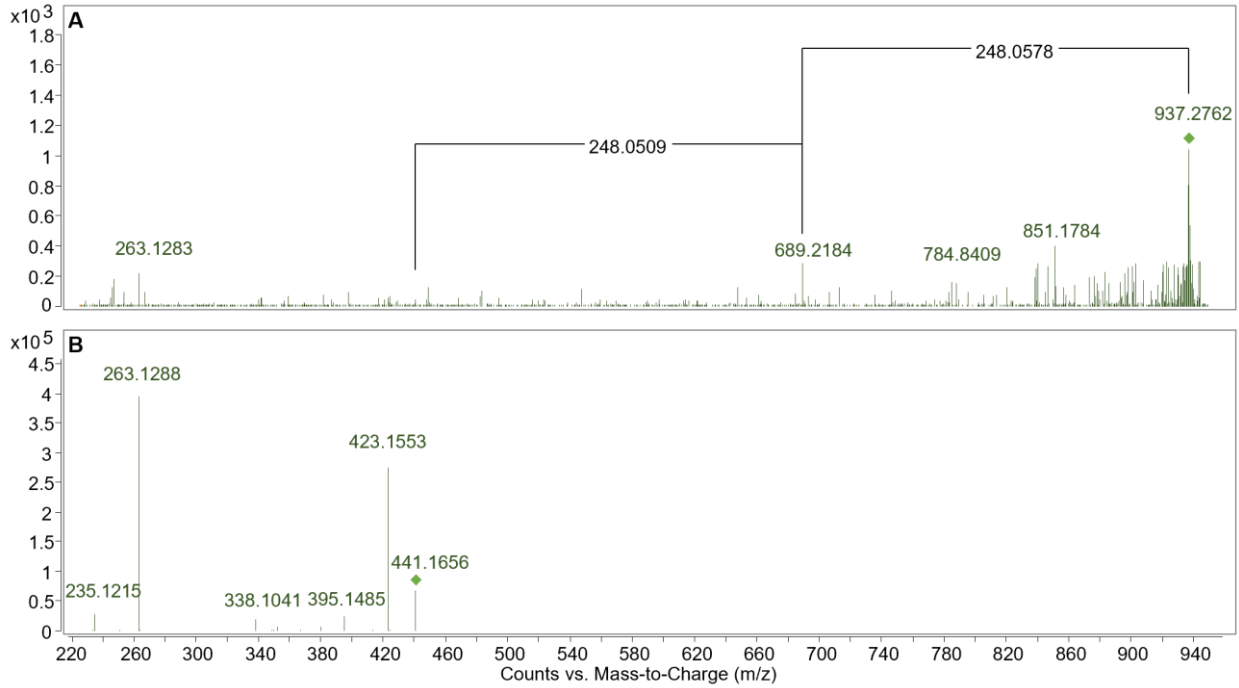

Figure 43: MS^2 spectrum of CAN-Glc-Glc-Mal-Mal (m/z 937.28; A) in a turnip green sample fragmented with a CE of 10 V in comparison to an MS^2 spectrum of CAN (441.16; B)

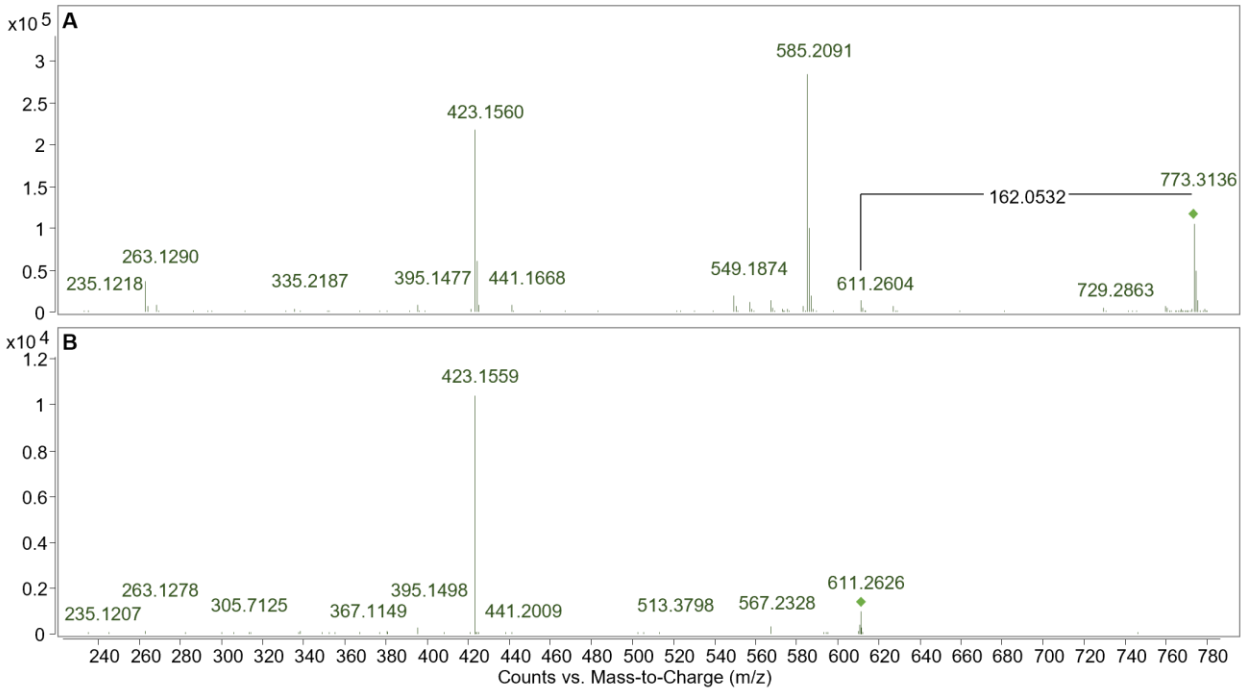

Figure 44: MS^2 spectrum of CDC-Glc (m/z 773.31; A) in a maize root sample fragmented with a CE of 10 V in comparison to an MS^2 spectrum of CDC (611.26; B).

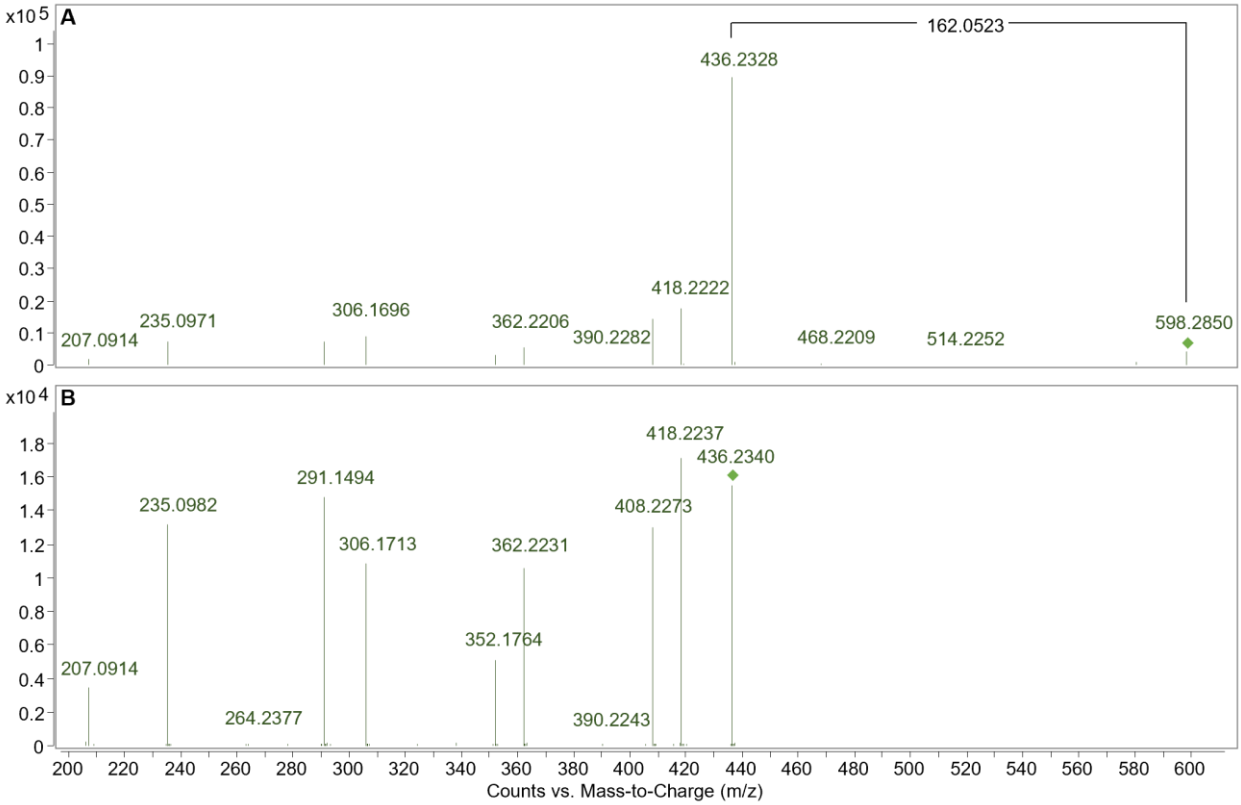

Figure 45: MS^2 spectrum of VAL-Glc (m/z 598.29; A) in a pea root sample fragmented with a CE of 3 V in comparison to an MS^2 spectrum of VAL (436.23; B)

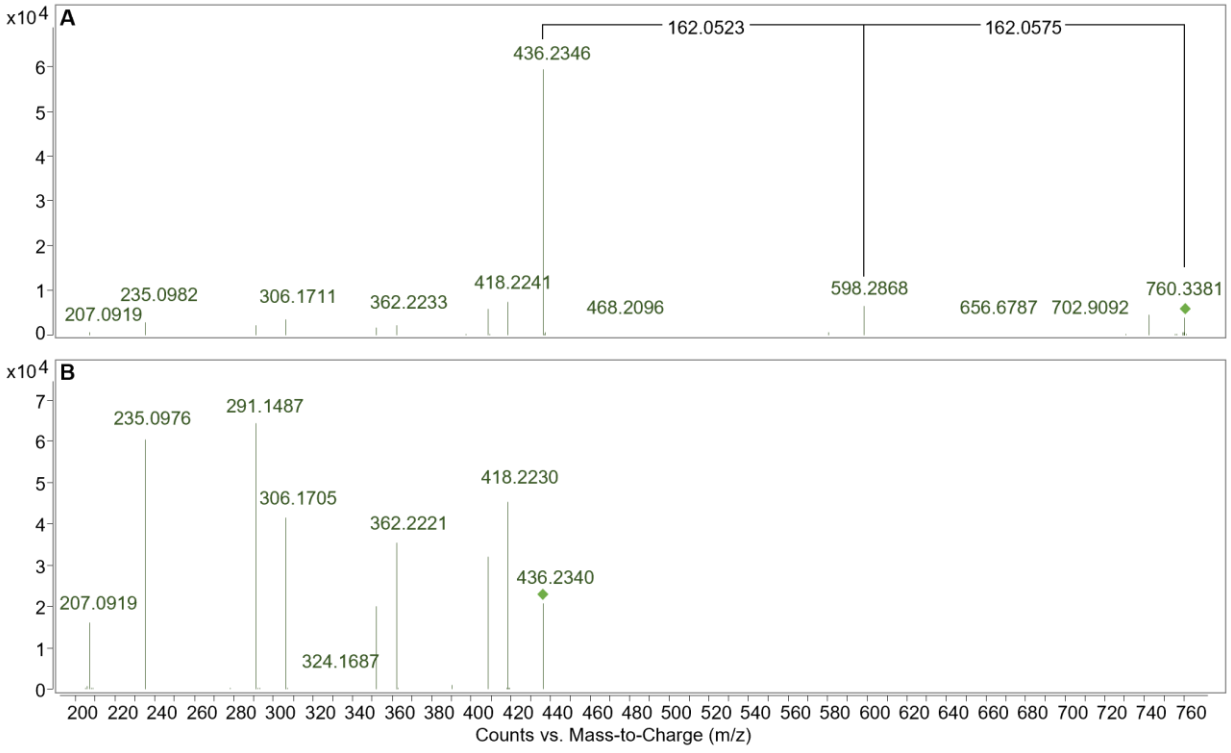

Figure 46: MS^2 spectrum of VAL-Glc-Glc (m/z 760.34; A) in a turnip greens sample fragmented with a CE of 5 V in comparison to an MS^2 spectrum of VAL (436.23; B)

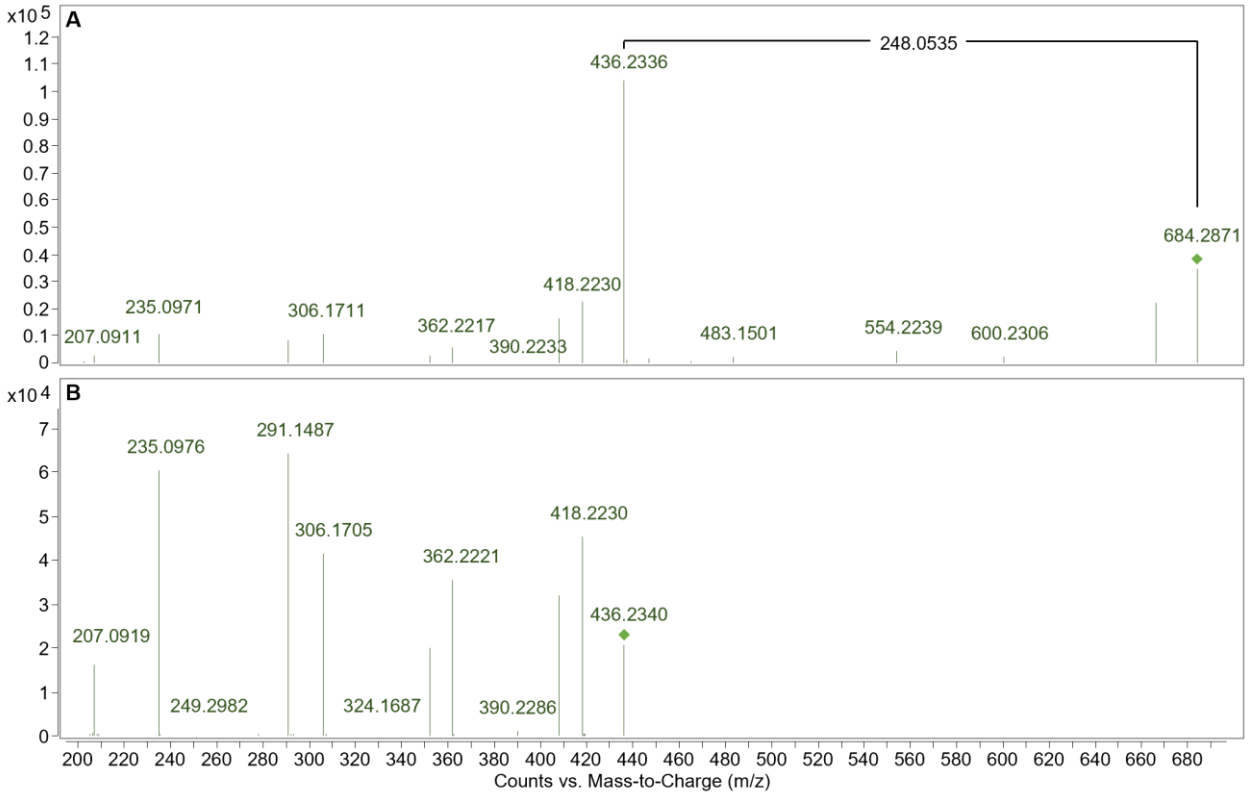

Figure 47: MS^2 spectrum of VAL-Glc-Mal (m/z 684.29; A) in a turnip greens sample fragmented with a CE of 5 V in comparison to an MS^2 spectrum of VAL (436.23; B)

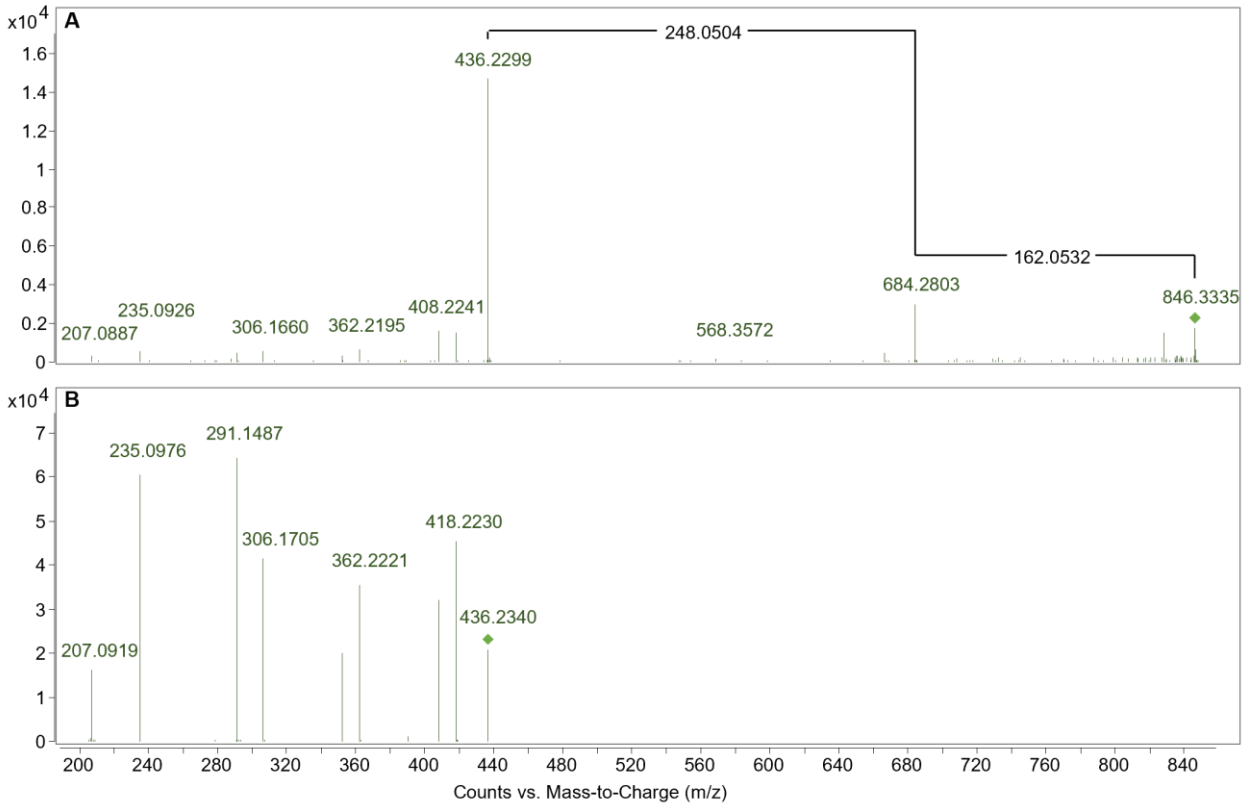

Figure 48: MS^2 spectrum of VAL-Glc-Glc-Mal (m/z 846.33; A) in a turnip greens sample fragmented with a CE of 5 V in comparison to an MS^2 spectrum of VAL (436.23; B)